SPECTRAL DECOMPOSITION AND ATTRIBUTES FOR EVALUATING SEISMICALLY THIN LAYERS

A Dissertation Presented to

the Faculty of the Department of Earth and Atmospheric Sciences

University of Houston

In Partial Fulfillment

of the Requirements for the Degree

Doctor of Philosophy

By

Jian Zhou

May 2017

SPECTRAL DECOMPOSITION AND ATTRIBUTES FOR EVALUATING SEISMICALLY THIN LAYERS

Jian Zhou

APPROVED:

Dr. John Castagna, Chairman
Department of Earth and Atmospheric Sciences

Dr. Evgeni Chesnokov
Department of Earth and Atmospheric Sciences

Dr. Robert Stewart
Department of Earth and Atmospheric Sciences

Dr. Alex Martinez
ExxonMobil

Dean, College of Natural Sciences and Mathematics

ACKNOWLEDGEMENTS

First and foremost, I would like to express gratitude to my advisor, Dr. John Castagna for his guidance and support during my study and research work here. His brilliance and dedication to push the limit for better geophysical technique will always be something that I aspire for. Also I would like to thank my committee members. Dr. Evgeni Chesnokov emphasizes that basic laws of physic should be used as guideline, which I will always remember. I am grateful to Dr. Robert Stewart and Dr. Alex Martinez for their comments, questions, and suggestions that eventually improved the quality of my dissertation significantly.

I wish to thank all the professors from whom I learned a lot in their classes. I thank the Department of E.A.S. for the financial support, and Dr. Jinny Sisson for coordinate my teaching duties. I am grateful to department Chairman Dr. Hua-Wei Zhou, graduate advisor Dr. Aibing Li, and all the administration staff for helping me every step of my way. I thank ExxonMobil for donating the 3D seismic data to University of Houston for research, and Earth Science Associates giving me access to the complete well log dataset that I used. I want to thank every one of my colleagues and friends at University of Houston, unfortunately their names are too many to list here. I might have learnt as much from them as from everywhere else, if not more. Their company made my study

experience here much more memorable. Last but not least, I couldn't have gone so far without the love, patience, and support from my family.

A wise man once told me, that going to graduate school is not just about the degree, but also the experience you gained along the way. I am delighted that I am about to get both in the end.

SPECTRAL DECOMPOSITION AND ATTRIBUTES FOR EVALUATING SEISMICALLY THIN LAYERS

An Abstract of a Dissertation

Presented to

the Faculty of the Department of Earth and Atmospheric Sciences

University of Houston

In Partial Fulfillment

of the Requirements for the Degree

Doctor of Philosophy

By

Jian Zhou

May 2017

ABSTRACT

The reflectivity series and resulting waveform for a generalized-simple layer (arbitrary reflection coefficients on top and base) can be separated into unique even and odd components, each having a different tuning curve. Amplitudes at peak frequency of pure-impulse pairs are independent of thickness, for either the original reflectivity, its odd, or even component. For seismic data with a non-flat spectrum, dividing the data spectrum over some useable band by the wavelet spectrum results in amplitudes at peak frequency that are independent of thickness. Comparing peak-frequency amplitudes for even and odd components to that of the total waveform, provides clues as to the nature of the layering.

Correlations between spectral-isofrequency-amplitude traces (time-varying-spectral amplitude at individual frequencies) provide a means of finding frequency notches induced by layer reflectivity. Isofrequency-amplitude traces tend to be strongly correlated amongst frequencies at spectral nulls; and amongst those that are not at those frequency notches. Spectral-principal-component-amplitude attributes take advantage of this property, and are indicative of layer thickness. With proper trace scaling and spectral balancing, spectral-PC amplitudes are independent of layer's reflection coefficients. Layers with only odd and even pair reflection coefficients have distinctive-spectral-principal component to thickness relationships in synthetic-wedge models.

Three spectral-PC attributes individually delineate amplitudes from: 1) an isolated reflection not affected by tuning; 2) tuning of an even reflection pair; and 3) tuning of an odd reflection pair in a 3-D-synthetic-channel model. As with the synthetic model, a good attribute versus true-reservoir-thickness relationship is seen in real seismic and well data from the Hoover field in the Gulf of Mexico.

TABLE OF CONTENTS

LIST OF FIGURES

Chapter 1

Introduction

Quantifying and visualizing frequency-dependent-seismic responses is a key objective of quantitative-seismic interpretation. These responses include effects such as thin-bed tuning (Chen et al., 2008), fluid-induced-reflectivity variation, attenuation and dispersion (Castagna et al., 2003, Korneev et al., 2004), waveform variation with offset (Yang, 2003), etc. Understanding these frequency-dependent responses may help differentiate fluid effects from stratigraphic variation in reflectivity. However, direct correlation of seismic amplitude and frequency content to reservoir properties is difficult when these factors simultaneously influence seismic responses (Chen et al., 2008, Li et al., 2011, Liner and Bodmann, 2010).

The thickness-amplitude relationship, as one of the earlier seismic-geology relationships studied, is complex due to the involvement of variation in layer-acoustic properties as well as frequency content in seismic data. Widess (1973) illustrated the relationship between seismic-reflection amplitude and layer thickness for an isolated-thin layer (a tuning curve). He also introduced the idea of a seismic-tuning thickness, i.e., the thickness corresponding to approximately a half-period of the dominant frequency of the seismic wavelet, at which thickness maximum constructive interference between top and base reflectors occurs. Kallweit and Wood (1982) dealt with the fact that the "Widess model" is not general and corresponds to the special case of equal- and opposite-reflection coefficients at the top and base of a layer. They showed that the tuning curve is inverted when reflection coefficients are the same sign; in that case, maximum-destructive interference occurs at half-period-time thickness and maximum constructive interference occurs at zero thickness. Chung and Lawton (1995) and Puryear and Castagna (2008) studied the tuning behavior of the more-general case of arbitrary pairs of reflection coefficients.

One of the ideas to investigate frequency-dependent seismic responses is to first study seismic response at individual frequencies. Taner et al. (1979) used instantaneous-spectral attributes from the complex seismic trace, which is an extension of the conventional-seismic trace. Partyka et al. (1999) applied spectral decomposition to seismic data to image thickness changes and subtle discontinuities. Since that time, many authors have investigated spectral decomposition as an interpretation tool. Castagna et al. (2003) and Sinha et al. (2005) discuss using spectral decomposition as a direct-hydrocarbon indicator. Marfurt and Kirlin (2001) and Liu and Marfurt (2007) demonstrate that using peak-amplitude, peak-frequency and coherence attributes give better visualization of channel features. Khare and Martinez (2008) show that amplitude ratios of frequency components are indicative of thickness variations.

Multiattribute-analysis techniques can make use of spectral decomposition, treating each frequency as an individual attribute. As one of the common types of multiattribute techniques, principal component analysis (PCA), can be useful in showing correlation relations between all frequency components (Guo et al., 2009). Principal components of a time-frequency analysis are orthogonal-linear combinations of individual frequencies ranked by the variance of the data that they account for. Principle component analysis (1) allows for reduction of the data dimensionality by elimination of insignificant principal components, (2) aids in multiattribute analysis due to the superiority of orthogonal attributes in multiple regression, and (3) provides independent visualizations of the geology, each PC potentially highlighting different geological features. We begin with the concept of the spectral isofrequency-amplitude trace, which represents amplitude versus time at a given frequency and investigate correlations between isofrequency traces and layer thickness. Also, we explore the use of Varimax rotation of principal components to separate frequency responses. The Varimax norm was formerly applied to test seismic data spikiness (Wiggins, 1978), zero-phase correlation (Levy and Oldenburg, 1987) and focusing (Fomel et al., 2007). When applied to balanced frequency gather data, the Varimax rotation of the first few spectral PCs, which usually represent most of information, finds their best correlation to specific frequency bands. As a result, each Varimax-rotated-spectral PC represents, for the most part, an independent band of frequencies.

In this dissertation, we first discuss the seismic-tuning effect from a generalized-simple layer in chapter 2. Any seismic reflection or seismogram from a layer can be decomposed into a real- and an imaginary-Fourier component, given that the center of layer is known. Frequency-domain-tuning curves prove to be superior to time-domain-tuning curves, having better resolution, and independence from reflection-coefficient change. In chapter 3, we demonstrate the concept and properties of an isofrequency-amplitude trace, and correlations between isofrequency traces, which are determined by thickness of layers. Chapter 4 introduces how principal component analysis of isofrequency-amplitude trace data takes advantage of the correlations, and produces statistically significant and independent spectral PCs. Also, Varimax rotation is explored as an interpretation tool of spectral PCs for their frequency content and geophysical meaning. In Chapter 5, 2D-synthetic-layer and wedge models, 3D-synthetic model containing a turbidite channel, and real datasets from the Fort-Worth basin, Texas and the Gulf of Mexico are used to test the effectiveness of spectral-PC attributes in delineating thickness variation. Chapter 6 summarize this dissertation briefly with conclusions.

Chapter 2

Generalized Tuning of Seismic-Reflection Events From Simple Layers

2.1 Background

Widess (1973) illustrated the relationship between seismic reflection amplitude and layer thickness for an isolated thin layer (a *tuning curve*). He also introduced the idea of a seismic *tuning thickness* (the thickness corresponding to approximately a half-period of the dominant frequency of the seismic wavelet at which maximum constructive interference between top and base reflectors occurs; see Figure 2.1a). Kallweit and Wood (1982) dealt with the fact that the "Widess model" is not general and corresponds to the special case of equal and opposite reflection coefficients at the top and base of a layer. They showed that the tuning curve is inverted (Figure 2.1b) when reflection coefficients are the same sign; in that case, maximum destructive interference occurs at half-period time thickness and maximum constructive interference occurs at zero thickness. Chung and Lawton (1995) and Puryear and Castagna (2008) studied the tuning behavior of the more-general case of arbitrary pairs of reflection coefficients. Various time domain attributes are tested in the same fashion as the tuning curve in the "Widess model", "Kallweit-Wood model" and two examples of the generic models. The results are included in Appendix A. One can conclude from these studies that tuning curves based on the Widess model can be seriously in error when applied to a layer with arbitrary reflection coefficients and that a more-general approach for understanding resolution is, thus, needed.

It is apparent from the Partyka et al. (1999) seminal paper on spectral decomposition that, in the frequency domain, for an isolated layer and a flat wavelet spectrum, the maximum amplitude of the reflectivity spectrum is independent of the layer thickness. Marfurt and Kirlin (2001) generalized this conclusion to an arbitrary pair of reflection coefficients. Application of this fact to interpretation of real seismograms is complicated when the seismic wavelet has a non-flat amplitude spectrum over the band of the data, and when wave propagation is not adequately described by a simple convolutional model. As a first step, these papers suggest that proper consideration of tuning must consider what happens in both the time and frequency domains. In light of these developments, the purpose of this chapter is, within the context of the convolutional model, to (1) synthesize and illustrate improvements in our understanding of seismic resolution, (2) review the current state-of-the-art, and (3) recommend best practices for seismic interpretation purposes.

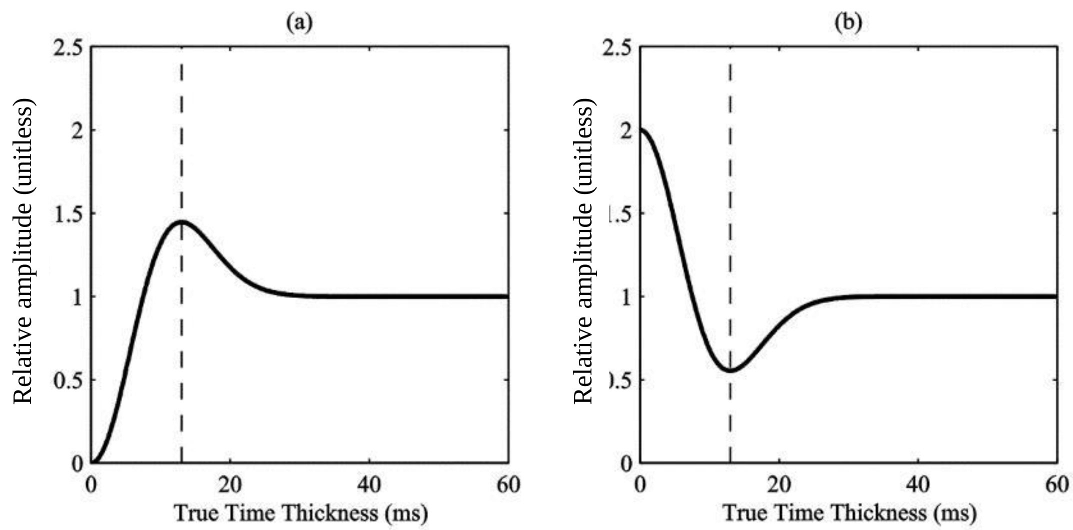

Figure 2.1 Classical tuning curves of time domain peak amplitude versus thickness for a 30 Hz Ricker wavelet (a) Widess (1973) model (b) Kallweit and Wood (1982) model.

2.2 Reflectivity Spectrum of a Generalized-Simple Layer

We define a *simple layer* as one with only two reflection coefficients; one at the top and one at the base. In practice, impedance profiles are rarely that simple, but (1) a simple layer is a good starting point to understand more complex behavior, and (2) reflectivity sequences can sometimes be approximated by an equivalent simple layer that exhibits similar behavior to a more complex sequence of reflection coefficients, particularly in an earth with a blocky impedance profile. As compared to the treatments by Widess (1973) and Kallweit and Wood (1982), we will investigate the case of a *generalized simple layer* where the reflection coefficients need not be equal in magnitude and can have arbitrary sign.

Following Puryear and Castagna (2008) the generalized simple layer can be represented as:

$$g(t) = r_1\delta(t\text{-}T/2) + r_2\,\delta(t+T/2) \quad , \tag{2.1}$$

where, $g(t)$ is the reflectivity series as a function of time, T is the layer two-way time thickness, r_1 and r_2 are the reflection coefficients at top and base of the layer respectively, and δ is the Dirac-delta function.

As any time series can be uniquely divided into even and odd parts (Bracewell, 1965), we now define even, $g_e(t)$, and odd, $g_o(t)$, reflectivity series components by

$$g_e(t) = r_e\delta(t\text{-}T/2) + r_e\,\delta(t+T/2) \tag{2.2}$$

and

$$g_o(t) = r_o\delta(t\text{-}T/2) + r_o\,\delta(t+T/2) \tag{2.3}$$

where, $g_e(t)$ and $g_o(t)$ sum to $g(t)$ and r_e and r_o are the even and odd reflection coefficients given by

$$r_e = (r_1 + r_2)/2 \tag{2.4}$$

and

$$r_o = (r_1 - r_2)/2\ . \tag{2.5}$$

The frequency spectrum, $G(f)$, is then

$$G(f) = (2r_e)cos(\pi fT) + i(2r_o)sin(\pi fT) \quad . \tag{2.6}$$

The real part of the complex spectrum, $Re[G(f)]$, is the spectrum of the even part of the reflectivity series while the imaginary part of the complex spectrum, $Im[G(f)]$, is the spectrum of the odd part of the reflectivity series. Each of these is a sinusoidal variation of amplitude with frequency with maxima equal to twice the even or odd reflectivity.

Equation (2.6) can be manipulated to reveal some interesting behavior and help us understand the resolution of a generalized layer. We first consider the spectrum of the even part of the reflectivity series, $Re[G(f)]$, which upon differentiation gives:

$$\frac{\partial Re[G(f)]}{\partial f} \Big/ Re[G(f)] = -\pi T \tan(\pi f T) \quad . \tag{2.7}$$

This equation allows computation of layer thickness from the real part of the reflectivity spectrum without knowing the reflection coefficient magnitudes. The form of equation (2.7) also reveals strong sensitivity to thickness even as the layer thickness becomes very small. This suggests strong sensitivity of the spectrum to thickness even below tuning for the even part of the signal (in the absence of noise). This should not be surprising given Kallweit and Wood's (1982) tuning curves which show strong amplitude sensitivity at small thicknesses below ¼ period. This equation provides a thickness estimate for every frequency within a given useable band, and thus, in the simple layer case, can produce reliable estimates of thickness when averaged over many frequencies;

while variations of thickness estimates for different frequencies can reveal poor data quality or more complex layering.

Similarly, for the odd part of the reflectivity series we obtain:

$$Im[G(f)] / \frac{\partial Im[G(f)]}{\partial f} = (1/\pi T)\tan(\pi f T) \quad . \qquad \textbf{(2.8)}$$

From inspection of equation (2.8), one can conclude that as time thickness goes to zero, estimation of T from the spectrum of the odd part of the reflectivity becomes unstable. This can be seen by taking the limit of the right-hand side of equation (2.8) as T approaches zero; which is simply f. Thus, as Widess (1973) concluded with wedge modeling, there is no sensitivity to thickness for very thin layers with equal and opposite reflection coefficients. On the other hand, from the spectrum of the even component, as thickness goes to zero the right-hand side of equation (t) becomes linear in f with a coefficient proportional to T^2; in other words, equation (2.7) is highly sensitive to thickness even for thin layers. It can readily be shown that ratioing equations (2.7) and (2.8) yields a simple direct solution for T which is unfortunately also unstable as thickness approaches zero and thus is not given here. Similarly, multiplying (2.5) and (2.6) provides a useful, if more complex, direct solution that is not restricted to thin layers.

$$-arctan\{\frac{\partial Re[G(f)]}{\partial f} Im[G(f)] \Big/ \frac{\partial Im[G(f)]}{\partial f} Re[G(f)]\}^{1/2} = \pi f T \quad . \tag{2.9}$$

Puryear and Castagna (2008) show that once thickness is obtained from equations (2.7 and 2.8), the reflection coefficients can be determined from the real and imaginary parts of equation (2.6). Of course, any frequency where the amplitude in any denominator term approaches zero should be avoided in these calculations. These manipulations suggest that the even part of a seismic signal has better resolution than the odd part for very thin layers. This is the basis for spectral inversion (Puryear and Castagna, 2008) but can also be used to better understand signals from thin layers as discussed below.

2.3 An Example

Assuming the center of a simple layer is known, it is possible to solve and separate the even and odd pair of any reflection in time and frequency domain by simply using the Fourier transform. The detailed workflow can be seen in Appendix B. For illustration, let us consider a 10 ms thick general simple layer with a top reflection coefficient $r_1 = .2$ and a base reflection coefficient $r_2 = -.1$ (Figure 2.2). The maximum amplitude of the reflectivity spectrum is given by $|r_1| + |r_2|$ and the minimum amplitude is $|r_1 - r_2|$. The reflection coefficients of the even part are $r_e = .05$ at top and base, and the odd reflection coefficients are $r_o = .15$ at the top and $-r_o = -.15$ at the base. These layer reflectivities are, respectively, even and odd impulse pairs which have sinusoidal frequency spectra. The amplitude spectrum of the reflectivity (Figure 2.3a) is the square root of the sum of the squares of the real and imaginary parts of the complex reflectivity spectrum given by equation (2.6). The amplitude spectrum of the even part of the reflectivity is a rectified cosine function (Figure 2.3b) and the amplitude spectrum of the odd part of the reflectivity is a rectified sin function (Figure 2.3c). The maximum amplitude at the frequency peaks for the reflectivity spectrum of the even part of the reflectivity is equal to $2r_e$ and equal to $2r_o$ for the odd part of the reflectivity. In both cases the minimum amplitude is zero. For a broad band wavelet with a flat spectrum, the resulting amplitude at any peak frequency is thus independent of thickness, which makes it a fundamentally different quantity than peak amplitude in the time domain. Similarly, as pointed out by Partyka et al., (1999) the peak frequencies, and spacing between spectral peaks, depends only on time thickness and is independent of reflection coefficient.

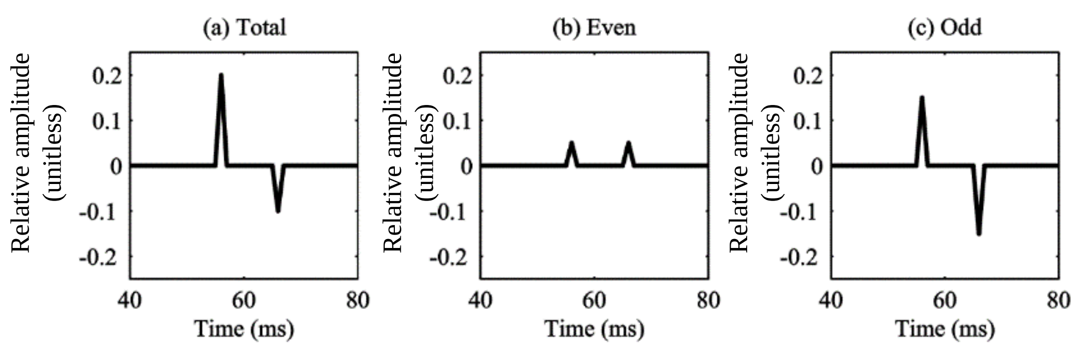

Figure 2.2 Reflectivity for for a 10 ms thick layer and has reflection coefficients of .2 at the top and -.1 at the base. (a) Reflectivity series. (b) Even part of the reflectivity. (c) Odd part of the reflectivity.

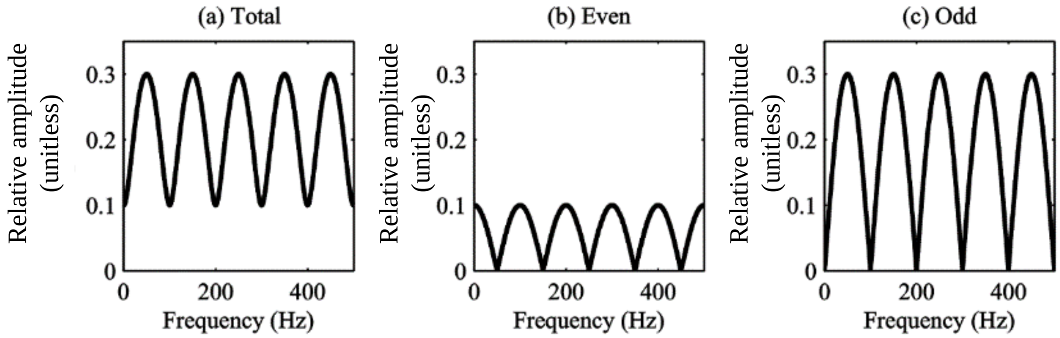

Figure 2.3 Reflectivity spectra for a 10 ms thick layer and has reflection coefficients of .2 at the top and -.1 at the base. Amplitude spectrum of (a) reflectivity series; (b) even part of reflectivity, (c) odd part of the reflectivity.

Of course, the example above does not include the effects of a band-limited seismic wavelet with general frequency and phase. For our purposes, we will assume that the wavelet is stable enough, and smooth enough in the frequency domain (without frequency nulls) over some useful bandwidth, such that the wavelet spectrum can be divided out, and that resulting spectra can be treated as reflectivity spectra over some useable band.

2.4 Generalized-Tuning Curves for a Wedge Model

To model a realistic thin-layer situation, we convolve the reflectivity spectra with a 30 Hz Ricker wavelet and measure amplitudes at peak frequency (Figure 2.4) as layer thickness thins well below tuning. Note that since the Ricker wavelet amplitude spectrum is not flat, the behavior is similar to that observed in the time domain (see Figure 2.1) for even and odd components. The total amplitude is dominated by the odd component near tuning where the odd component constructively interferes and the even component destructively interferes. As the layer thins, the odd component becomes weaker while the even component becomes stronger. As thickness approaches zero, amplitude does not go to zero as in the Widess model, but rather the even component dominates for very thin layers. This behavior is similar to that observed in the time domain (Puryear and Castagna, 2008). This is a consequence of the fact that the Ricker wavelet spectrum is not flat. We can shape the wavelet spectrum to a flat response over a desired bandwidth by dividing the data by the Ricker wavelet spectrum. The result are amplitudes at peak frequency that are independent of thickness (Figure 2.5).

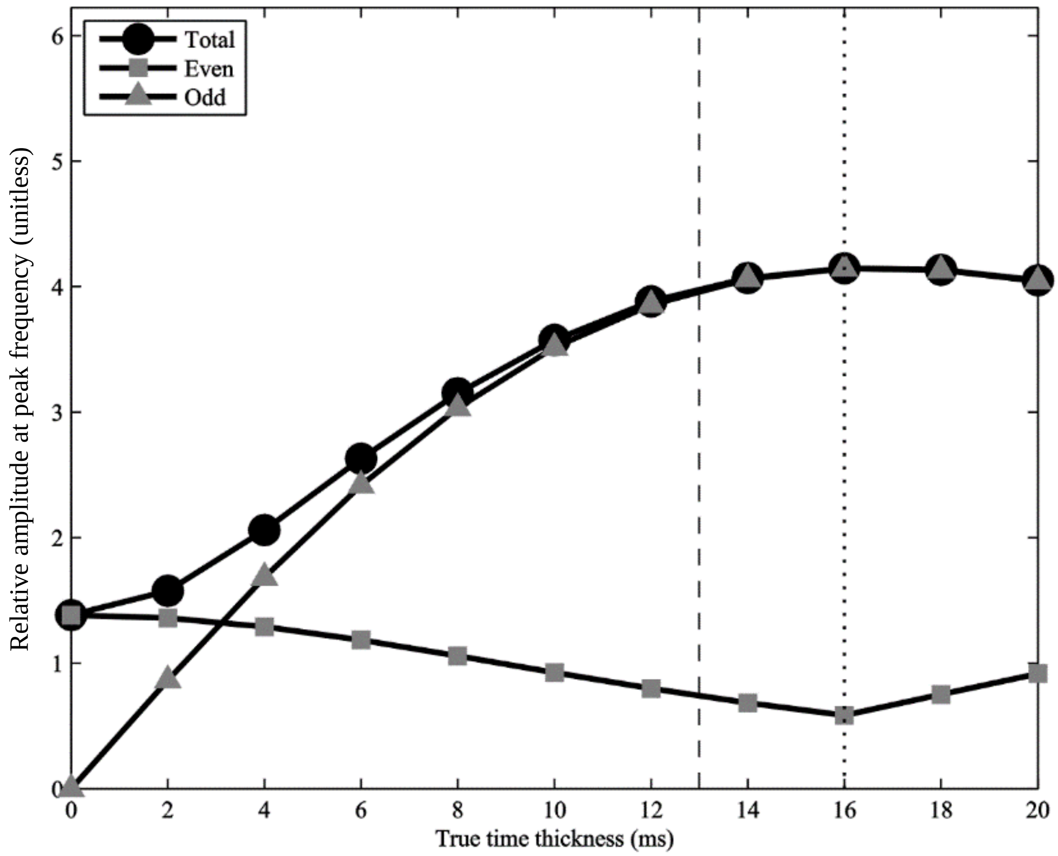

Figure 2.4 Amplitude at peak frequency for a wedge model using a 30 Hz Ricker wavelet. Reflection coefficients is .2 at the top and -.1 at the base. The dashed and dotted line represents tuning thickness of the Ricker wavelet and a 30 Hz sinusoid, respectively.

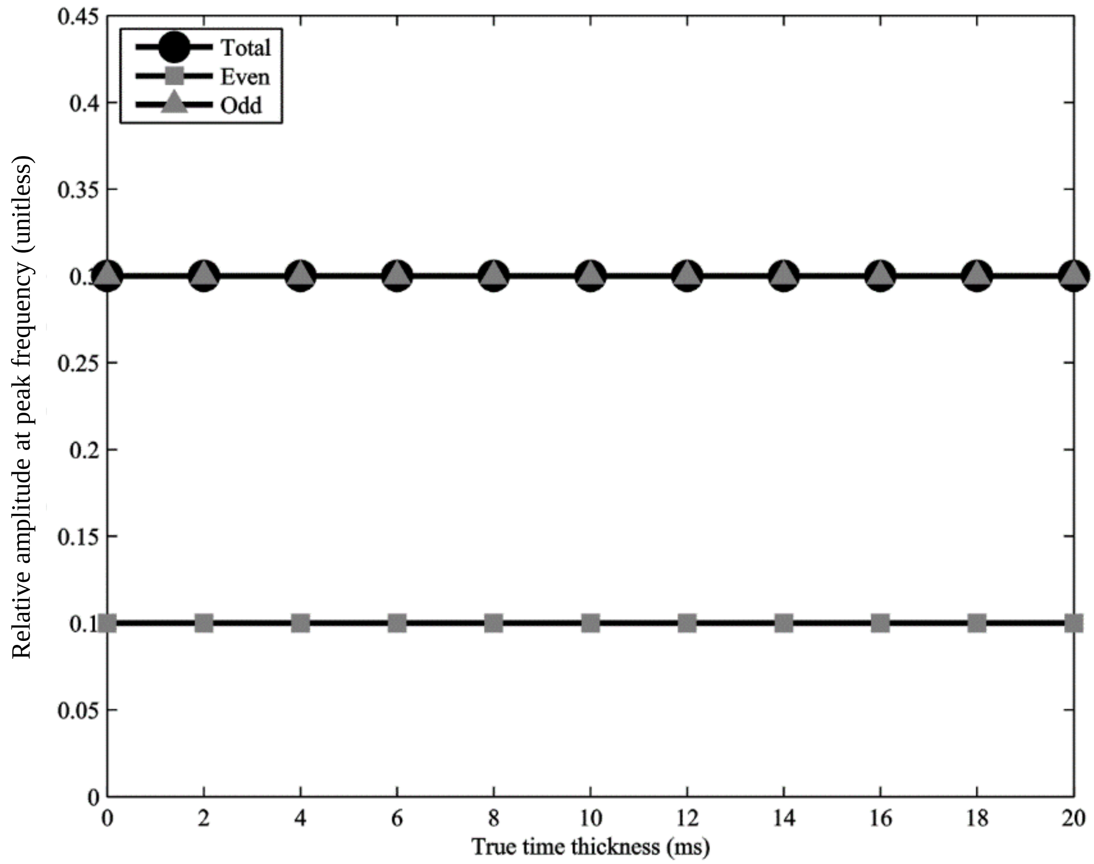

Figure 2.5 Amplitude at peak frequency for a wedge model using a 30 Hz Ricker wavelet with the Ricker wavelet spectrum divided out over the useable bandwidth. Reflection coefficients is .2 at the top and -.1 at the base.

The significance of this is important for seismic interpretation and multiattribute analysis. In analyses making use of amplitudes, we of course assume that overburden variations, and any other non-local factors, affecting amplitudes have been corrected for. For conventional time-domain amplitudes, below tuning, if thickness changes, amplitudes change. Thus, when seismic amplitude changes in a thin layer, it is unknown whether that amplitude change is caused by a rock properties change (and a corresponding reflection coefficient change) or a layer thickness change. For amplitudes at peak frequency on properly frequency balanced spectra (with the wavelet divided out) as shown in Figure 2.5, a local amplitude change can be related directly to reflection coefficient changes. This makes amplitude analysis more robust and powerful.

Another interesting effect evident in Figure 2.5 is that the amplitude at peak frequency is virtually the same as the amplitude of the odd component. This is not always the case. Since the amplitude at a peak frequency for a general impulse pair, A_{total}, is given by

$$A_{total} = |r_1| + |r_2| \tag{2.10}$$

The amplitude at a peak frequency for the even part, A_{even}, is then

$$A_{even} = |r_1 + r_2| \tag{2.11}$$

and the amplitude at a peak frequency for the odd part, A_{odd}, is

$$A_{odd} = |r_1 - r_2| \tag{2.12}$$

If r_1 and r_2 are the same sign (as would result from an impedance staircase) then

$$A_{even} = |r_1 + r_2| = |r_1| + |r_2| = A_{total} \tag{2.13}$$

On the other hand, if r_1 and r_2 are opposite sign (as would result from an isolated layer of abnormally high or low impedance encased in material with equal impedance above and below the layer) then

$$A_{odd} = |r_1 - r_2| = |r_1| + |r_2| = A_{total} \tag{2.14}$$

Thus, by comparing the amplitudes at peak frequency of the even and odd components to that of the total waveform, one can determine if one is dealing with either of these idealized simple layers or a more complex situation, in which case neither component may exhibit the same amplitude at peak frequency as the total waveform.

Finally, amplitude tuning curves for even and odd components for peak amplitudes in the time and frequency domains (Figure 2.6) are compared. It is important to note that the amplitude tuning effects are larger in the frequency domain when the spectra have not been normalized by the wavelet spectrum.

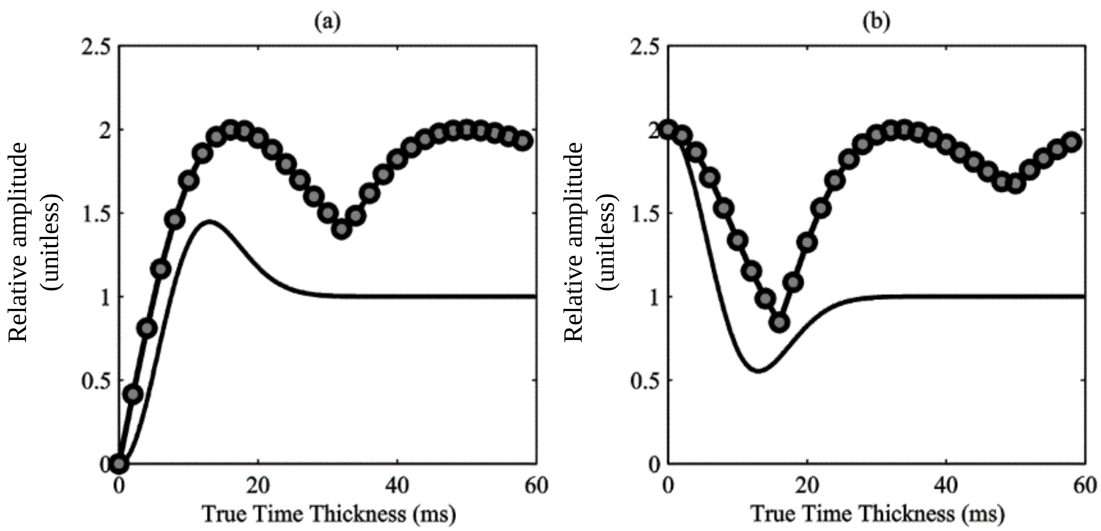

Figure 2.6 Peak amplitude in time (line) and frequency domain (circle) for wedge model with (a) odd reflection pair, and (b) even reflection pair after convolved with 30 Hz Ricker wavelet.

2.5 Summary

In the general case of arbitrary reflection coefficients at the top and base of a simple layer, amplitude tuning may deviate significantly from the Widess model. This is particularly true for layers well below tuning. When observing the total tuning response, such behavior can be complex and difficult to understand. However, tuning phenomena can be greatly simplified by (1) separating tuning responses for the unique even and odd components of a waveform, and (2) looking at amplitudes at peak frequencies of the spectral response. Most significantly, we find that the even component of the reflectivity dominates amplitudes as thickness approaches zero, and provides the possibility of resolving reflectors well below tuning. Furthermore, by flattening the wavelet spectrum over some useful frequency band, we find that the amplitude at peak frequency is independent of layer thickness. This has potentially important consequences for amplitude analysis. Finally, comparing amplitudes at peak frequency for even and odd components to that of the total waveform provides clues as to the nature of the layer being investigated.

Chapter 3

Spectral Decomposition and Correlation Between Isofrequency Traces

3.1 Spectral decomposition, spectral amplitude, and the isofrequency trace

Since the inception of the Fourier Transform, frequency components of an arbitrary time series or signal can be revealed by transforming the signal from the time domain into the frequency domain. The process of the Fourier transform cross-correlates the input signal and a series of sine and cosine waves of different frequencies, which can be viewed as template functions. For a windowed signal calculated, the process of Fourier transform is equivalent to measuring similarity between the signal and the template functions. The output frequency information consists of spectral amplitude, which are correlation coefficients between the signal and the bases functions, as for variable frequency and phase.

However, for an arbitrary signal, the Fourier transform cannot provide time-varying information since it considers the input signal as a whole. Gabor (1946) introduced the short-time Fourier transform by using an analysis window that slides through the signal over time. At each time sample, a time-specific Fourier transform of the windowed signal is performed. The spectrum of truncated signal is assigned to the time sample at the center of the window. To capture the "short duration" temporal variation in the signal, using a shorter window is desirable. However, using a shorter window, which means more shortly truncated bases functions, distorts the signal spectrum by convolving it with the window spectrum. This is one example of the uncertainty principle, which indicates that for a given algorithm of time-frequency analysis, the product of time- and frequency- resolution is fixed with a constant value as the window length varies. For more recent spectral decomposition techniques that use windows of variable length or a dictionary of wavelets, product of time- and frequency-resolution at a given frequency can differ from that of the short-time Fourier transform. However, there should always be a limit of the resolution product for each method; hence there is always a trade-off between time- and frequency-resolution.

For an arbitrary signal (Figure 3.1a), to interpret its amplitude spectrum variation over time, instead of plotting the amplitude spectrum for each truncation of the signal as a function of time (Figure 3.1b), it is now standard procedure to use some key feature of the amplitude spectrum as a spectral attribute. These include frequency at which amplitude reaches maximum (peak frequency), amplitude at peak frequency (peak amplitude), bandwidth, spectral shape, etc. To display a complete spectral decomposition amplitude spectrum, it is usually plotted as a time-frequency panel (Figure 3.1c). At each point on the panel, the color or intensity represent spectral amplitude, which are also correlation coefficients of truncated signal to basis. To show spectral amplitude variation over time, it is also possible to plot spectral amplitude for each single frequency as an individual attribute, referred to here as an "isofrequency-amplitude trace" or "isofrequency trace". The smoothly varying spectral amplitude over time at each individual frequency can be plotted as seismic traces (Figure 3.1d). Here, the isofrequency-amplitude trace is a frequency domain seismic attribute. No inference related to properties of a regular seismic time trace, such as phase or frequency should be drawn from the isofrequency-amplitude trace.

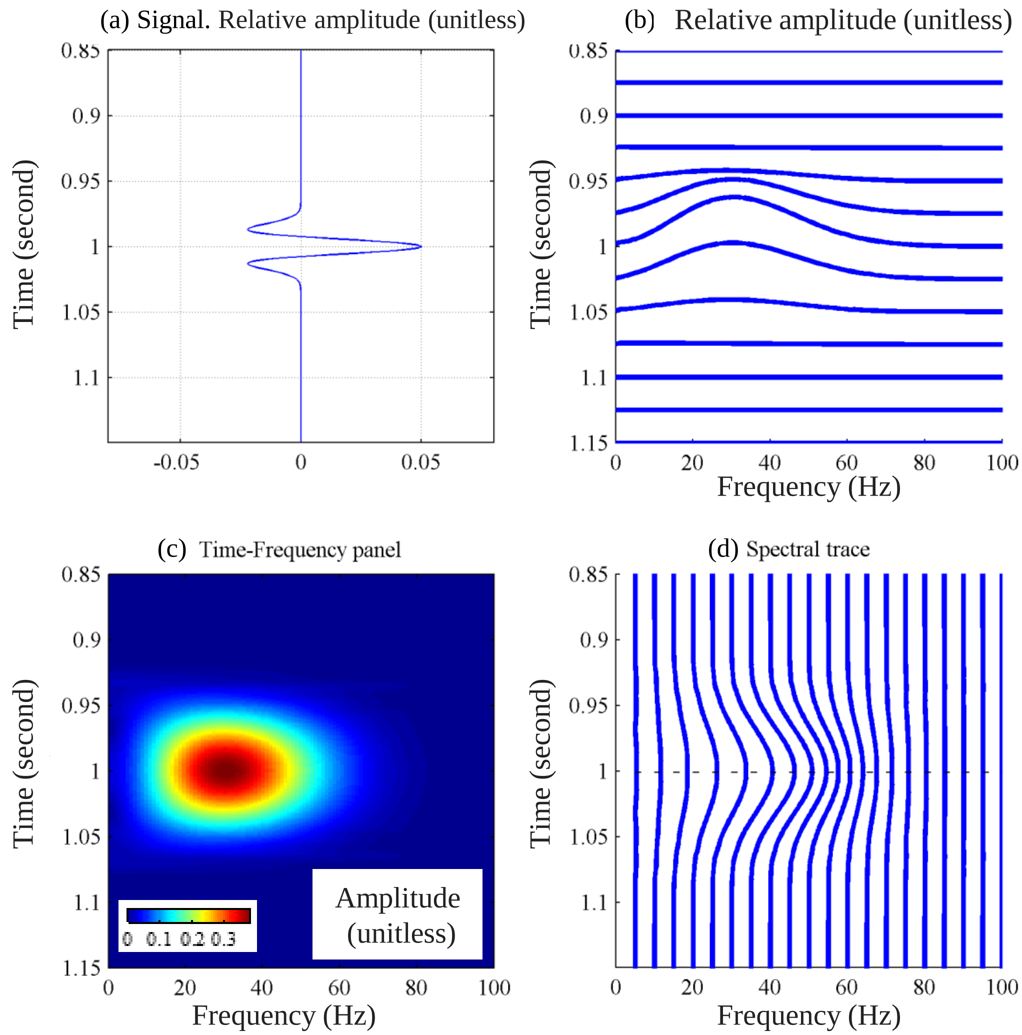

Figure 3.1 Comparison of an arbitrary signal (a), its spectral amplitude result displayed as amplitude spectrum at time samples (b), time-frequency intensity panel (c), and isofrequency-amplitude traces.

3.2 Correlation between isofrequency-amplitude traces

Correlation between isofrequency-amplitude traces of a signal can be the result of similarity between isofrequency-amplitude traces of the reflectivity series and the wavelet, as well as due to the poor resolution of the spectral decomposition algorithm, e.g., as would be caused by the window effect. From the Fourier convolution theorem, the amplitude spectrum of a signal equals the product of the reflectivity series spectrum and the wavelet spectrum. For example, the amplitude spectrum of a 30 Hz Ricker wavelet has amplitude frequency variation that is a continuous curve (Figure 3.2a). This suggest that isofrequency-amplitude traces are highly correlated, regardless of variation in amplitude magnitude over frequency. For the simplest situation, if the truncated reflection series contains only one reflector, the amplitude spectrum and isofrequency-amplitude trace waveforms of the reflectivity series remain unchanged over frequency. Hence the amplitude spectrum of the signal and the shape of isofrequency-amplitude traces will only be determined by those of the wavelet (Figure 3.2, b-d).

The correlation matrix (r) is usually applied to quantify the correlativeness between multiple measurements from a few sample points. The correlation coefficient is a calculation of how well measurements x and y acquired at k observation points fit around the linear regression of the points. The equation for calculating correlation coefficient is:

$$r_{xy} = \frac{\sum_{i=1}^{k}(x_i-\bar{x})\,(y_i-\bar{y})}{\sqrt{\sum_{i=1}^{k}(x_i-\bar{x})^2}\,\sqrt{\sum_{i=1}^{k}(y_i-\bar{y})^2}} \quad . \tag{3.1}$$

Here $\boldsymbol{\bar{x}}$ and $\boldsymbol{\bar{y}}$ are mean values of all points from isofrequency-amplitude traces x and y, respectively. Also, x_i and y_i are the i^{th} sample of measured points. In our application, each point on the matrix is the correlation coefficient between two isofrequency-amplitude traces x and y (r_{xy}). A schematic illustrating this process is given in Figure 3.3.

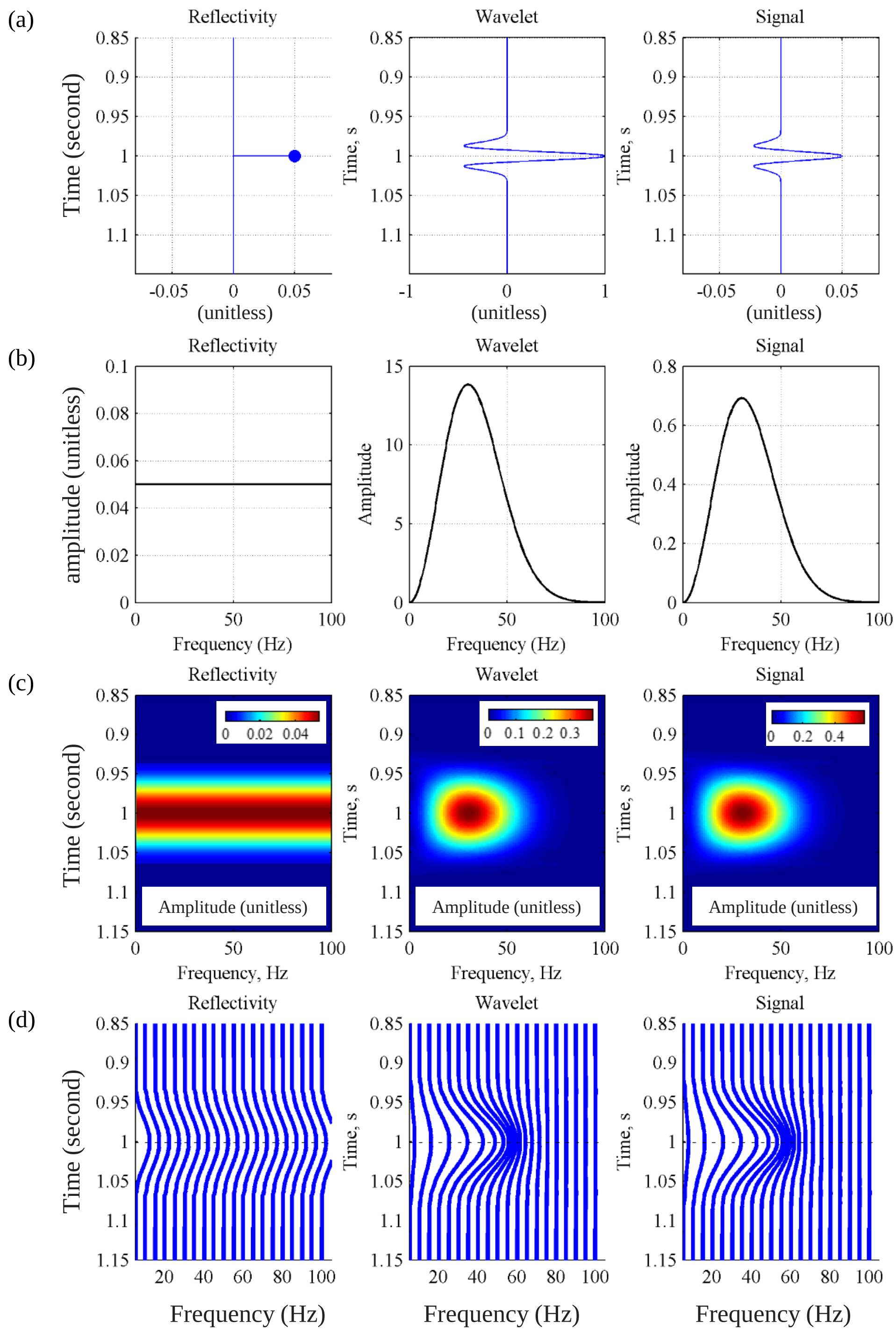

Figure 3.2 Time view (a), amplitude spectrum view (b), spectral intensity view (c), and isofrequency trace view (d) of a one-reflector model, a 30 Hz Ricker wavelet, and the convolved signal.

(a)

d	o_1	o_2	o_3	o_4	o_5	$o_{...}$	o_k
f_1	d_{11}	d_{12}	d_{13}	d_{14}	d_{15}	…	d_{1k}
f_2	d_{21}	d_{22}	d_{23}	d_{24}	d_{25}	…	d_{2k}
f_3	d_{31}	d_{32}	d_{33}	d_{34}	d_{35}	…	d_{3k}
$f_{...}$	…	…	…	…	…	…	$d_{...k}$
f_m	d_{m1}	d_{m2}	d_{m3}	d_{m4}	d_{m5}	$d_{m...}$	d_{mk}

(b)

r	f_1	f_2	f_3	$f_{...}$	f_m
f_1	r_{11}				
f_2	r_{21}	r_{22}			
f_3	r_{31}	r_{32}	r_{33}		
$f_{...}$	…	…	…	…	
f_m	r_{m1}	r_{m2}	r_{m3}	$r_{m...}$	r_{mm}

Figure 3.3 Schematic showing isofrequency-amplitude traces d (*k* samples and *m* frequencies) (a), and correlation matrix (b) calculated from the isofrequency-amplitude traces.

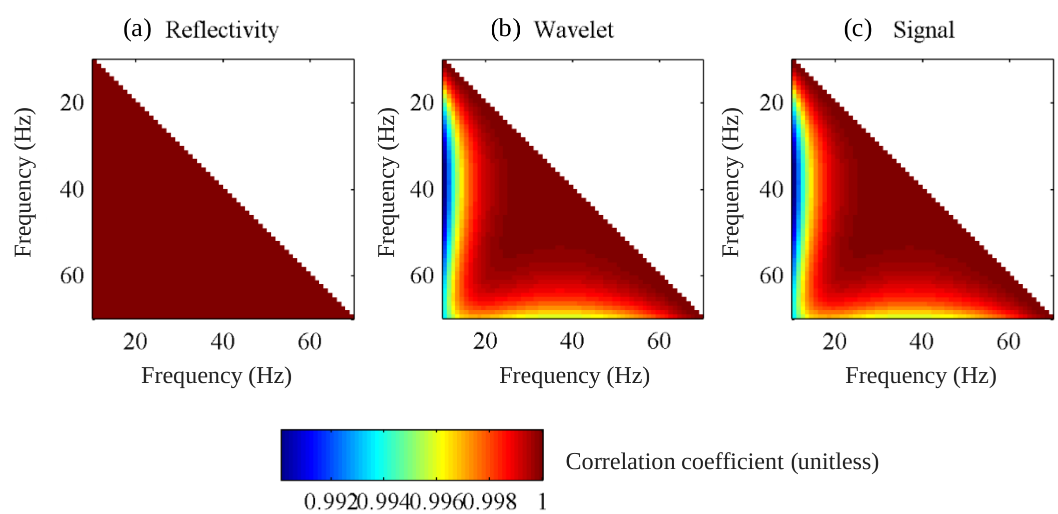

Figure 3.4 Correlation coefficient between isofrequency-amplitude traces within typical bandwidth (10-70 Hz) of Reflectivity of one reflector (a), 30 Hz Ricker wavelet (b) and signal constructed by convolution of the previous two (c).

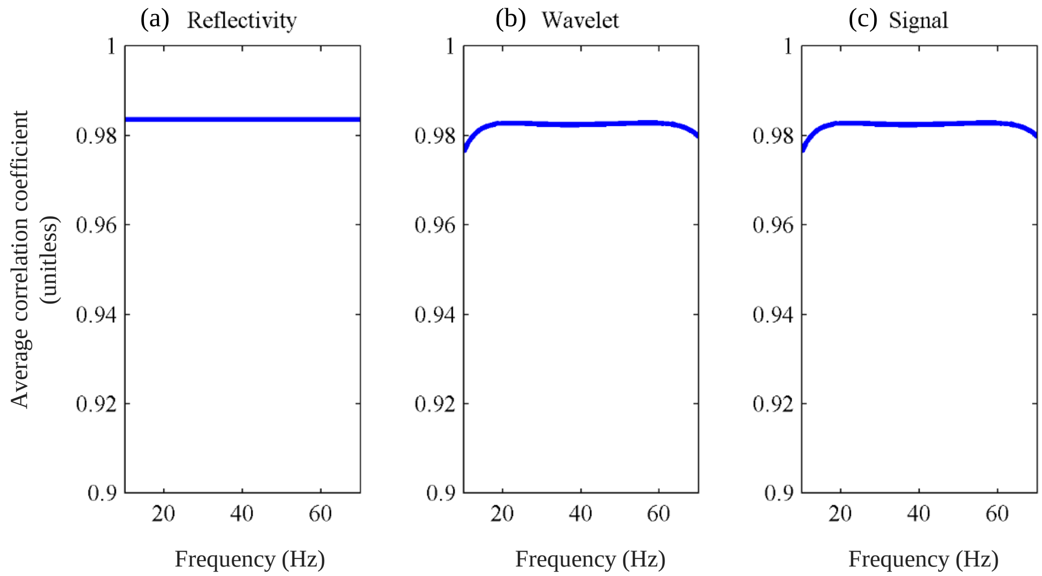

Figure 3.5 Average correlation coefficient between isofrequency-amplitude traces within typical bandwidth (10-70 Hz) of reflectivity for one reflector (a), 30 Hz Ricker wavelet (b) and signal constructed by convolution of the previous two (c).

Figure 3.4 shows the correlation matrix of isofrequency-amplitude traces of the (a) reflectivity, (b) wavelet and (c) signal of the above model with one simple reflector. The upper-right half of the matrices are zeroed out because that would be the identical to the lower-left half. Because isofrequency traces of reflectivity in this model are frequency independent, (a), the correlation matrix of the signal isofrequency traces, (c), show correlation relations mainly controlled by that of the wavelet, (b). One could also calculate a simple average of correlation coefficients for each isofrequency-amplitude trace to all other isofrequency traces over the entire bandwidth (Figure 3.5), which would be equivalent to calculating the average correlation coefficient for each row or column in Figure 3.3(b). The average correlation coefficient plot in Figure 3.5 shows the same trend as in Figure 3.4.

As reflectivity series become more complex, especially when seismically-thin layers are involved, correlation between isofrequency-amplitude traces can be complex as well, especially at frequencies where spectral notches occur. A spectral notch forms when reflections from the top and bottom of a layer most destructively interfere with each other. Partyka et al. (1999) point out that the frequency of a spectral notch is directly determined by the time thickness of the layer. From the derivation of Marfurt and Kirlin (2001), we summarize simply that for a model with one simple layer (reflection on top and bottom having the same magnitude) of time thickness Δt, the most destructive frequency (F_{des}) occurs at:

(1) For same magnitude and opposite sign reflections:

$$F_{des} = \frac{N}{\Delta t}; \qquad \textbf{(3.2)}$$

(2) Or, same magnitude and same sign reflections:

$$F_{des} = \frac{N + 0.5}{\Delta t}; \qquad \textbf{(3.3)}$$

where N = 0, 1, 2, 3... .

Figure 3.6(a) shows an example with one simple layer of 24 ms time thickness which has the same and opposite sign reflection coefficients on top and bottom. The seismic time signal is created by convolving the reflectivity with a 30 Hz Ricker wavelet. The notches in trace amplitude spectrum (Figure 3.6b) of reflectivity are "passed on" to the spectrum of signal, especially within the typical usable bandwidth of the wavelet. They are also reflected in the time-frequency panel, with low amplitudes shown at notch frequencies (Figure 3.6c). This results in poorly correlated spectral waveforms at notch frequencies (Figure 3.6d).

Figure 3.7(a) compares the correlation matrix of isofrequency traces of reflectivity, wavelet and signal. For the wavelet, within usable bandwidth of a 30 Hz Ricker wavelet (10 to 70 Hz), high correlations are found between all isofrequency traces. While for the reflectivity series, clear low correlation occurs around the notch frequency, i.e., 42 Hz, for this 24 ms layer model. If we calculate a simple average of correlation coefficients over all frequencies (Figure 3.7b), isofrequency traces of the signal show low correlation coefficients around notch frequencies almost identical to that of the reflectivity series, which is determined by layer thickness.

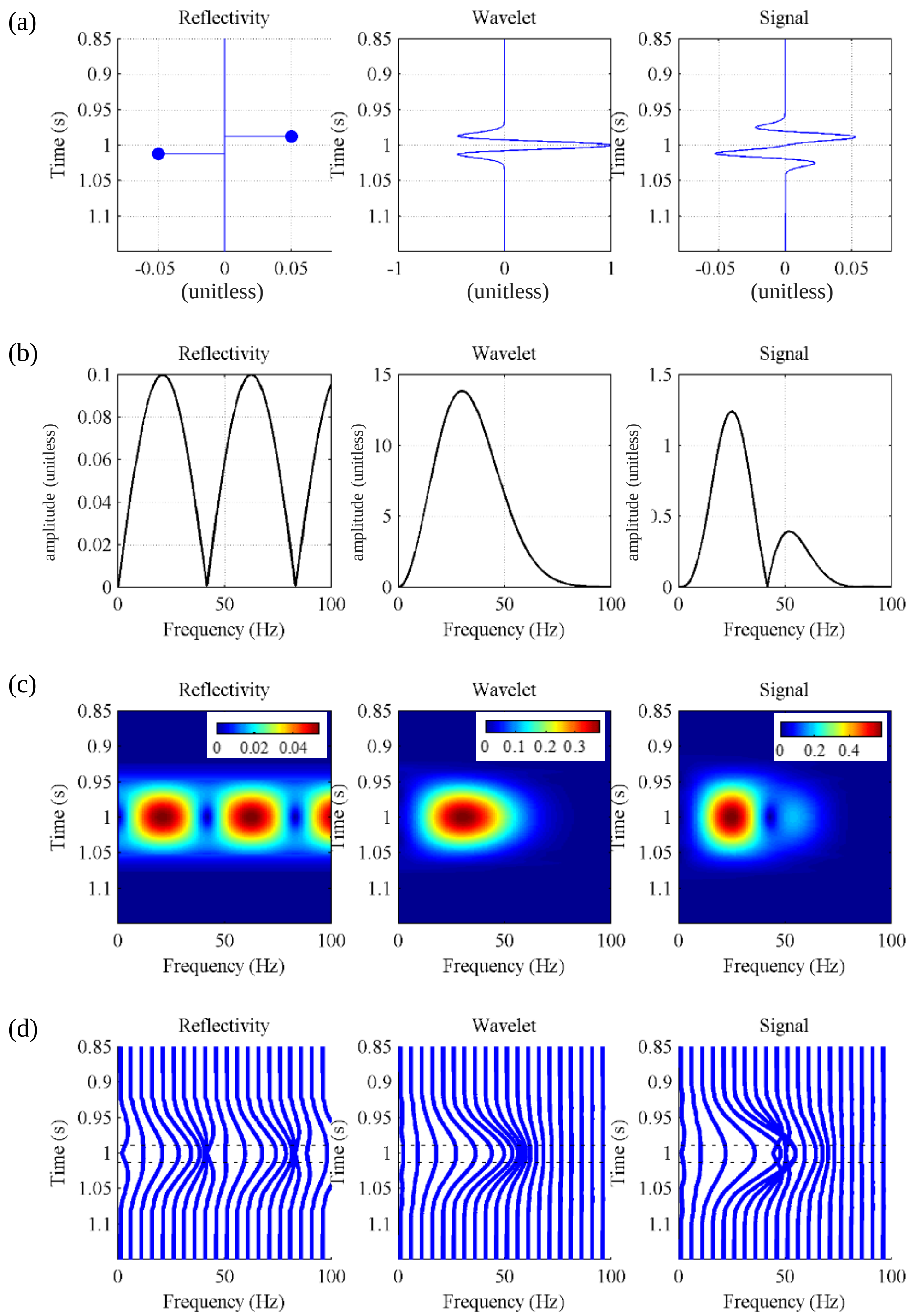

Figure 3.6 Time view (a), amplitude spectrum view (b), spectral intensity view (c), and isofrequency trace view (d) of a 24 ms layer with pure odd reflection pair, a 30 Hz Ricker wavelet, and the convolved signal.

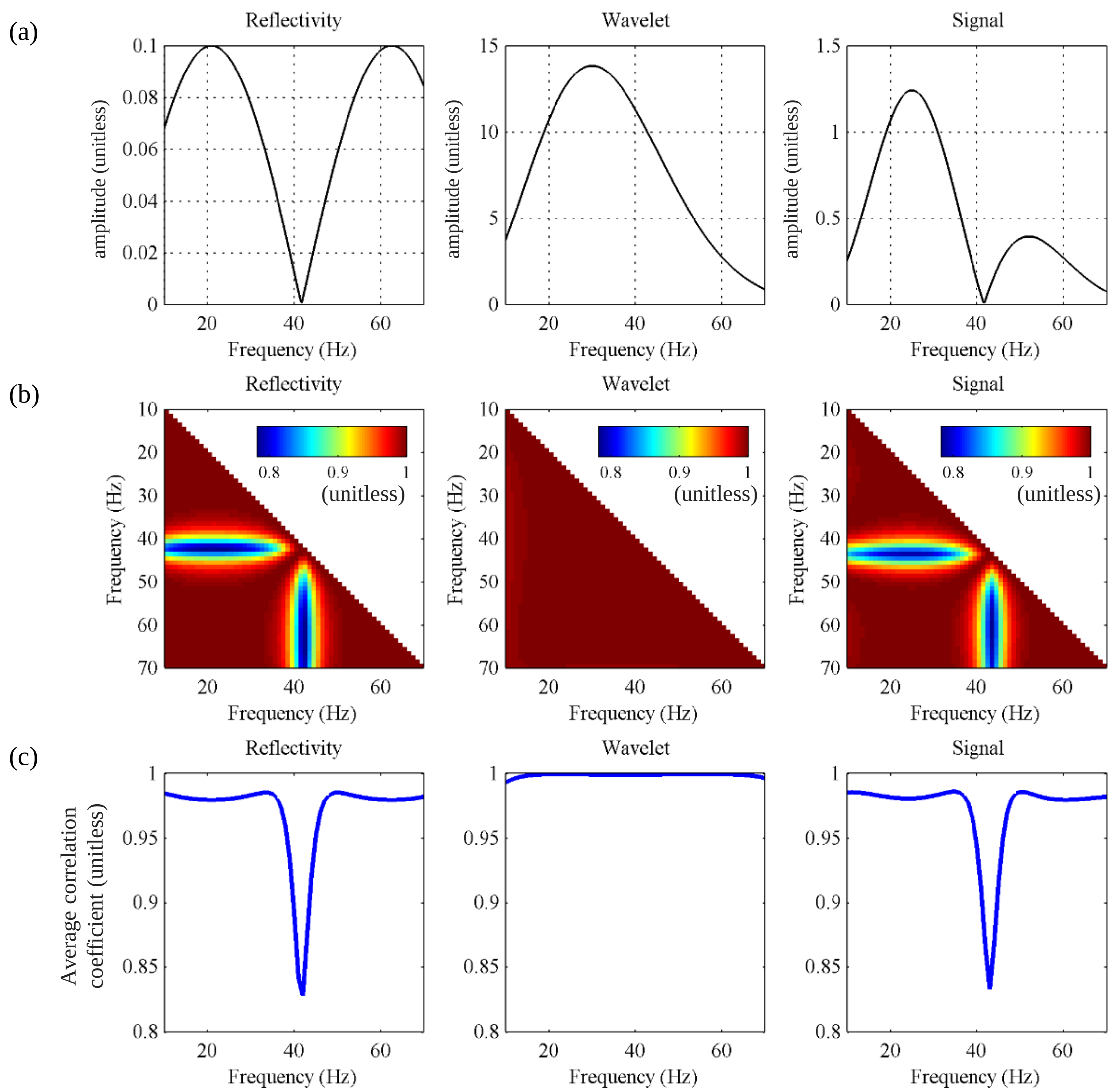

Figure 3.7 Amplitude spectrum (a), Correlation coefficient between isofrequency traces (b), Average correlation coefficient (c) of the one layer reflectivity model, wavelet, and signal within typical usable bandwidth of the wavelet used (10 to 70 Hz).

Using these simple examples, we have seen that understanding of the correlation behavior between isofrequency-amplitude traces provide a simple means to find spectral notches in the seismic signal within the usable bandwidth, given that amplitude spectrum of the wavelet is null-free. Because spectral notch frequency is generally considered directly connected to geology, by simply isolating those poorly correlated isofrequency-amplitude traces that are well correlated to each other, we can develop a spectral amplitude attribute that is narrow band or geologically oriented.

This objective could be reached, as shown in the one-layer model, by calculating the average correlation coefficient over the usable frequency bands (Figure 3.7c). However, in some more complex situations, simple arithmetic averaging couldn't successfully find notch frequencies in the data. Figure 3.8 describes a slightly more complex model consisting of five reflectors with the same and opposite sign reflections. The four layers that compose the model time thicknesses of 28, 24, 24, and 28 ms. From Figure 3.8 we can clearly see that in the frequency domain, frequency notches and the "zone" of low correlation in the correlation matrix (Figure 3.9b) is far too complex to be represented using an arithmetically averaged correlation coefficient curve (Figure 3.9c).

Here, eigen-decomposition will be used as a tool to extract eigen-amplitude attributes that contain most of the information from the correlation matrix. In addition, a hyperspace rotation technique will be applied on the truncated eigenvector matrix to unveil and interpret key independent factors for each extracted eigen-amplitude attribute.

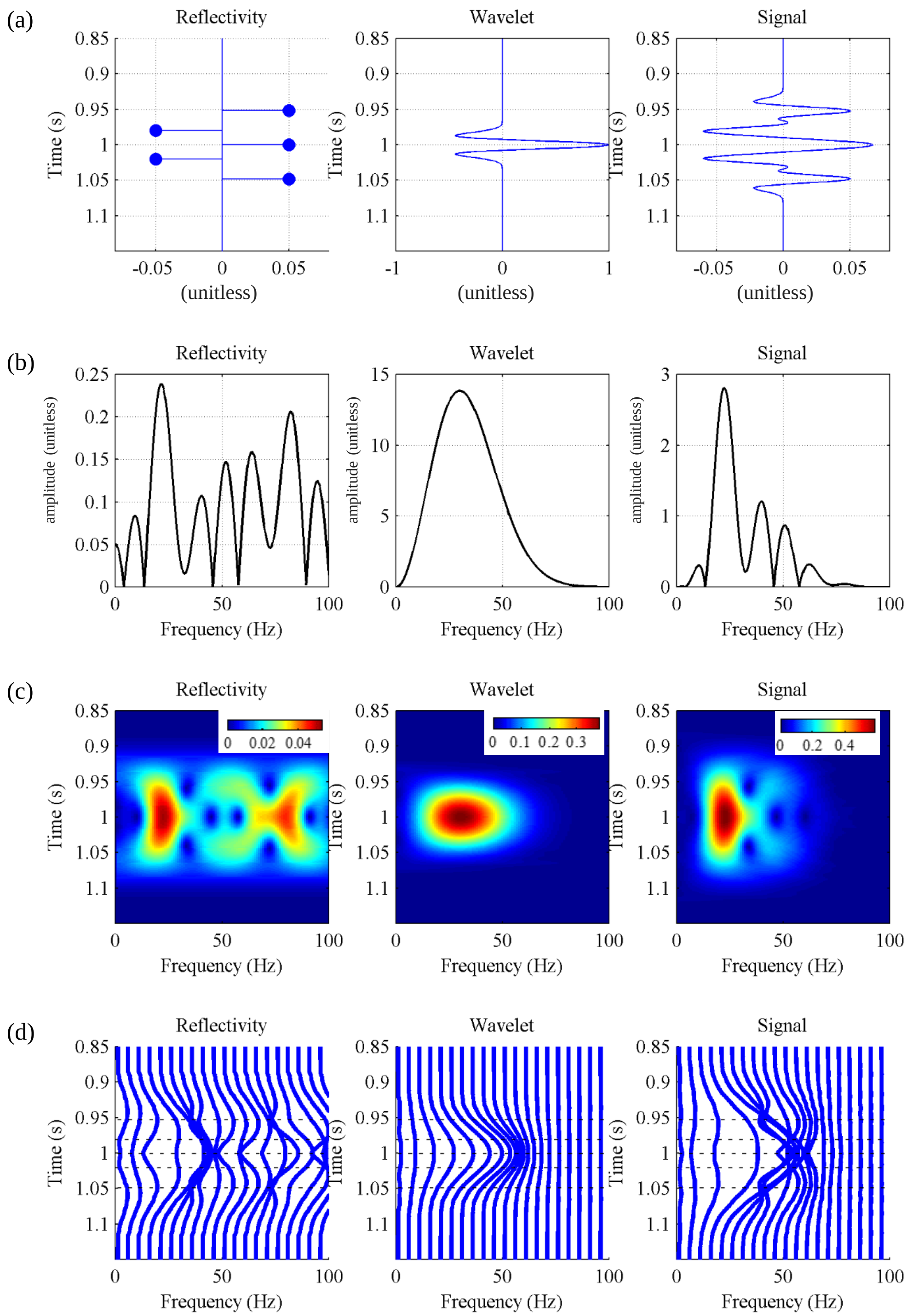

Figure 3.8 Time view (a), amplitude spectrum view (b), spectral intensity view (c), and isofrequency trace view (d) of a complex reflectivity model of four layers with mixed thickness (28, 24, 24, and 28 ms), a 30 Hz Ricker wavelet, and the convolved signal.

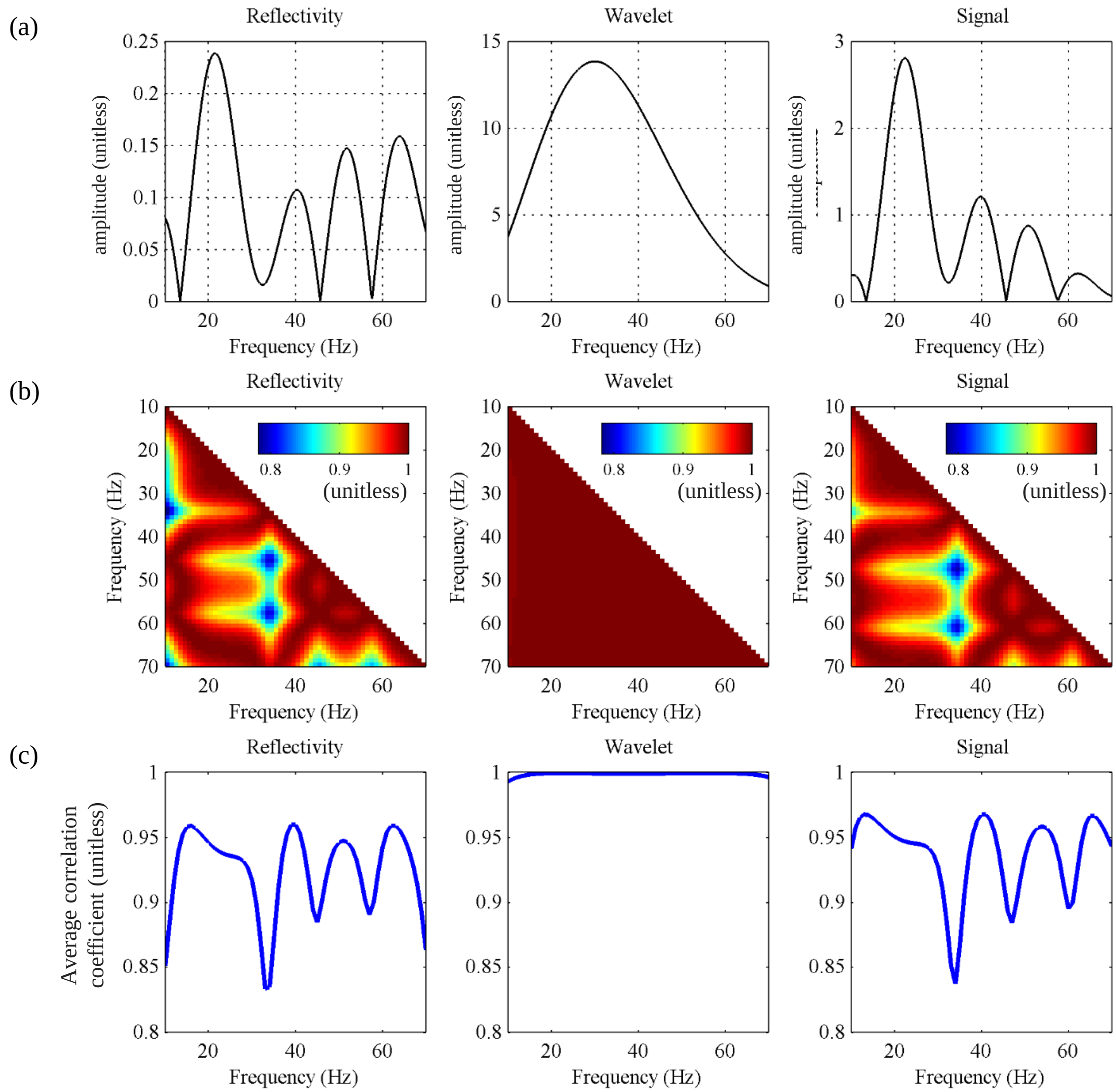

Figure 3.9 Amplitude spectrum (a), Correlation coefficient between isofrequency traces (b), Average correlation coefficient (c) of the complex reflectivity model, wavelet, and signal within typical usable bandwidth of the wavelet used (10 to 70 Hz).

Chapter 4

Spectral Principal Component (PC) Analysis

As discussed in the previous chapter, isofrequency-amplitude traces tend to be strongly correlated between frequencies at spectral nulls; and amongst those that are not at those frequency notches. To take advantage of this clustering behavior, we show in this chapter methods including principal component analysis (PCA), an eigen-decomposition based mathematical tool to try to extract individual events behind isofrequency-amplitude traces; and Varimax rotation method to understand or interpret more easily the extracted spectral-PC attributes in physically meaningful terms, i.e., individual frequencies.

4.1 PC analysis of isofrequency-amplitude traces – dimension reduction

The mathematical basis of PCA is eigen-decomposition of a correlation matrix or covariance matrix for multi-variat data. The correlation coefficient is equivalent to covariance normalized by the mean values of the variables, hence we apply it here for its simplicity. Because the correlation matrix is always diagonalizable, using eigen-decomposition we can write correlation matrix as the sum of its m eigenvalues (λ) multiplied by the corresponding eigenvectors (V_i) and the transpose of each (V_i^T):

$$r = \begin{pmatrix} V_{11} & \cdots & V_{1m} \\ \vdots & \ddots & \vdots \\ V_{m1} & \cdots & V_{mm} \end{pmatrix} \begin{pmatrix} \lambda_1 & \cdots & 0 \\ \vdots & \ddots & \vdots \\ 0 & \cdots & \lambda_m \end{pmatrix} \begin{pmatrix} V_{11} & \cdots & V_{m1} \\ \vdots & \ddots & \vdots \\ V_{1m} & \cdots & V_{mm} \end{pmatrix} \quad , \tag{4.1}$$

or in shorter form

$$r = \sum_{i=1}^{m} \lambda_i * V_i * V_i^T \quad . \tag{4.2}$$

Again, here *r* represent correlation matrix of isofrequency-amplitude traces, same as in chapter 3 (equation 3.1). In this expression, eigenvalues indicate the amount of variance that is represented by each eigenvector. Comparing all *m* eigenvalues, usually only the first few (e.g., 1st, 2nd… *p*st) are large enough to be significant. As a result, we can create a matrix by excluding the non-significant terms, without losing much variance in the original ***r*** matrix. The process can be written as:

$$r' = \begin{pmatrix} V_{11} & \cdots & V_{1p} \\ \vdots & \ddots & \vdots \\ V_{p1} & \cdots & V_{pp} \end{pmatrix} \begin{pmatrix} \lambda_1 & \cdots & 0 \\ \vdots & \ddots & \vdots \\ 0 & \cdots & \lambda_p \end{pmatrix} \begin{pmatrix} V_{11} & \cdots & V_{p1} \\ \vdots & \ddots & \vdots \\ V_{1p} & \cdots & V_{pp} \end{pmatrix} \approx r \ , \tag{4.3}$$

or in shorter form:

$$r \approx \sum_{i=1}^{p} \lambda_i * V_i * V_i^T = r'. \tag{4.4}$$

Furthermore, if we rearrange above equation by incorporate scalar $\boldsymbol{\lambda}$ into the two matrices, we would have:

$$r' = \begin{pmatrix} \sqrt{\lambda_1}V_{11} & \cdots & \sqrt{\lambda_1}V_{1p} \\ \vdots & \ddots & \vdots \\ \sqrt{\lambda_p}V_{p1} & \cdots & \sqrt{\lambda_p}V_{pp} \end{pmatrix} \begin{pmatrix} \sqrt{\lambda_1}V_{11} & \cdots & \sqrt{\lambda_p}V_{p1} \\ \vdots & \ddots & \vdots \\ \sqrt{\lambda_1}V_{1p} & \cdots & \sqrt{\lambda_p}V_{pp} \end{pmatrix} \approx r \ , \tag{4.5}$$

or in shorter form:

$$r' = \left(\sqrt{\lambda_1}\, V_1 \sqrt{\lambda_2}\, V_2 \cdots \sqrt{\lambda_p}\, V_p\right) \begin{pmatrix} \sqrt{\lambda_1}\, V_1^T \\ \sqrt{\lambda_2}\, V_2^T \\ \cdots \\ \sqrt{\lambda_p}\, V_p^T \end{pmatrix} \approx r. \qquad \textbf{(4.6)}$$

Here if we define vectors

$$R'_i = \sqrt{\lambda_i} V_i, \qquad \textbf{(4.7)}$$

where i range from 1 to p, each R'_i vector can be seen as the original eigenvector or PC coefficient normalized by square root of the eigenvalue, i.e., $\sqrt{\lambda_i}$, which equals to its standard deviation. Then the original r matrix can be reconstructed with a significant degree of confidence by multiplication of matrix R' and its transpose. In other words, we can create a correlation matrix r' only using a reduced number of p vectors but still representing most information in the original r matrix:

$$r' = R' * R'^T \approx r. \qquad \textbf{(4.8)}$$

The amount of variance represented by the new matrix (r') with selected $\boldsymbol{p}$ eigenvectors can be estimated using the proportion that sum of selected eigenvalues out of the sum of all eigenvalues, the equation can be:

$$f_{var} = \frac{\sum_{i=1}^{p} \lambda_i}{\sum_{i=1}^{m} \lambda_i} \quad . \qquad \textbf{(4.9)}$$

Here f_{var} represent the fraction of variance. This can be used as a criterion to determine the value of p. Usually the selected p eigenvectors need to collectively represent variance greater than a threshold, e.g., in some cases 85% of total variance. The second criterion is, for an m-variable matrix, eigenvalues that are less than 1 are usually considered insignificant. Sometimes a third criterion is to find p at which point there is a change of slope occurred in an eigenvalue-PC number plot, or scree plot (Figure 4.1). For example, for the two-layer synthetic model we used in the last section, the first two PCs are selected to be significant. The reason is that the two PCs account for more than 90% of the variance, the eigenvalues corresponding to them are all greater than one, and the selection of the first two PCs doesn't violate the scree plot rule.

In addition to the three criteria applied to determine the selection of PCs, one can double check the ability for a limited number of eigenvector to represent most of the variation from the original input data by comparing the original correlation matrix and the reconstructed correlation matrix with selected PCs. Figure 4.2 and 4.4 compare the (a) original correlation matrix to that reconstructed with (b) only the first PC; (c) the first two PCs; and (d) the first three PCs. The residue correlation matrix plots (Figure 4.2 and 4.4, e-g) and the residue histogram plots (Figure 4.3 and 4.5) show that using the first two PCs is good enough to reduce the level of residue to under 0.5% and 2% on the average respectively, which may be judged adequate.

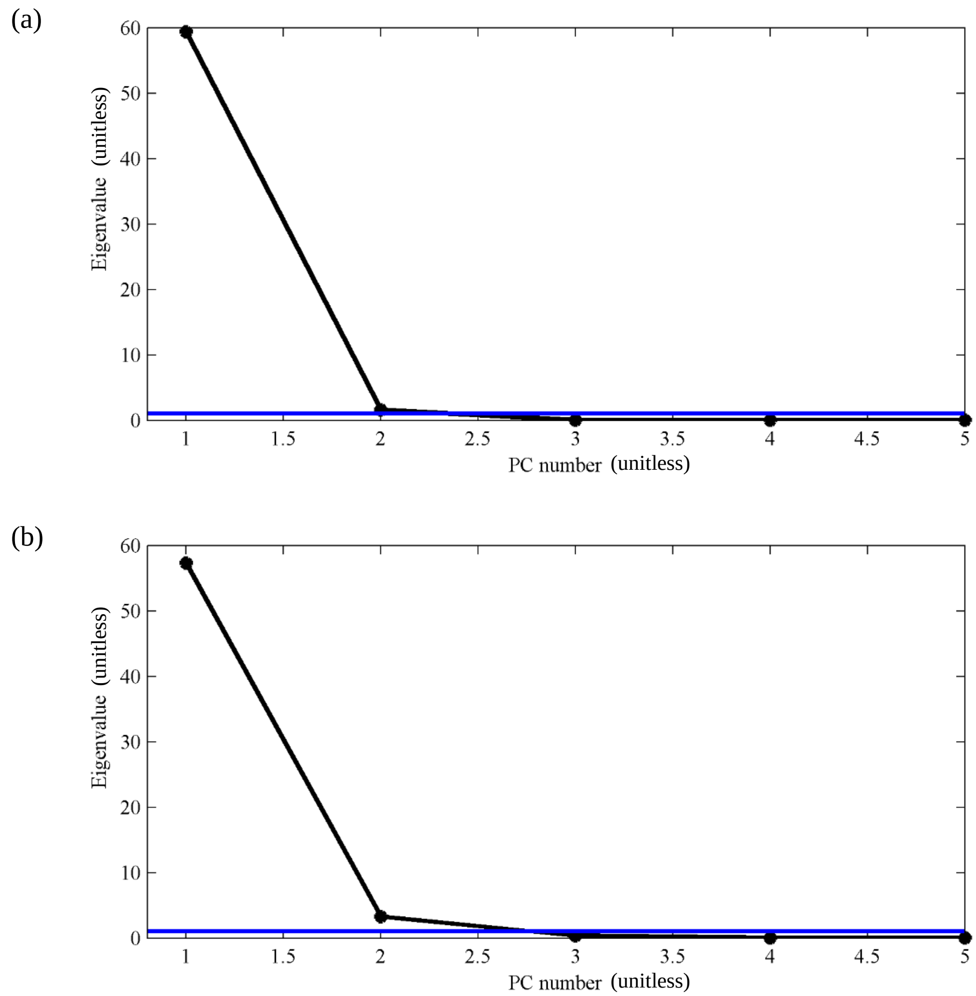

Figure 4.1 Scree plot for (a) the simple 24 ms layer model as seen in Figure 3.5; (b) the complex layer model, as seen in Figure 3.7. The blue horizontal lines indicate eigenvalue equal to one. In both cases, only the first two PCs have eigenvalues greater than zero.

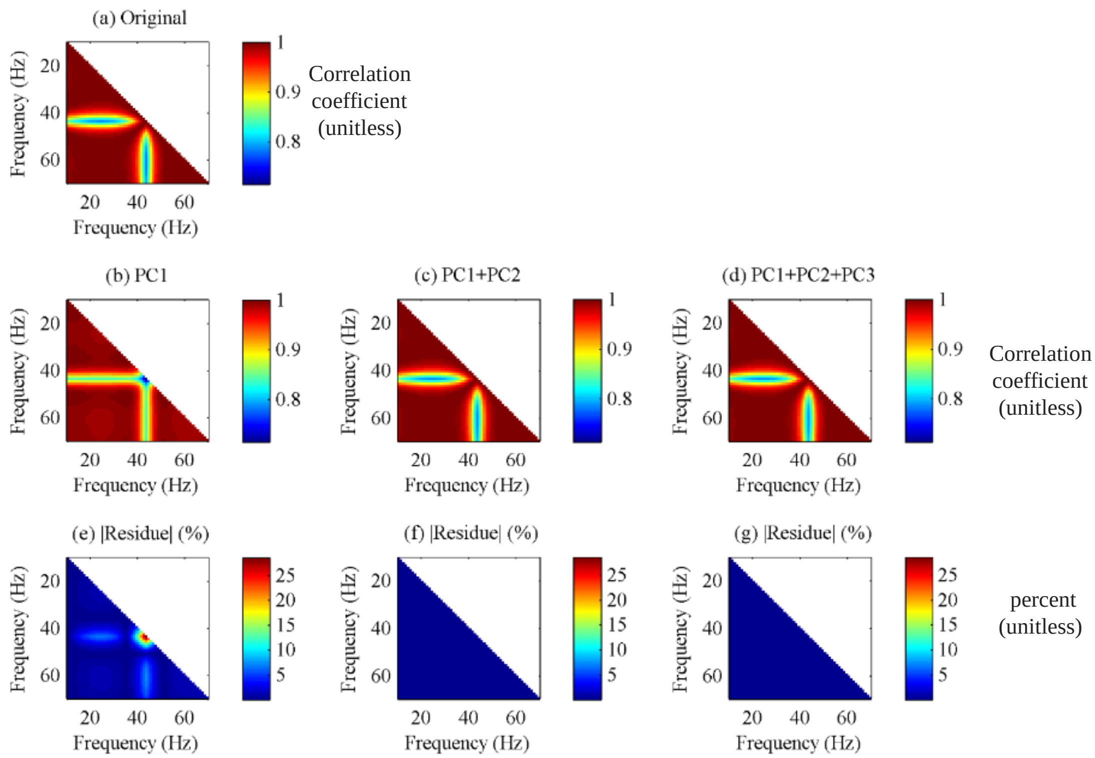

Figure 4.2 Correlation matrix original signal (Figure 3.6) (a); one reconstructed with only PC1 (b); (c) PC1 and PC2; and (d) PC1 through PC3. Residue correlation matrix from the original (e, f, g).

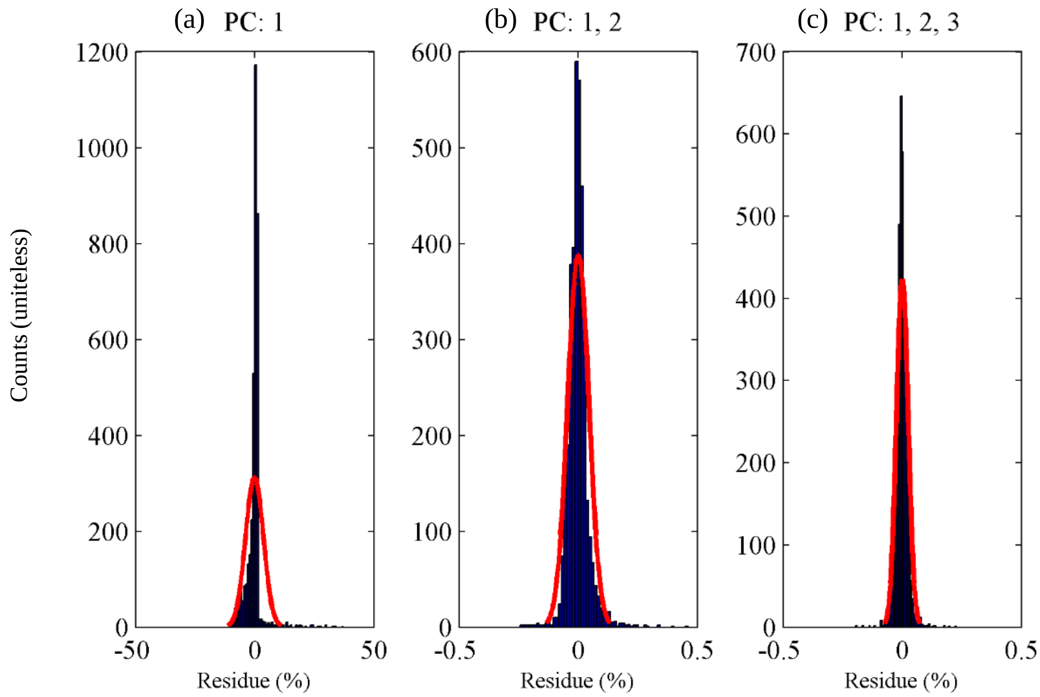

Figure 4.3 Histogram and a Gaussian fit of residue (red lines) after recreating the correlation matrix using only PC1 (a), PC1 and PC2 (b), and summation of PC1, PC2, and PC3 (c) for the simple layer model.

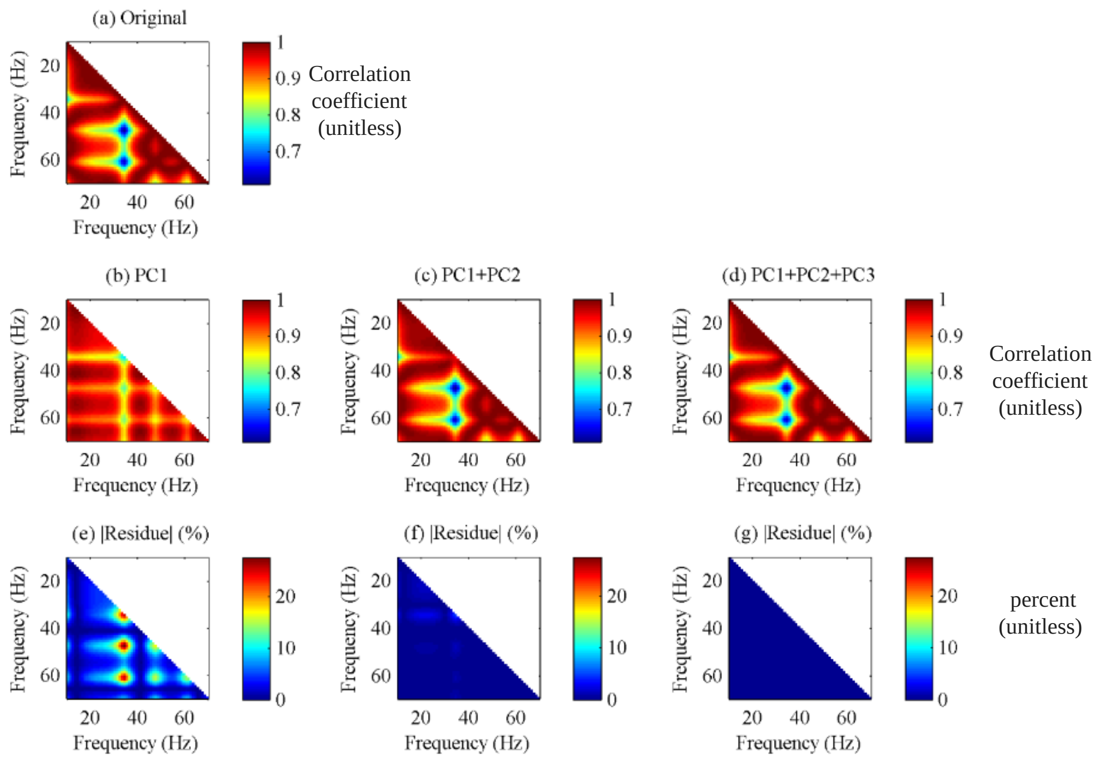

Figure 4.4 Correlation matrix of original signal (Figure 3.8) (a); reconstructed with only PC1 (b); (c) with PC1 and PC2; and (d) with PC1 through PC3. Residue correlation matrix from the original (e, f, g).

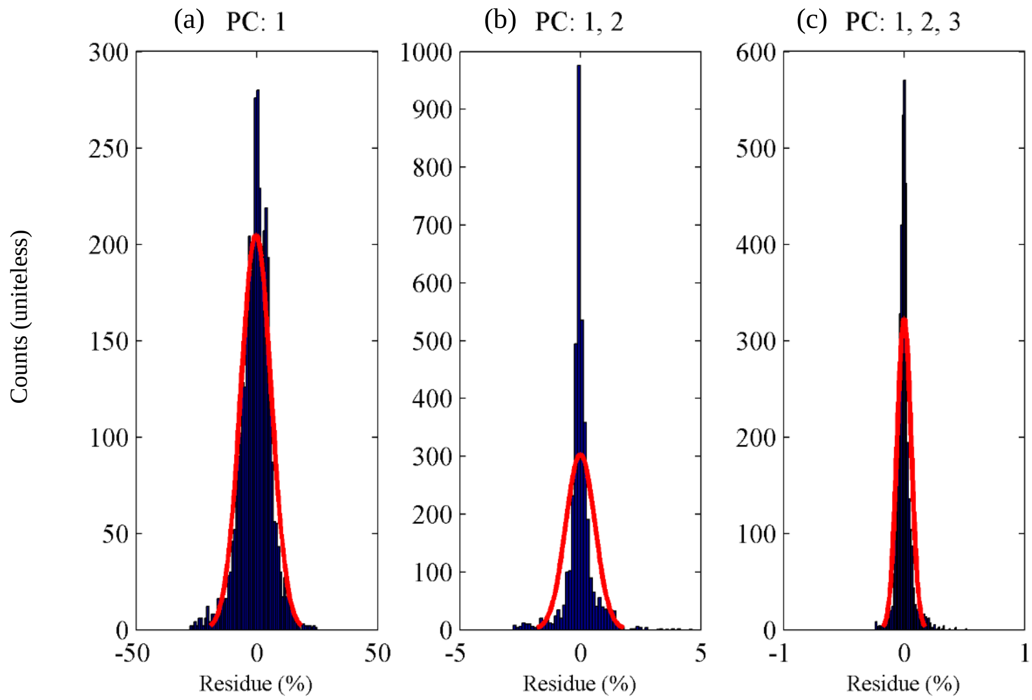

Figure 4.5 Histogram and a Gaussian fit of residue after recreating the correlation matrix using only PC1 (a), PC1 and PC2 (b), and summation of PC1, PC2, and PC3 (c) for the complex layer model.

After determining the number of PCs to keep (value of p), typically the most frequent application of the p number of eigenvectors is to use them as coefficients to project the original data in their most significant directions. Here we define D as a matrix of isofrequency-amplitude for the m frequencies and k samples. With the p number determined, it is common to calculate a PC score for each eigenvector by multiplying the input data D by the p eigenvectors:

$$\begin{pmatrix} PC_{11} & \cdots & PC_{1k} \\ \vdots & \ddots & \vdots \\ PC_{p1} & \cdots & PC_{pk} \end{pmatrix} = \begin{pmatrix} V_{11} & \cdots & V_{1m} \\ \vdots & \ddots & \vdots \\ V_{p1} & \cdots & V_{pm} \end{pmatrix} \begin{pmatrix} D_{11} & \cdots & D_{1k} \\ \vdots & \ddots & \vdots \\ D_{m1} & \cdots & D_{mk} \end{pmatrix} , \qquad \textbf{(4.10)}$$

or in shorter form

$$PC_i = V_i^T * D, \qquad \textbf{(4.11)}$$

where i range from 1 to p.

Before the multiplication procedure, the isofrequency-amplitude matrix D is usually balanced to remove relative amplitude variation inherited from wavelet. For this study we applied the same algorithm as in Liu and Marfurt (2007). After the multiplication procedure, the calculated PC score can be considered a projection of input data D in the new p directions that are orthogonal to each other and show the most variation.

For the two-layer model examples, as seen Figure 4.6 and 4.7), the spectral PC1 and PC2 traces show different amplitude. Compared to the isofrequency-amplitude trace (mid panel), it has been shown that the spectral-PC trace takes advantage of the power of spectral decomposition while containing almost the same information but with less redundancy. Compared to the original seismic trace (left panel), each of the spectral-PC traces deliver a subset of information, which we will later be shown to be physically meaningful.

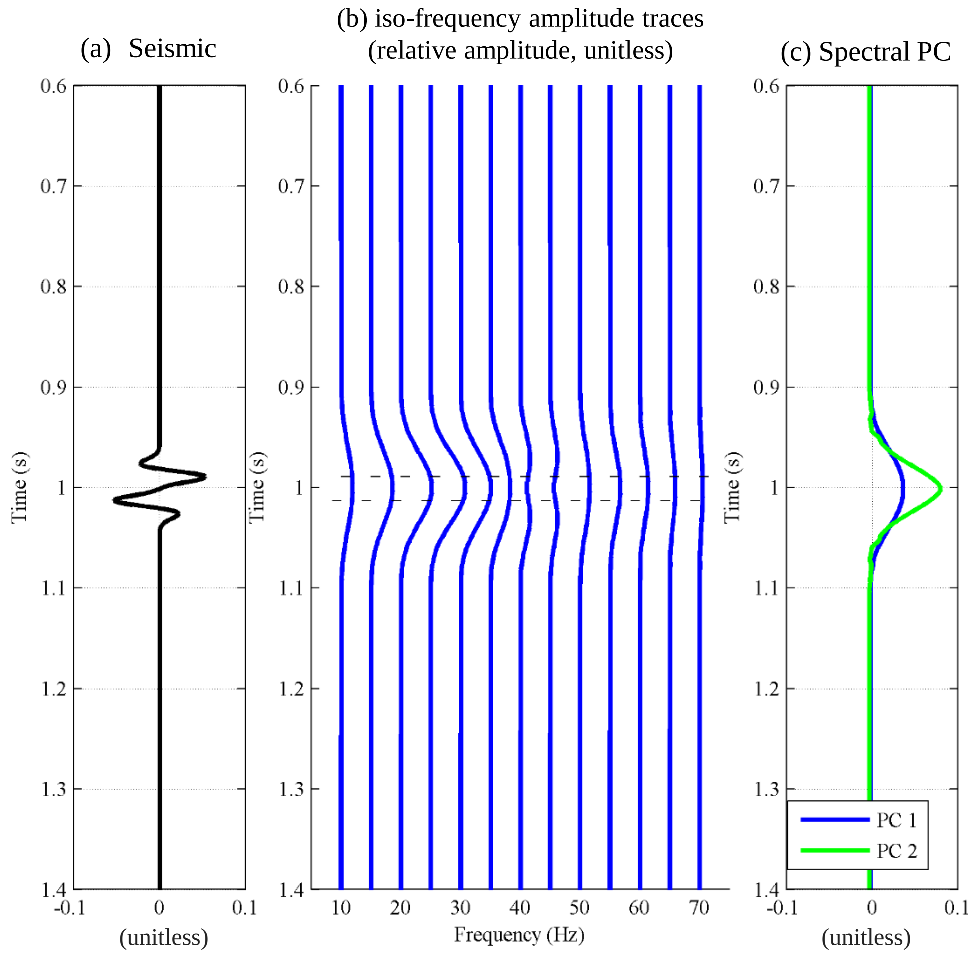

Figure 4.6 Original seismic trace from the simple layer model (a); isofrequency-amplitude traces within the usable bandwidth (10-70 Hz) (b); and trace of the first and second spectral PC (c).

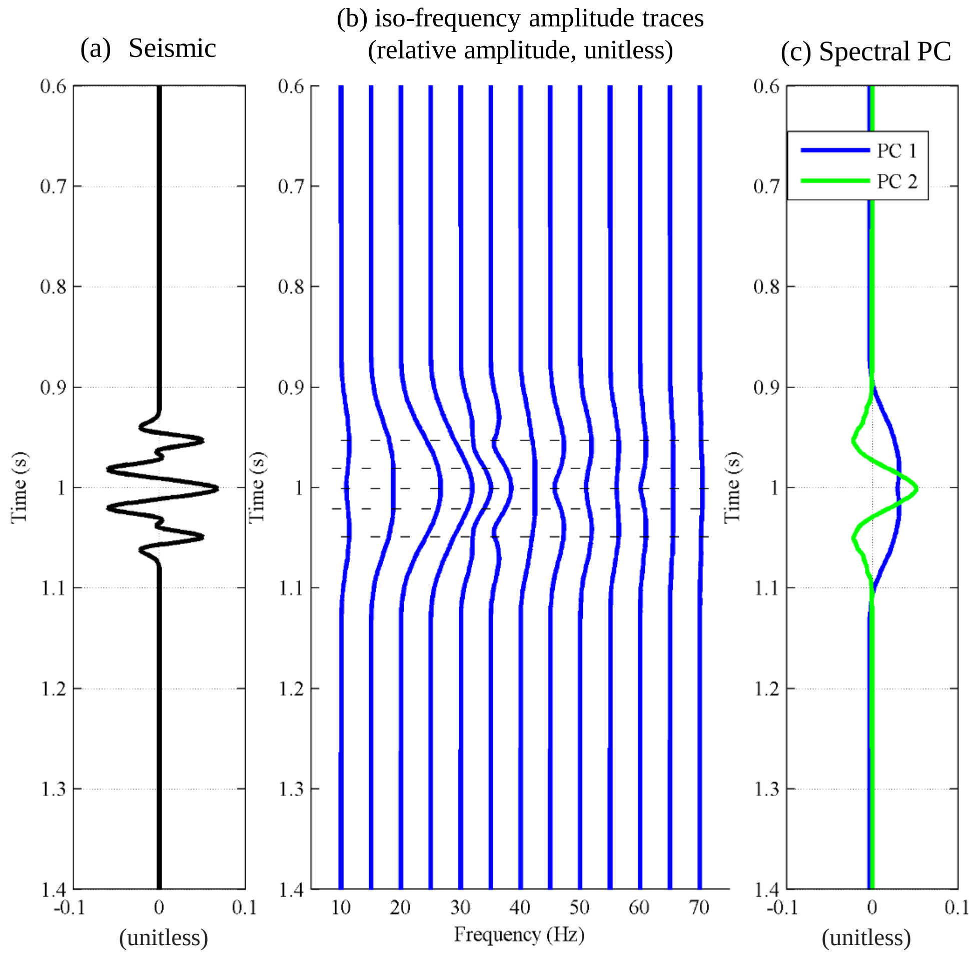

Figure 4.7 Original seismic trace from the complex layer model (a); isofrequency-amplitude traces within the usable bandwidth (10-70 Hz) (b); and trace of the first and second spectral PC (c).

4.2 Independence of PCs

If our only purpose is to remove random noise, the projected PCs as in right panel of Figure 4.6 and 4.7 would usually suffice. However, one important property of the eigen-decomposition is often neglected while doing so. By definition, the eigenvectors are algebraically uncorrelated/independent and geometrically orthogonal to each other. This would suggest a possibly more useful application of the projected PC scores, i.e., each one of the selected significant PCs, defined by the first p eigenvectors, should all represent one physical process that is independent in nature. In the two synthetic models we have been using, if we plot a reconstructed correlation matrix using only PC1, or PC2 and compare them to the original correlation matrix (Figure 4.8-a, and 4.9-a), we would see that the PC1 matrix bares the most resemblance to the original, which is consistent in the notion that PC1 should contain the most information compared to the other PCs. However, in comparison, the PC2 correlation matrices are always different to that of PC1 as also shown in Figure 4.8 (b) and 4.9 (b), which are the simple average of correlation coefficient values of all frequencies over frequency. In addition, for the complex model, the PC2 matrix even shows negative correlation between a low frequency band (15-40 Hz) to a high frequency band (40-65 Hz), suggesting complex relationships beyond what could be interpreted using a simple average. This would suggest the necessity of using a higher dimensional matrix manipulating method.

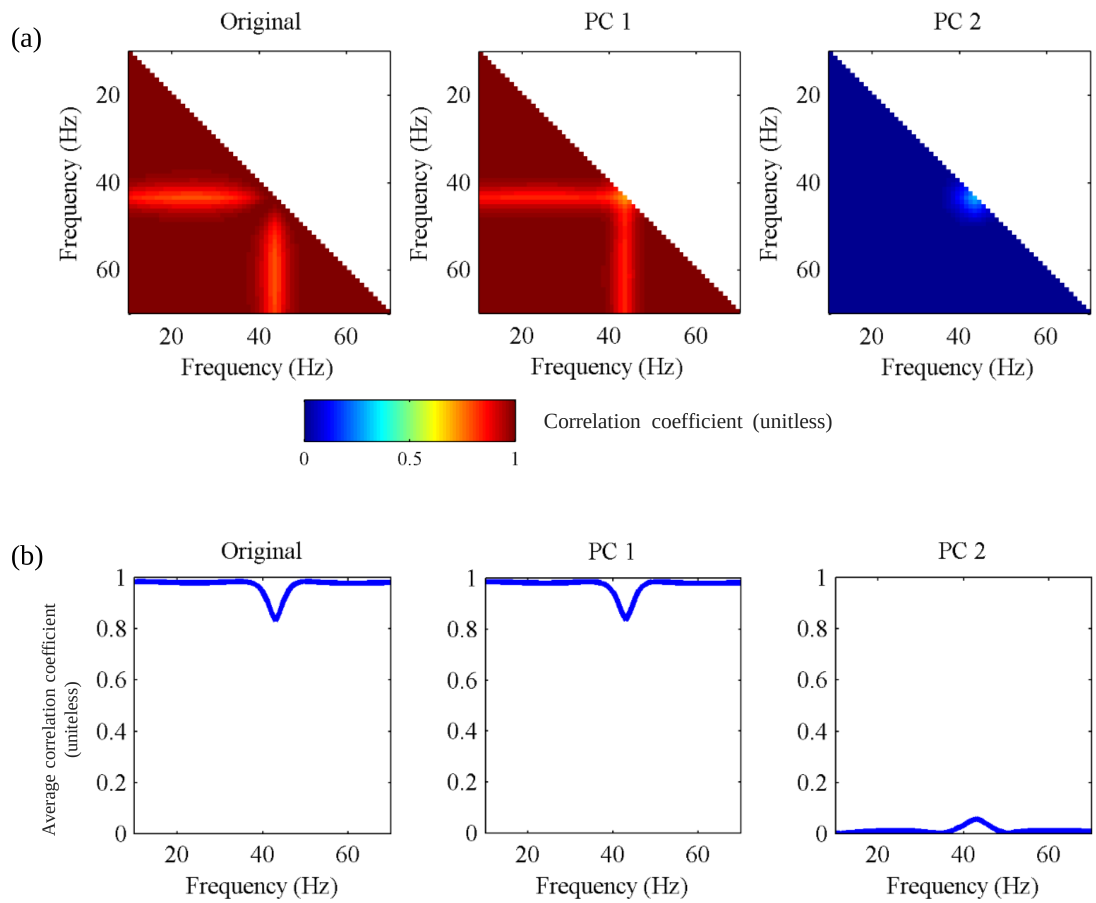

Figure 4.8 (a) Correlation matrix of original signal (Figure 4.2a); one reconstructed with only the first PC; and only the second PC. (b) Average correlation coefficient for the original signal; that reconstructed with only PC1; and that with only PC2.

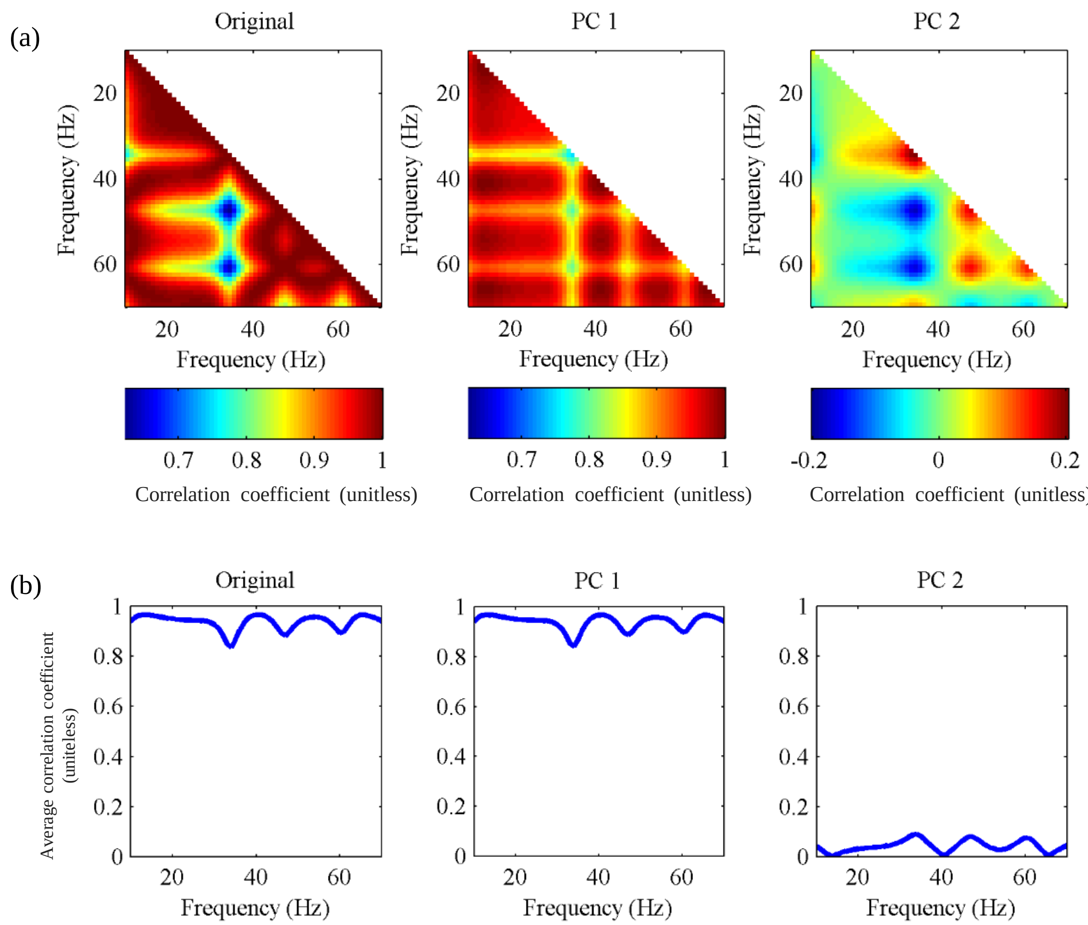

Figure 4.9 (a) Correlation matrix of original signal (Figure 4.4a); one reconstructed with only the first PC; and only the second PC. (b) Average correlation coefficient for the original signal; that reconstructed with only PC1; and that with only PC2.

4.3 Interpreting PCs – Rotation of PC coefficients

In previous derivations, the process of creating matrix r' (equation 4.8) can be seen as a simple model where the R' matrix is multiplied with its transpose. However, the making of this model is not unique. We should be able to find a number of p-by-p matrices X, where

$$X * X^T = I, \tag{4.12}$$

so that

$$r'_v = (R'X) * \left(X^T R'^T\right) = r' \tag{4.13}$$

is equivalent to the model r'. This is effectively a rotation of the r' matrix. In fact, there are an infinite number of orthogonal matrices X *that are possible*, each corresponding to a particular rotation to R'. We can take advantage of this property to find one particular angle of rotation so that the PCs defined previously by eigenvectors (equation 4.11) can be most easily interpreted.

Varimax rotation is one of the most common method for orthogonal matrix rotation. For data created from covariance matrix, Varimax rotation starts with scaling the R' coefficients. However, since our data model is created using correlation matrix, which is a normalized covariance matrix, the scaling can be skipped. A general expression of the Varimax criterion (Kaiser, 1958) is given as:

$$R'_v = argmax\left(\sum_{j=1}^{m}\sum_{i=1}^{p}(\Lambda R')_{ij}^4 - \frac{1}{p}\sum_{j=1}^{m}\left(\sum_{i=1}^{p}(\Lambda R')_{ij}^2\right)^2\right) \, , \qquad \textbf{(4.14)}$$

Where *argmax* means "arguments of the maxima". Symbol Λ indicates variance. There are multiple methods capable of solving for R'_v. One of the algorithms is by bivariate rotation, which is described in detail in Appendix C. The objective is to rotate the input p-by-p R' matrix so that the Varimax criterion is met in all p dimensions (columns) in R'. Data points would have the maximum variation along the new axes, or scattering as close to the axes as possible in the p dimension hyperspace. A schematic is shown in Figure 4.10 to show both (a) finding the eigenvector from a dataset by eigen-decomposition; and (b) rotate the selected p coordinates to obtain the maximum variation.

One of the important things about selecting a method of rotation is that the effect of rotating the coordinate should not change the information represented by the R' matrix that can be reconstructed using the new coefficients. The Varimax criterion is selected as a method of rotation, because it preserves the orthogonality in the R' matrix. We can examine whether this is the case using the two models we have seen earlier. In Figure 4.11 and 4.12, we compare the original correlation matrix of model (a), reconstructed correlation matrix using the p selected PCs (b), to the reconstructed correlation matrix with rotated p PCs (c). From the residue plots (d and e), the rotated and unrotated PCs have no difference in terms of information contained.

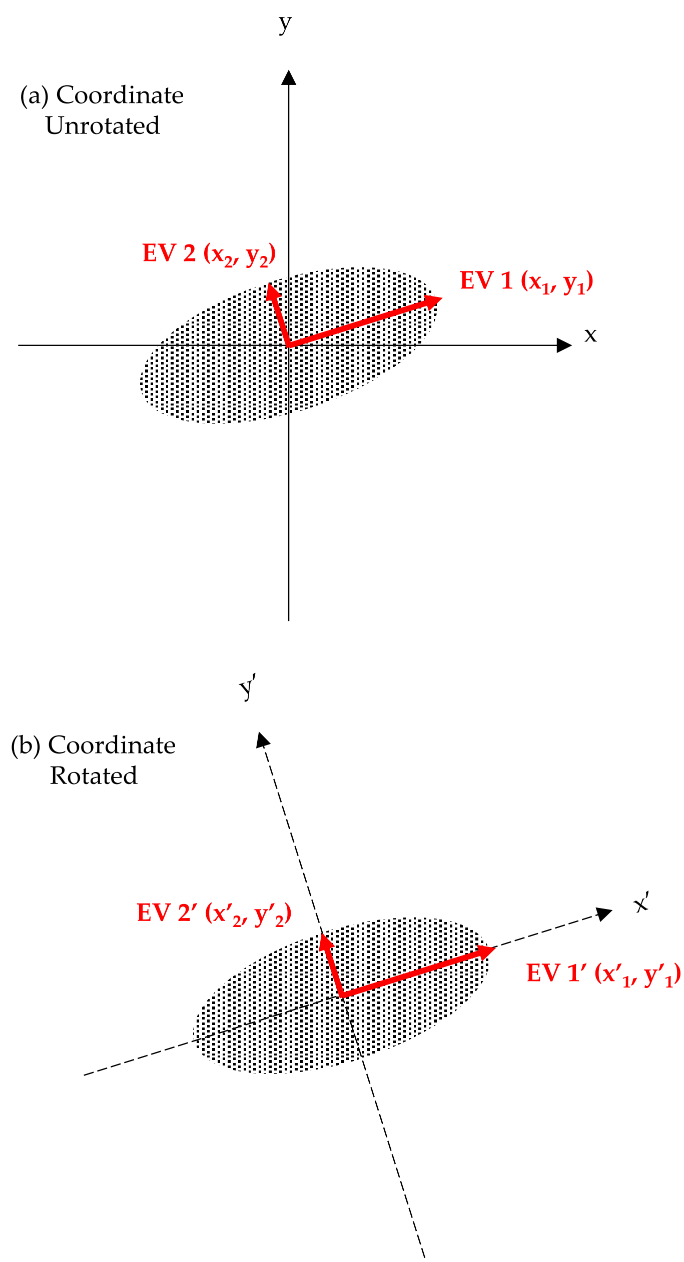

Figure 4.10 (a) Schematic showing finding the eigenvalue and eigenvector of PC1 and PC2 of the dataset (red arrows). (b) Varimax rotation of the original axes x and y maximize variation of PC1 and PC2 coordinates.

What we also hope is that after the rotation, the R' matrix can be interpreted with ease. The success of the rotation can be judged that R' values are driven towards either zero or their maximum possible absolute value (scaled to unity). This helps differentiate more easily, in rotated coordinates, variables with large absolute R' values, which are considered significant, and variables with near-zero R' values, which are not significant. From the same two synthetic models, the Varimax rotated PC coefficient ($R'v$) plot (Figure 4.13 and 4.14, d) has coefficients are more distinct compared to the original coefficients (Figure 4.13 and 4.14, c), making any coefficient-based automated interpretation much easier.

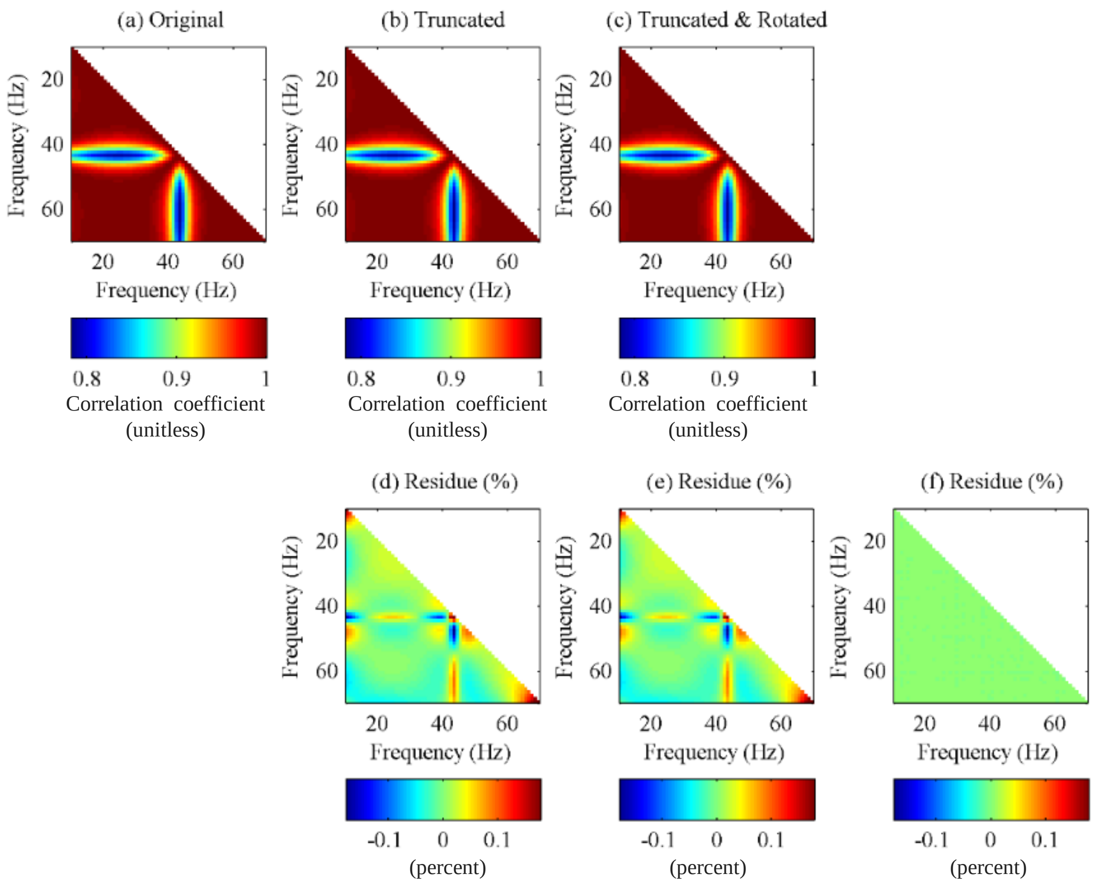

Figure 4.11 (a) Correlation matrix of the original simple layer model (Figure 4.2a); (b) that reconstructed with PC1 and PC2 in original coordinates; (c) that reconstructed with PC1 and PC2 in rotated coordinates after the Varimax criteria. Residue in percentage between (a) and (b), (a) and (c), and (d) and (e) is shown in (d), (e) and (f), respectively.

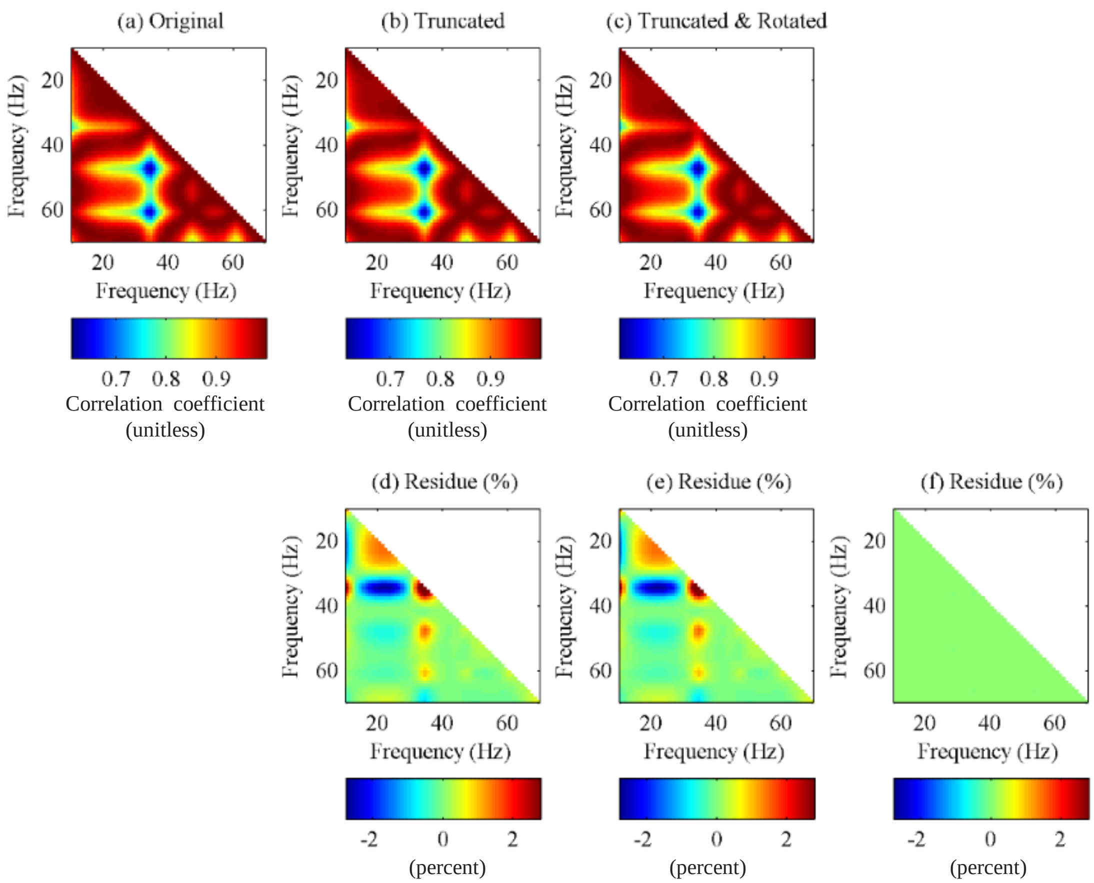

Figure 4.12 (a) Correlation matrix of the original complex layer model (same as in Figure 4.4a); (b) that reconstructed with PC1 and PC2 in original coordinates; (c) that reconstructed with PC1 and PC2 in rotated coordinates after the Varimax criteria. Residue in percentage between (a) and (b), (a) and (c), and (d) and (e) is shown in (d), (e) and (f), respectively.

Note that generally (for any type of data), what is unveiled from rotated R' is just a pattern that exists in the data. No causal inferences should be made directly from this interpretation unless the type of measurements in the original input data (variables in the linear combination, or eigenvectors) maintains a physical meaning. Luckily there *is* a physical basis for the variables we are dealing with – amplitude of the isofrequency trace, or in other words, correlation coefficient of original seismic trace to pure cosine waves of various frequencies. As we do see in multiple examples using isofrequency-amplitude data (Figure 4.13 and 4.14, d), in the rotated R' matrix, coefficients of some frequencies have more similar values compared to other frequencies. This is similar to, or in fact, the direct result of, the clustering behavior as we have seen in the correlation matrix presented earlier (Figure 4.11 and 4.12).

For the two synthetic model cases, using the Varimax rotated PC coefficients, we could see more clearly that each PC can be related to a few significant frequencies. The results show that PC1 has a preference for representing amplitude information of frequencies that is are affected by the tuning effect, while PC2 tends to reflect amplitude information that is affected by tuning (Figure 4.13 and 4.14, d).

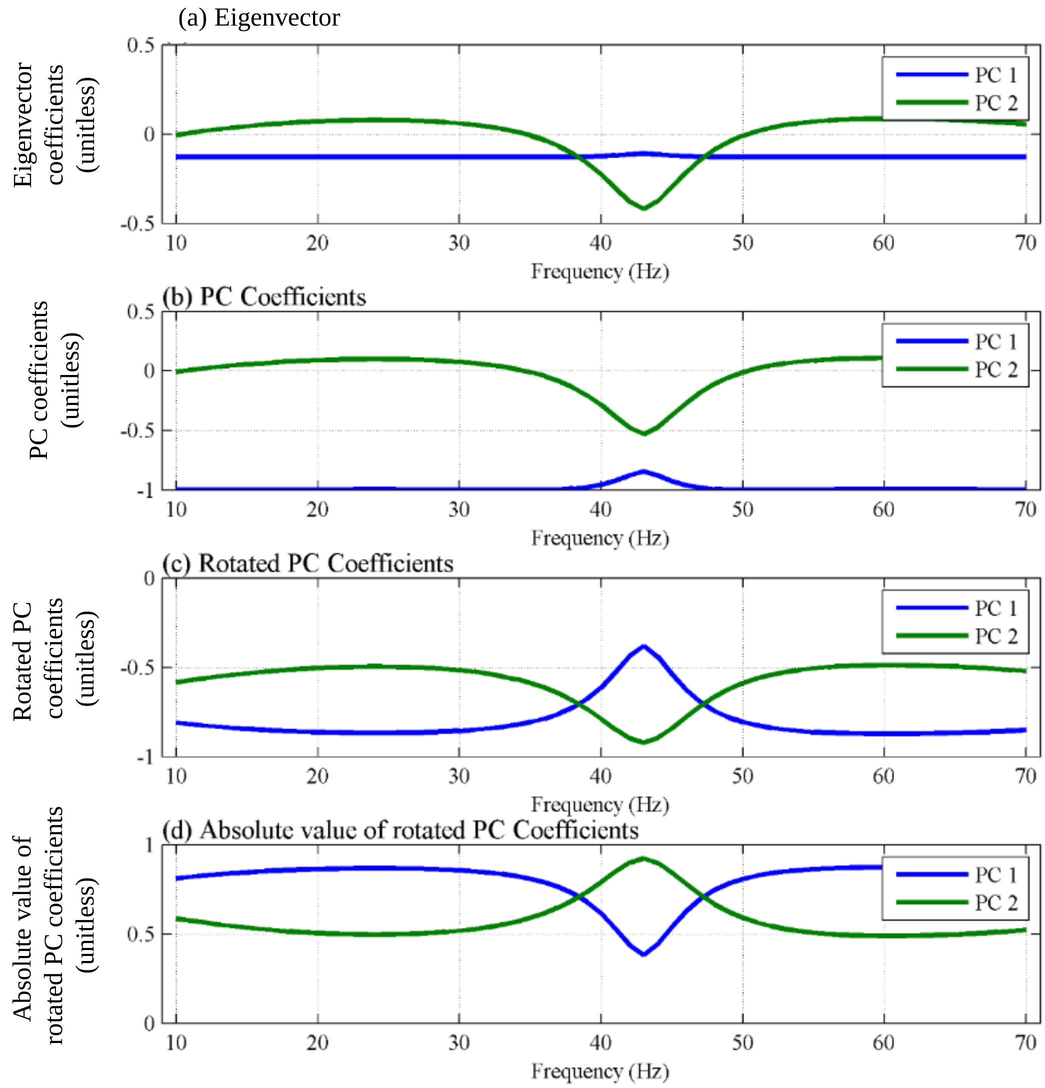

Figure 4.13 (a) Eigenvector coefficients, (b) PC coefficients (R), (c) rotated-PC coefficients (R'), (d) absolute value of rotated-PC coefficients of PC1 and PC2 for the simple layer model.

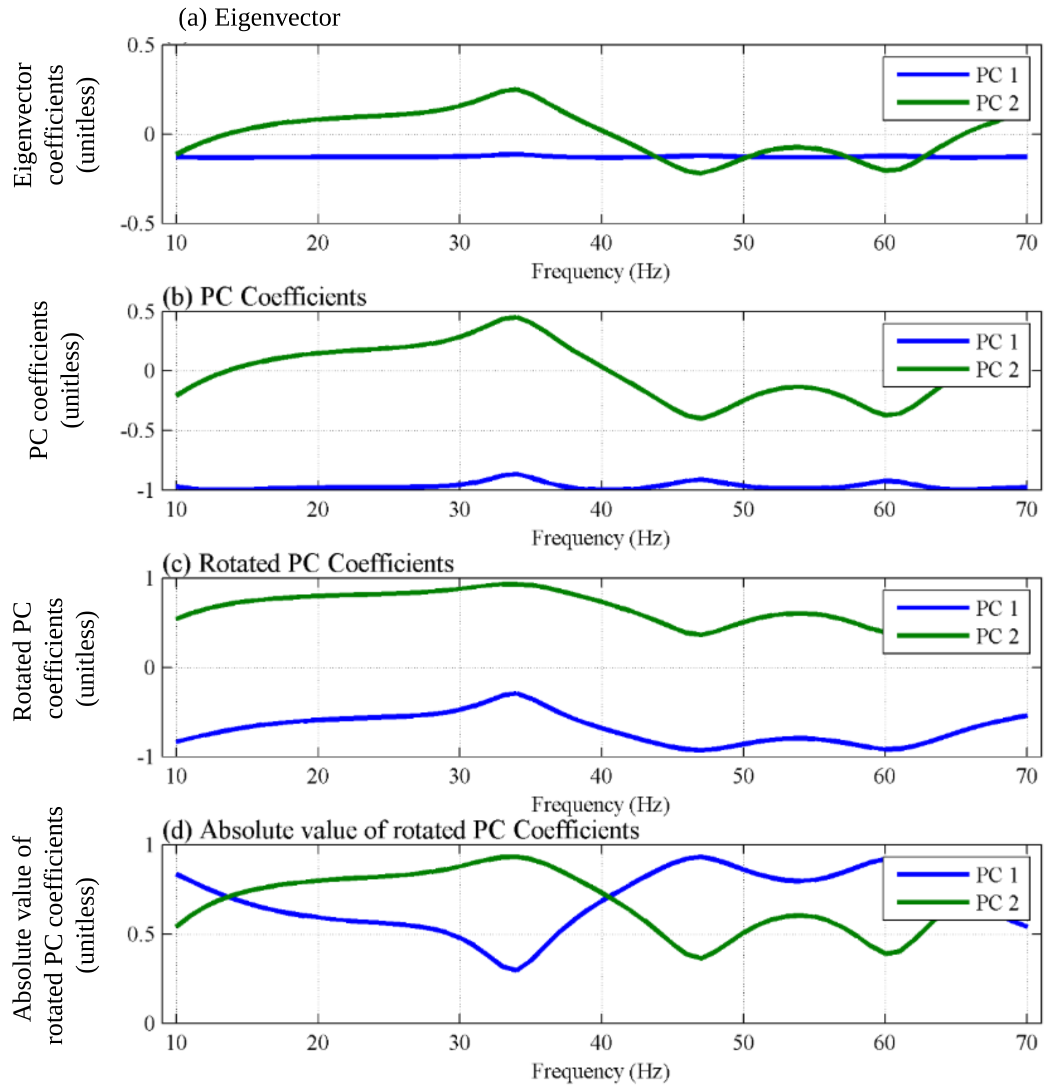

Figure 4.14 (a) Eigenvector coefficients, (b) PC coefficients (R), (c) rotated PC coefficients (R'), (d) absolute value of rotated PC coefficients of PC1 and PC2 for the complex layer model.

In summary, the rotated R' matrix shows that each eigenvector collectively responds to a few frequencies, with the next eigenvector capturing a different cluster of frequencies. The process of projecting input spectral amplitude data to a few selected (p) eigenvector or principal components that are orthogonal to each other is equivalent to band-passing the original time-domain seismic trace using a designed Fourier filter. The difference is that for a conventional band-pass filtering in the Fourier domain, parameters of a designed filter are determined arbitrarily or by experience. In contrast, in spectral-PC projection, it is the data itself that decide the coefficients for multiplication (i.e., eigenvector, equation 4.11), or the angle of projection, based on the inter-correlation relationship. Even though the reason for the decision of angle is not apparent in the original coefficients or eigenvector (*V*), yet by rotating the normalized truncated eigenvector (*R'v* matrix) the significant frequencies behind each projection direction (PC) is highlighted (Figure 4.13 and 4.14, d).

The value of this is that one can now interpret, with a certain confidence that each one of the spectral-PC-amplitude traces (Figure 4.6 and 4.7, c) result from a unique geophysical process. A flowchart is given in Figure 4.15 to show how this workflow can be applied to 3D seismic data. In the next chapter, synthetic and real data examples will test how amplitude of spectral-PC traces can be related to the thickness of layers.

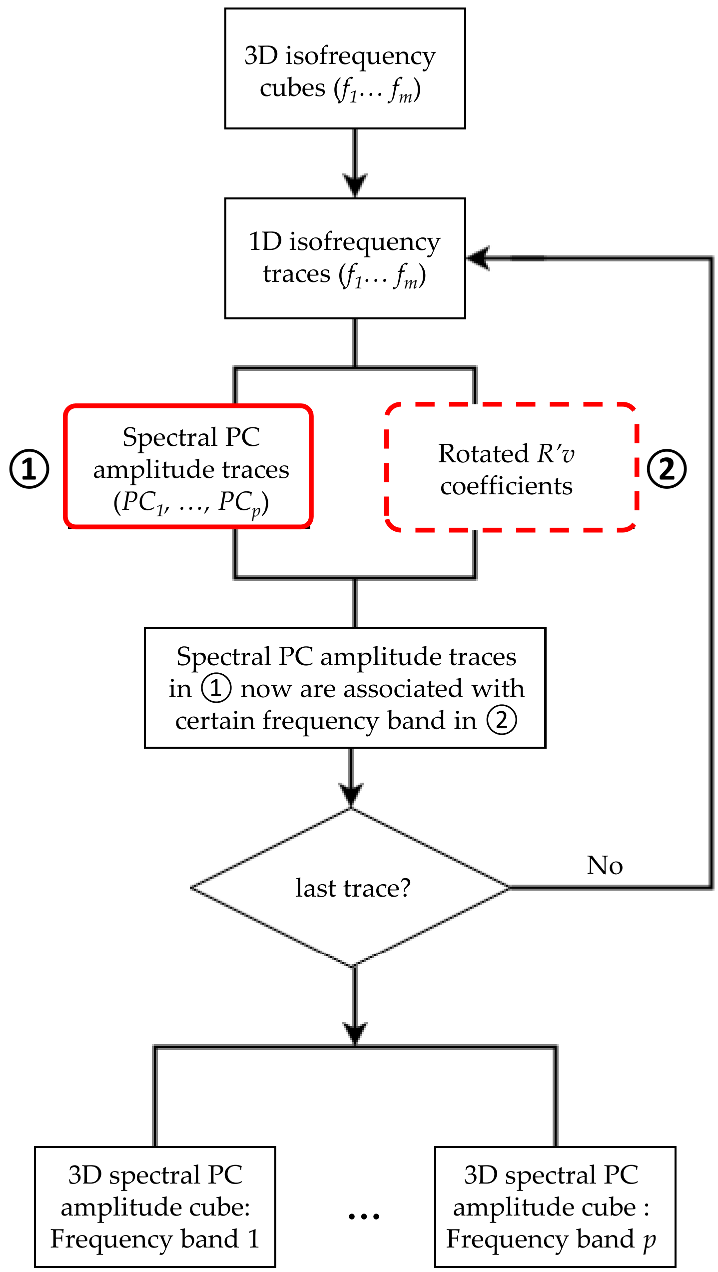

Figure 4.15 Flow chart to calculate spectral-PC amplitude for 3D seismic data from frequency cubes.

Chapter 5

Application of the Spectral-PC-amplitude attribute

In the previous chapter, steps to calculate spectral principal component (PC) amplitude traces from isofrequency-amplitude traces were described. We showed that using the Varimax rotation method, individual spectral-PC amplitude can be indicative of tuning or non-tuning. In this chapter we test this workflow using synthetic layer and wedge models, synthetic 3D model data of a turbidite channel system, and real 3D data that includes thickness variations associated with karst features in north Texas, USA and a producing field in the deep-water Gulf of Mexico.

5.1 Synthetic layer/wedge model

From equation 4.11, spectral-PC amplitude is determined from isofrequency-amplitude traces and the resulting eigenvectors selected. The amplitude of each time sample for a specific PC (PCi) is calculated by multiplying the (scaled and balanced) amplitude spectrum at that time by a vector of coefficients, which points to a direction of maximum variation in a hyperspace, i.e., an eigenvector. For any simple layer, amplitude of the spectral-PC trace is affected by the properties of the layer, e.g., reflection coefficient and layer thickness. In order to examine these influences on amplitude of the PC trace, a few simple layer or wedge models are tested accordingly using the same algorithm exemplified using the single trace case.

5.1.1 Constant-thickness odd pair, varying reflection coefficient

The first example is for a layer composed of two parallel reflectors with the same and opposite sign reflections on top and bottom of the layer. The reflection coefficient varies from 0.05 to 0.3, with layer thickness unchanged as 24 ms (Figure 5.1a). Processing the data (Figure 5.1b) using the same procedure outlined in the previous chapter (Figure 4.16) on a trace-by-trace basis, the resulting spectral-PC-amplitude trace (plotted as a waveform) and the amplitude in the center of layer (usually the same as the peak) is shown in Figure 5.2. The results indicate that for a layer of fixed thickness, both PC1 and PC2 amplitude is linearly proportional to reflection coefficient in the model. This can be seen as if the traces are scaled differently for various reflection coefficients. The reason for that is, as reflection coefficient (RC) increase, the amplitude spectrum of the reflectivity would increase, and the data amplitude spectrum would increase accordingly (Figure 5.3). As a result, the PC spectral waveforms have a peak amplitude that increases as a function of RC. However, if before the spectral decomposition algorithm, a scaling procedure is included that normalizes the input seismic trace by its peak amplitude, then the spectral decomposition result would be unaffected by RC, given that the wavelet stays unchanged and the noise level is low enough. As a result, if we re-do the same workflow on the same data with one extra scaling step, we would see that both PC 1 and 2 amplitude are now independent of RC magnitude (Figure 5.4).

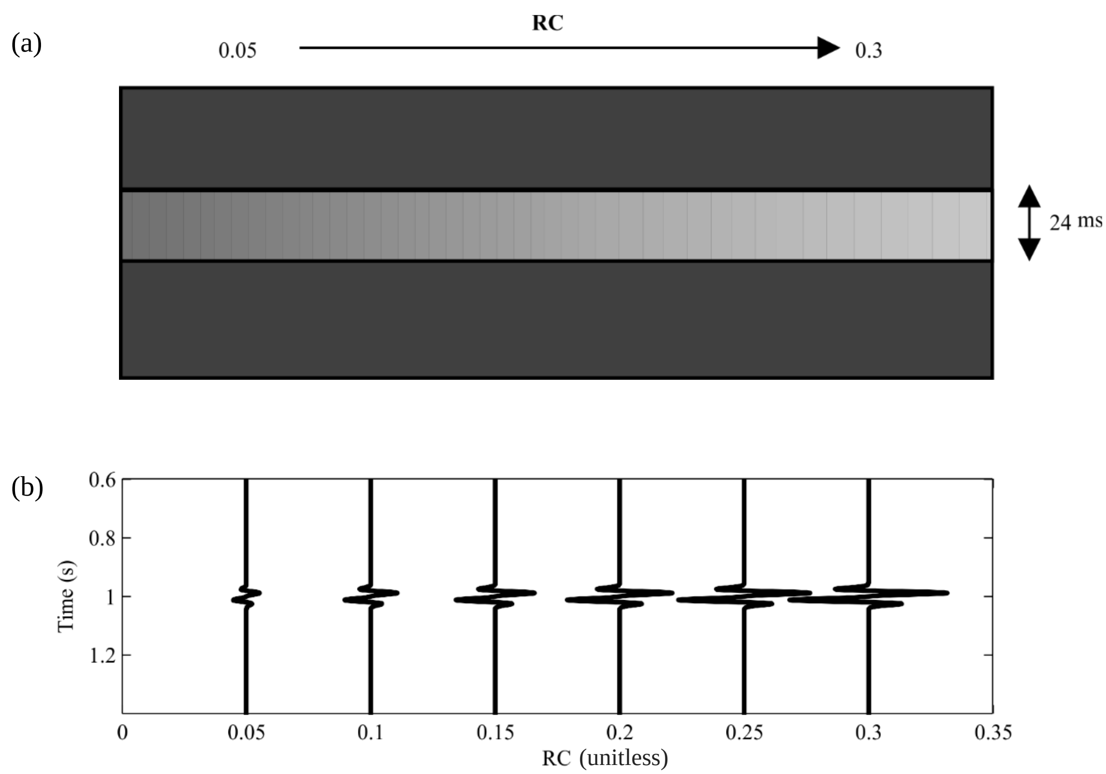

Figure 5.1 (a) Synthetic model containing one 24 ms-thick-low-impedance layer with same magnitude and opposite-sign reflection on top and base of layer. (b) Seismic traces generated from the model.

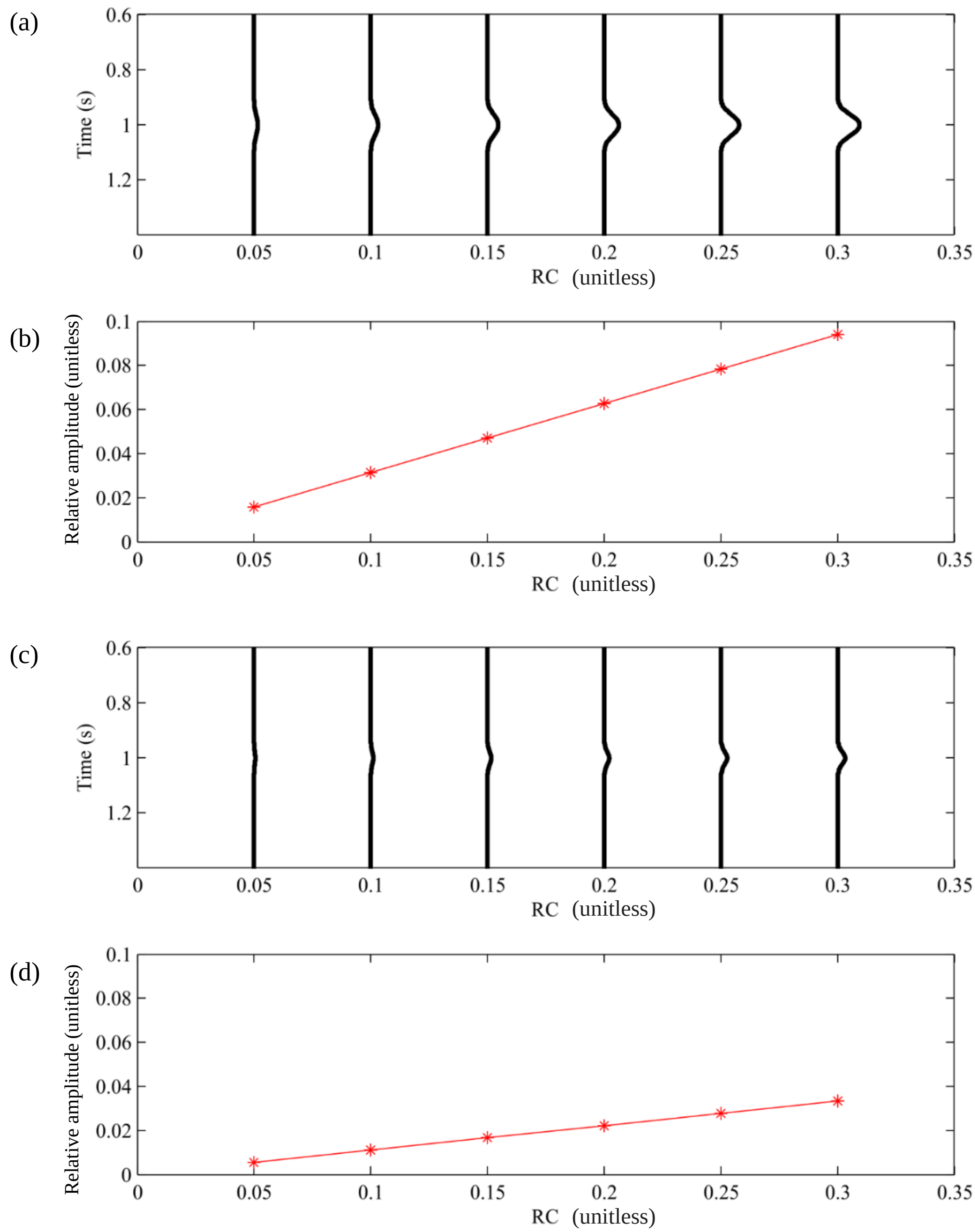

Figure 5.2 Spectral-PC-amplitude trace and peak amplitude for PC1 (a, and b) and PC2 (c, and d) of the layer model from analysis without normalizing isofrequency-amplitude traces.

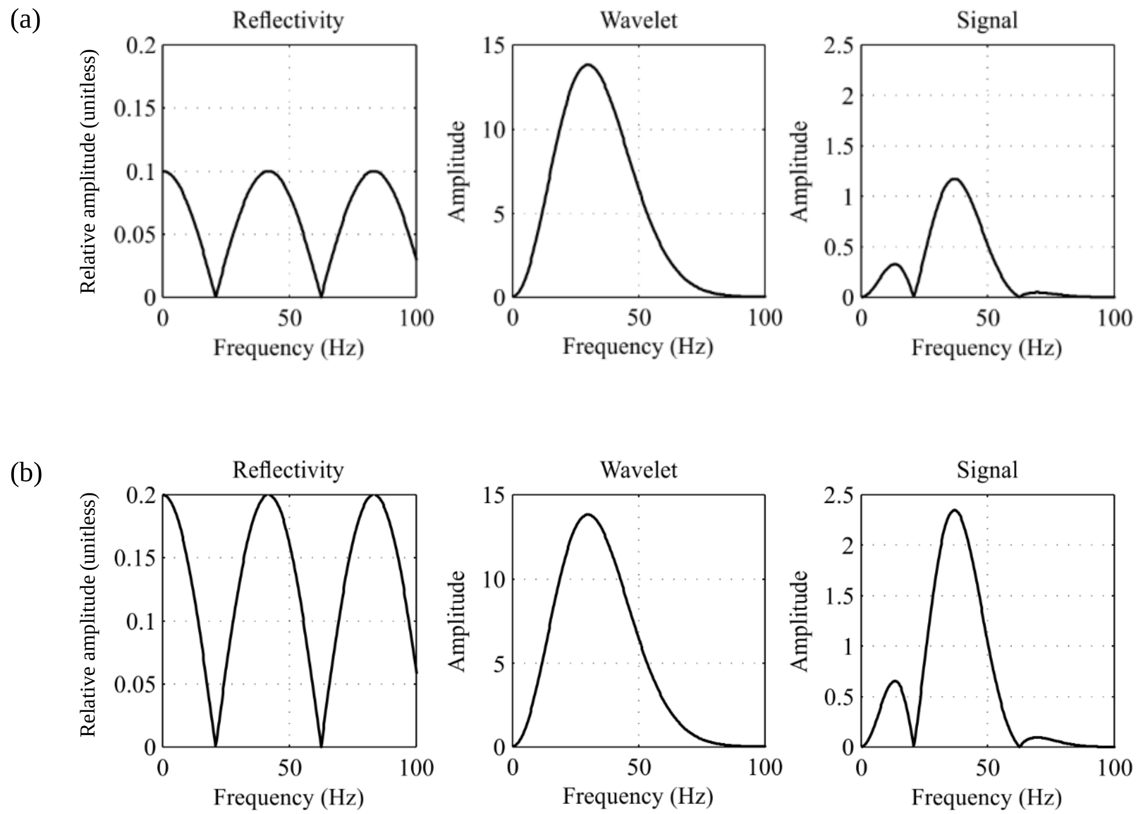

Figure 5.3 Amplitude spectrum of reflectivity, wavelet, and signal for a 24-ms thick, odd model with (a) -0.05 and +0.05 reflection pair; and (b) -0.1 and 0.1 reflection pair on top and base of layer, respectively.

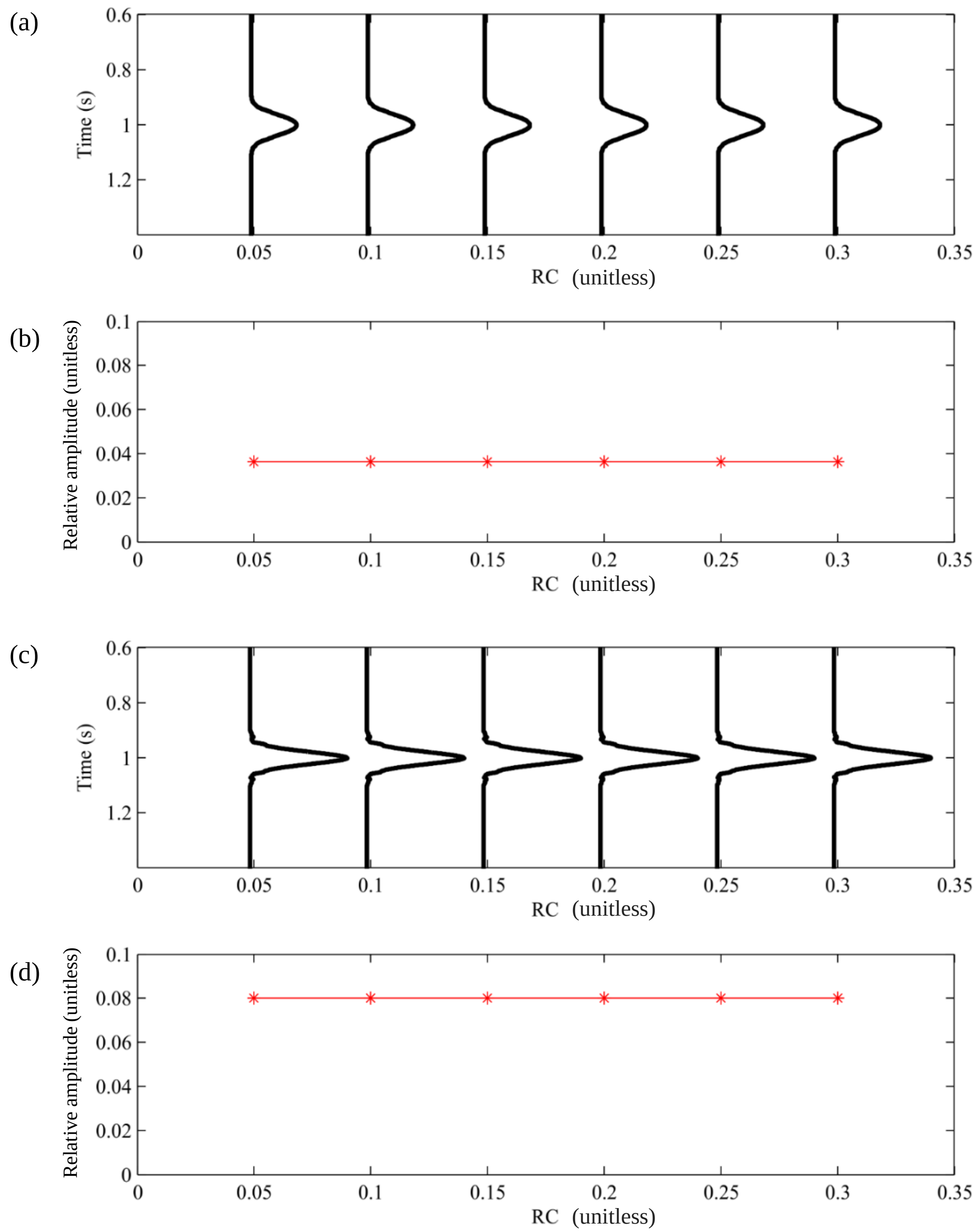

Figure 5.4 Spectral-PC-amplitude trace and peak amplitude for PC1 (a and b) and PC2 (c and d) of the layer model from analysis after normalizing isofrequency-amplitude traces.

5.1.2 Odd-reflection pair, varying thickness (wedge model)

As the effect of RC has been removed using a proper scaling, thickness variation is to be tested on how it affects spectral-PC traces. Model 2 consists of two reflections of the same magnitude and opposite sign so that a continuous thickness increase forms a "wedge" (Figure 5.5a). A synthetic seismogram is generated with the same 30 Hz wavelet (Figure 5.5b). Following the same workflow (Figure 4.16) in a trace-by-trace fashion, the resulting spectral-PC traces and amplitudes are shown in Figure 5.6. PC 1 waveform and amplitude is relatively constant over thickness comparing to PC2. For thickness over one period for the 30 Hz wavelet, PC 2 amplitude is fairly constant. However, as thickness decreases from 16 ms, which is the thickness where maximum interference is expected, PC2 amplitude increases almost linearly as a function of thickness (Figure 5.6b). An interpretation for this could be that, at thickness of maximum destructive interference (16 ms), reflection from top and base of layer (peak and trough in signal) overlap perfectly to the side lobes of one other (Figure 5.5b). As thickness decreases from thickness of maximum destructive interference to zero, although the period of the new waveform remains constant (that of the derivative of 30 Hz Ricker wavelet), the shape of waveform keeps changing and amplitude continues to decrease. This, on one hand can be observed by increased peak amplitude in a Fourier amplitude spectrum, and also can be shown by PC 2 amplitude increases because of intensified tuning.

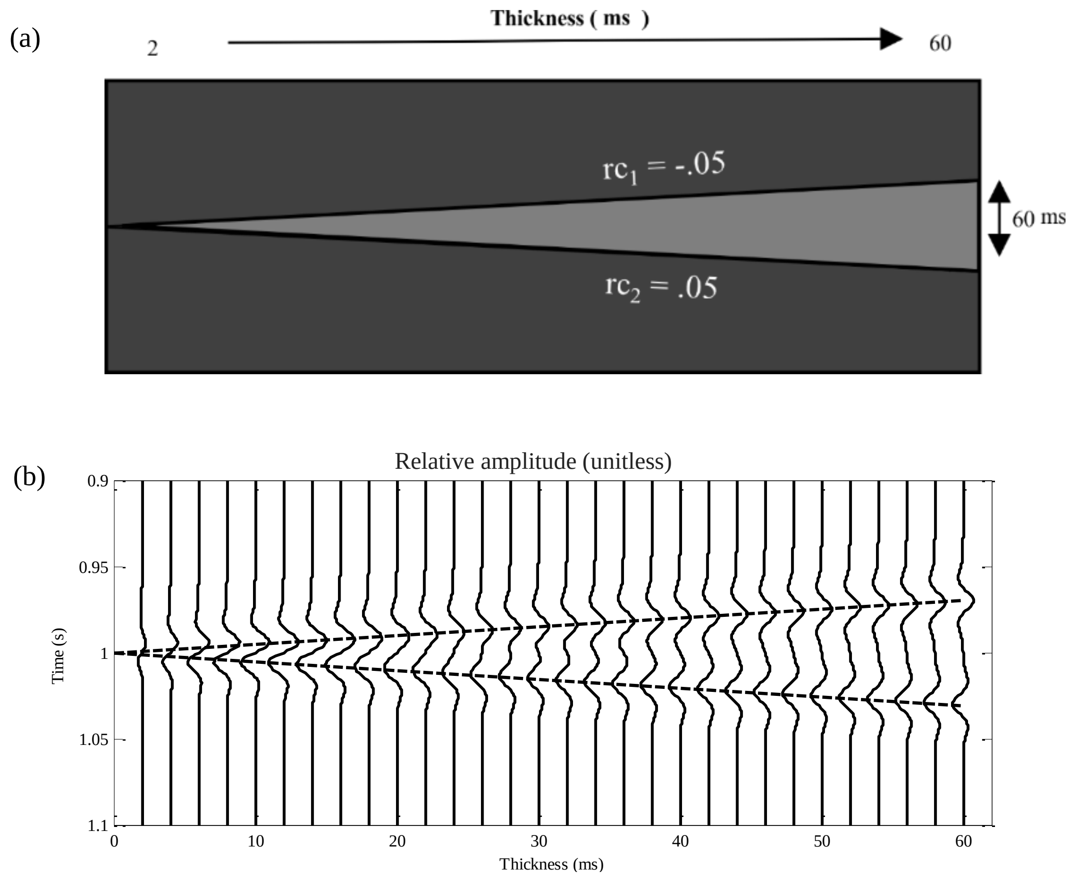

Figure 5.5 (a) Synthetic model containing one layer with unified impedance (low compared to media above and below) and gradually-increased thickness. (b) Seismic traces generated from the model.

Although in this sense, conventional peak amplitude and PC2 spectra amplitude seem to work equally well. However, in comparison, the benefit of using PC spectral amplitude over traditional time-domain peak amplitude is that, by doing spectral decomposition to the seismic trace and proper trace scaling, the effect of laterally changing reflection coefficients and overburden attenuation variations can be minimized, as shown in Figure 5.4. This property is especially useful where in most real situations, tracking peak or trough in time-domain seismic data in a regional or reservoir mapping situation is always the more practical and robust approach. As seismic traces are picked and scaled by peak amplitude (t), we would assume the effect of noise is minimized proportionally. Also, since the peak amplitude is only useful for the scaling step, it is not directly related to thickness as is required for conventional tuning curves. For the PC algorithm used here, where differentiating whether the peak/trough amplitude is caused by a single reflector or thin layer (below or above layer thickness) is *not* necessary, layer thickness information can be most effectively extracted with the tuning affected PC spectral amplitude.

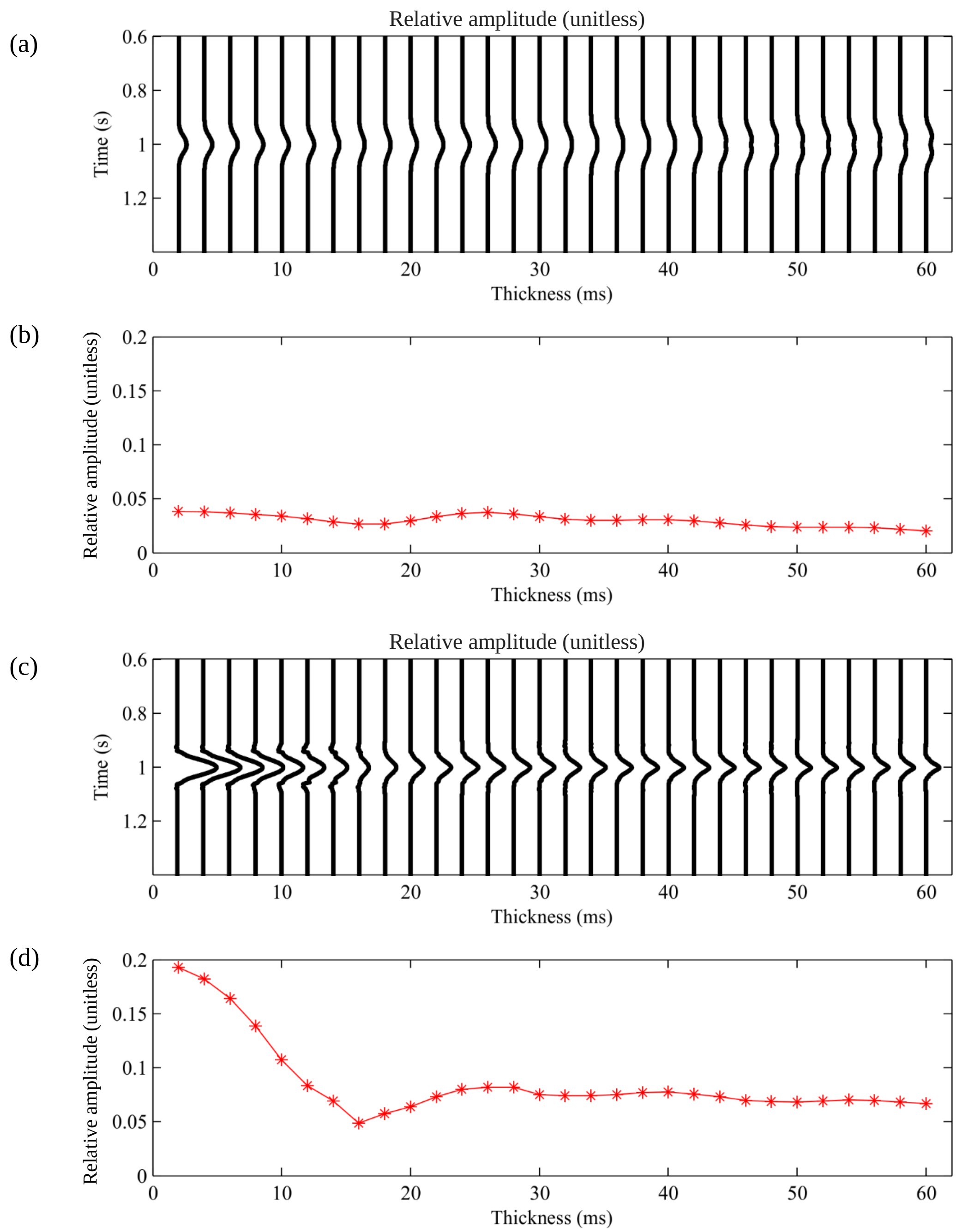

Figure 5.6 Spectral-PC-amplitude trace and peak amplitude for PC1 (a, and b) and PC2 (c, and d) for the wedge model (odd pair) for analysis after normalizing isofrequency-amplitude traces.

5.1.3 Even-reflection pair, varying thickness (wedge model)

We also tested the behavior of the spectral-PC trace and amplitude for a wedge model with the same magnitude and same sign of the reflection on top and base of the wedge (Figure 5.7). Similar to what is seen in the odd-pair model case (Figure 5.6a), PC1 spectral waveform and amplitude are fairly constant over thickness as compared to PC2, which tends to be representative of frequencies affected by tuning. However, PC2 sees high amplitudes *at* the tuning thickness, the one where destructive interference reaches maxima, while decreases as thickness approaches zero. Our interpretation is that, as thickness reaches 16 ms the side lobe of top or base precisely match the main lobe of base or top. This creates a double-peak shaped wavelet that represent the maximum waveform shape change compared to the original wavelet, hence the maximum tuning effect. In contrast, for very thin layers, e.g., 2 ms, although amplitude of the waveform is almost twice the original, the shape of waveform doesn't differ as much from a scaled original Ricker wavelet, meaning a much smaller tuning effect.

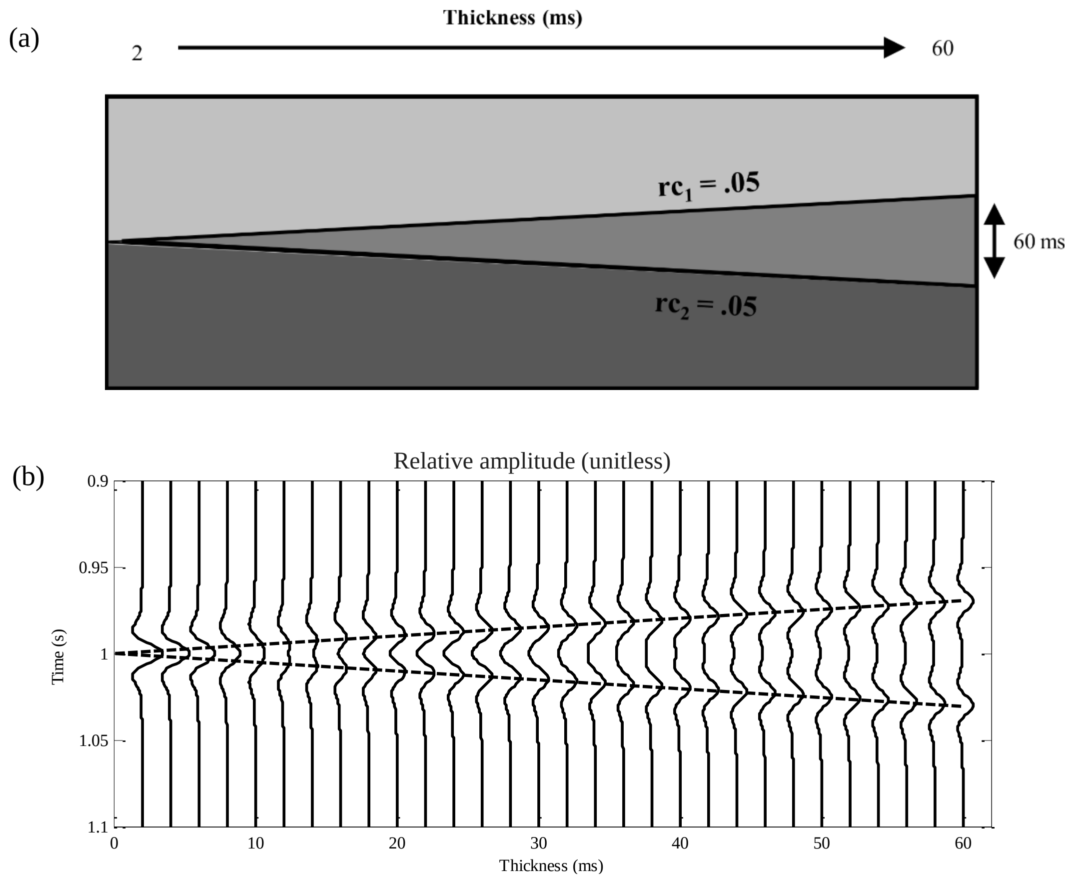

Figure 5.7 (a) Synthetic model containing one layer with unified impedance (medium compared to media above and below) and gradually-increased thickness. (b) Seismic traces generated from the model.

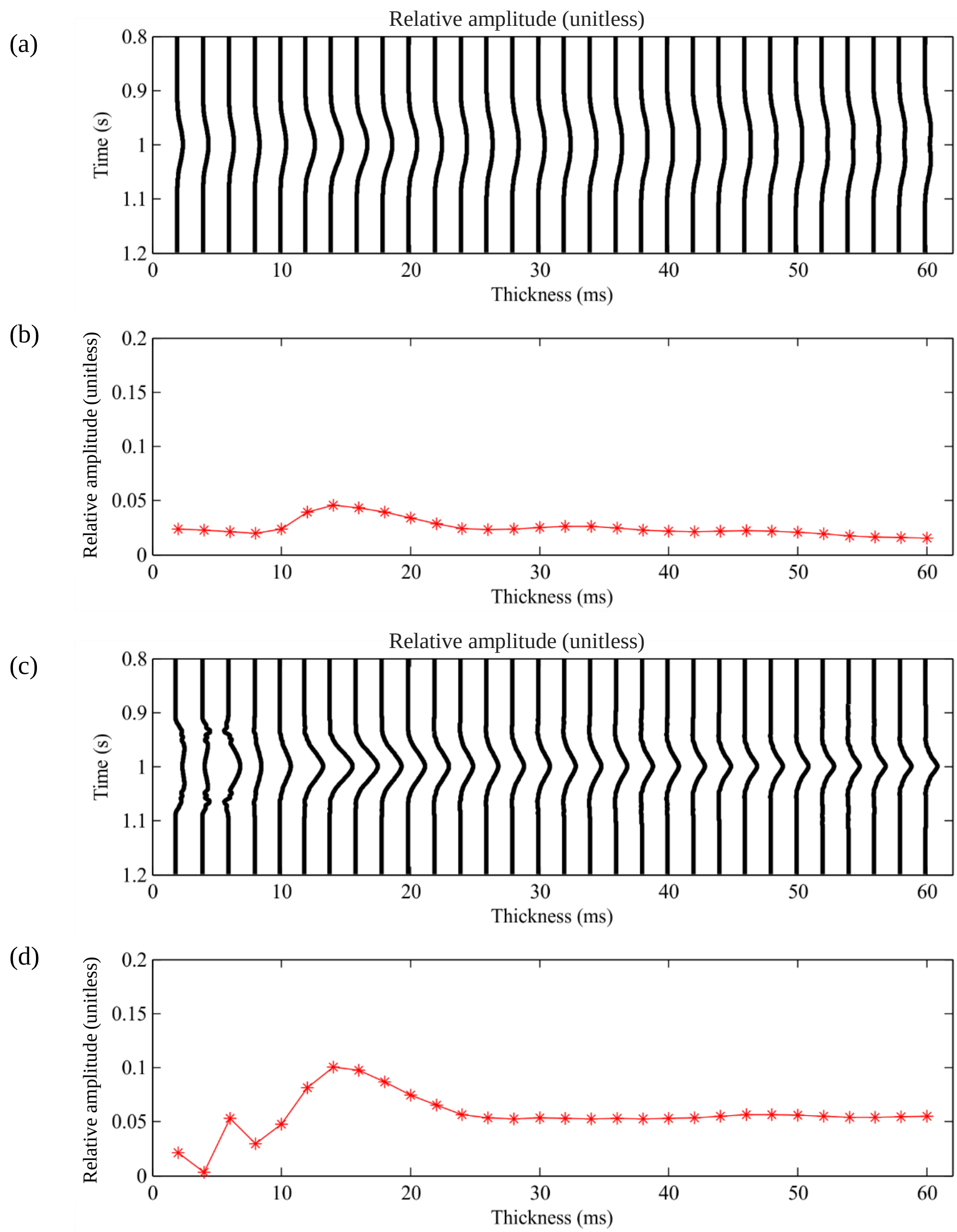

Figure 5.8 Spectral-PC-amplitude trace and peak amplitude for PC1 (a, and b) and PC2 (c, and d) for the wedge model (even pair) for analysis after normalizing isofrequency-amplitude traces.

5.1.4 Robustness of spectral-PC amplitude in the presence of noise

To test the robustness of the PC spectral amplitude attribute, we created noise-affected models by adding the noise-free odd model (Figure 5.5a) with noise traces of 10, 20, 30, and 40 percent root-mean-square (RMS) error. The error trace is created by generating a Gaussian distributed trace that has a mean of zero and desired standard deviation (RMS error) proportional to the input trace. For each noise level, 50 trials are tested at each thickness.

Figure 5.9 compares result of the noise-free model (a) to that of the noise-affected models (b-e). Point markers indicate mean amplitude out of 50 trials and the error bars show one standard deviation higher and lower from the mean. Generally, PC1 is much less affected by noise compared to PC2, and is also very close to the noise-free model result. This is because the PC1 amplitude is generated by projecting the amplitude spectrum to the most significant direction, hence would be less affected by noise. PC2 amplitude exhibits good stability and resemblance to the noise-free case when thickness is greater than 16 ms. For 2 to 16 ms traces, the mean-amplitude curve still fits the same general trend in the noise-free model with a higher standard deviation value. This suggests, in a scenario where a non-random moderate-level noise is present, the PC2 amplitude would still be able to maintain a thickness resolution.

Another possible application suggested here is that, since the PC1 amplitude is relatively stable over thickness in the presence of strong noise when a trace scaling is applied in the workflow, the PC1 amplitude alone can be used as an attribute for lateral reflection coefficient variation if the scaling is *not* included in the workflow. As seen in the noise-free case, the PC amplitude is linearly proportional to RC (Figure 5.2), so the PC1 amplitude would work better, especially in the presence of strong noise.

(a)

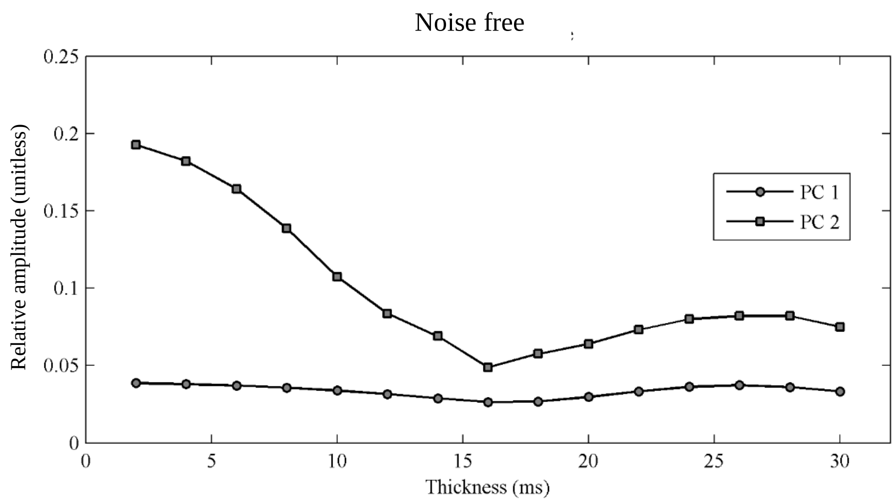

(b)

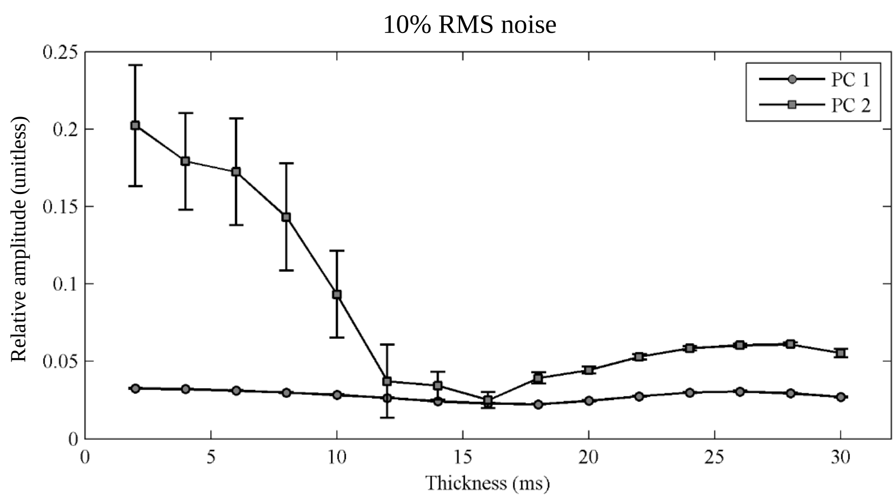

(c)

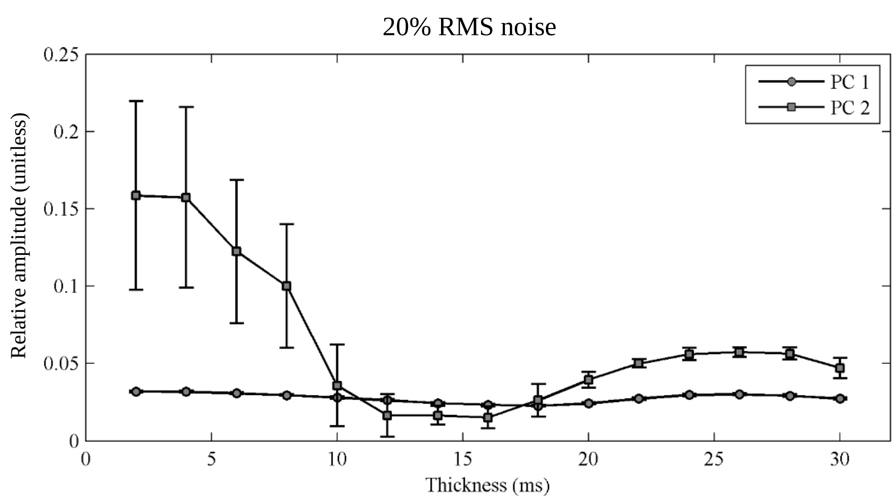

(continue on next page)

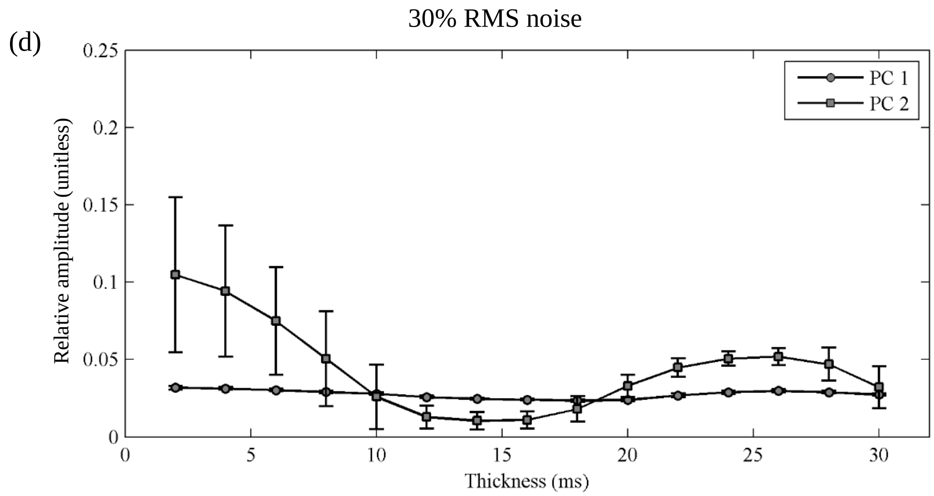

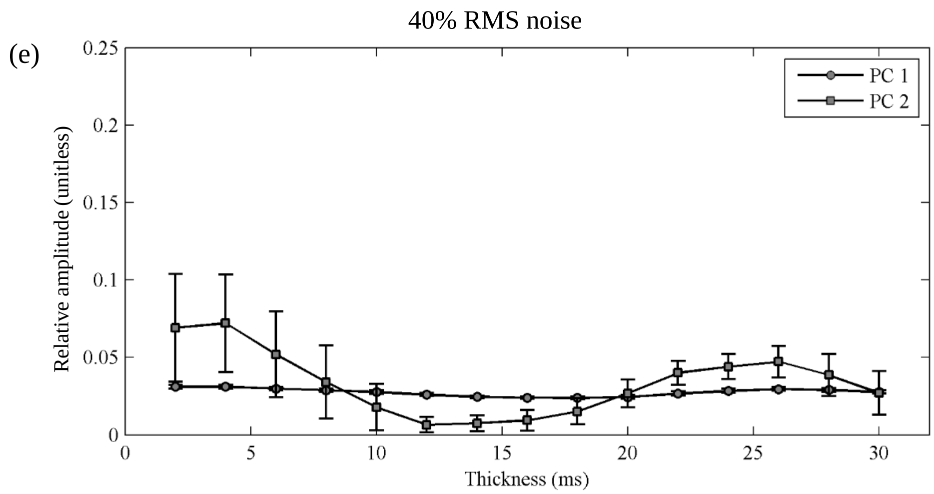

Figure 5.9 Peak amplitude of spectral PC1 and PC2 from (a) noise-free odd pair model; models with RMS noise of (b) 10%; (c) 20%; (d) 30%; (e) 40%. Vertical lines indicate one standard deviation above and below mean value after 50 trials.

5.2 Three-Dimensional-Synthetic-channel model

A 3D synthetic model involving a channel encased in thin layers is used to test the PCA workflow for 3D data (Figure 4.16). The synthetic data has an average dominant frequency of 20 Hz (Figure 5.10). Using conventional commercial software, we are able to pick a surface at the peak which should correspond to the horizon of the channel. The time structure and amplitude map is shown in Figure 5.11.

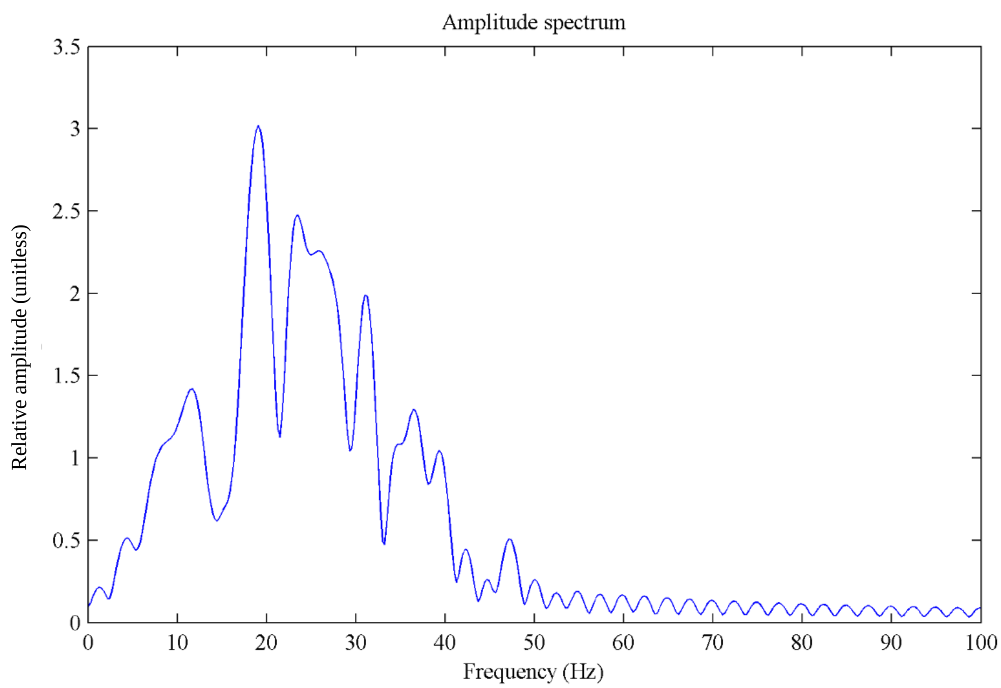

Figure 5.10 Amplitude spectrum of the synthetic-channel-model data centered at the horizon of the channel.

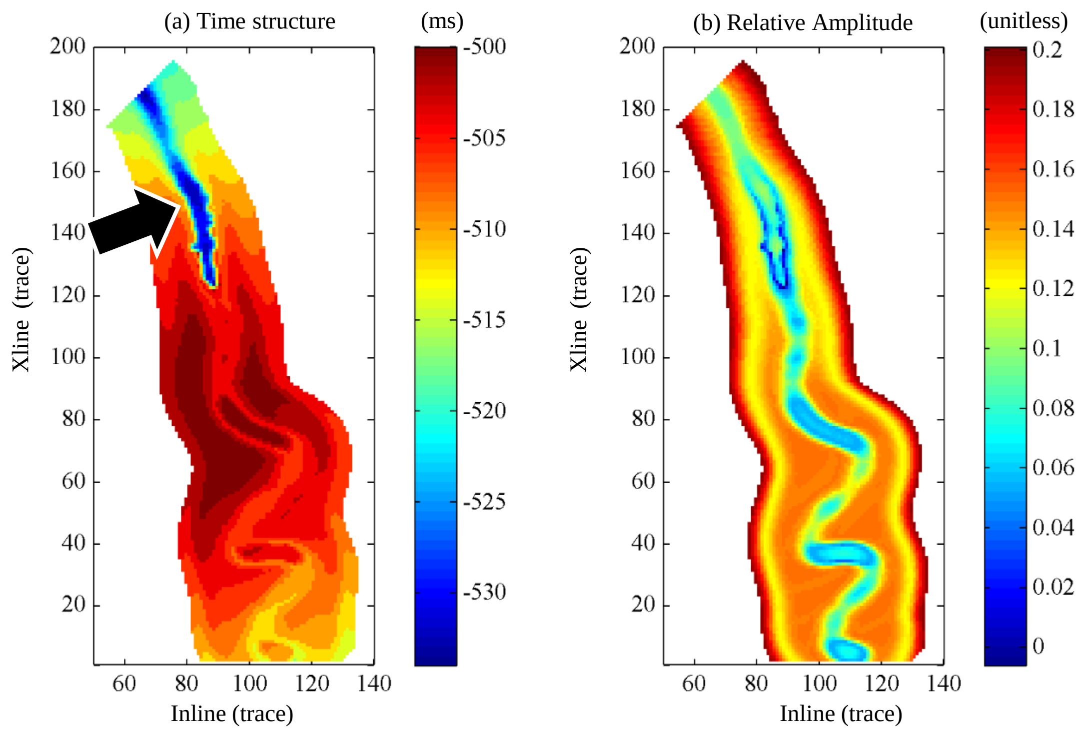

Figure 5.11 Time-structure map (a) and seismic-amplitude map (b) on the horizon of the channel. Black arrow show location of incised valley.

From the time structure map, a typical interpretation for this map would be that the channel is located on top of a dome-like structure. The center of the map is on a structural high compared to the north and south ends with clear two-way-time gradient. Also the channel in the north part of map (black arrow) is deeply incised compared to the south meander part. The amplitude map doesn't show any sign that would suggest otherwise. However, the impedance model and thickness map of the channel (Figure 5.12), shows that the north end of the channel is not that deep compared to some sections of the channel in the southern part (black arrow). This could result from the fact that the deepest section of channel has a thickness of about 40-45 ms, which is the around the tuning thickness for the 20 Hz dominant frequency of this data. In a conventional post-stack seismic data, thickness below the "tuning thickness" of the wavelet suggests the reflected waveform will approach the derivative of the original wavelet. As a result, the mapped time thickness following the "peak" would be different from the true thickness.

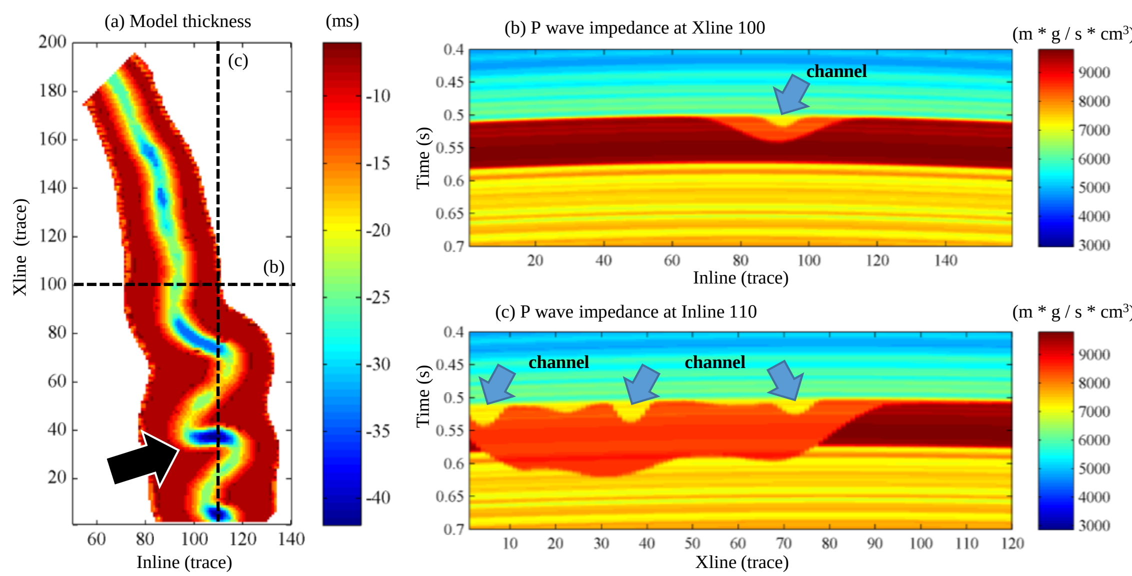

Figure 5.12 (a) True thickness of the channel as measured from impedance model; (b) and (c) shows impedance section of the model located on the two dash lines in (a).

In addition to the complex waveform shape, it is also hard to estimate thickness of the channel itself due to interference from very thin layers above and below. As shown in Figure 5.12, the studied channel in this model is encased between a soft layer of material on top, and a hard layer on the bottom. This would be more likely the situation of an even reflection pair for the most part. From the true model, thickness of the channel ranges from 10 to 42 ms, which make it always below "tuning thickness", i.e., impossible to pick from seismic.

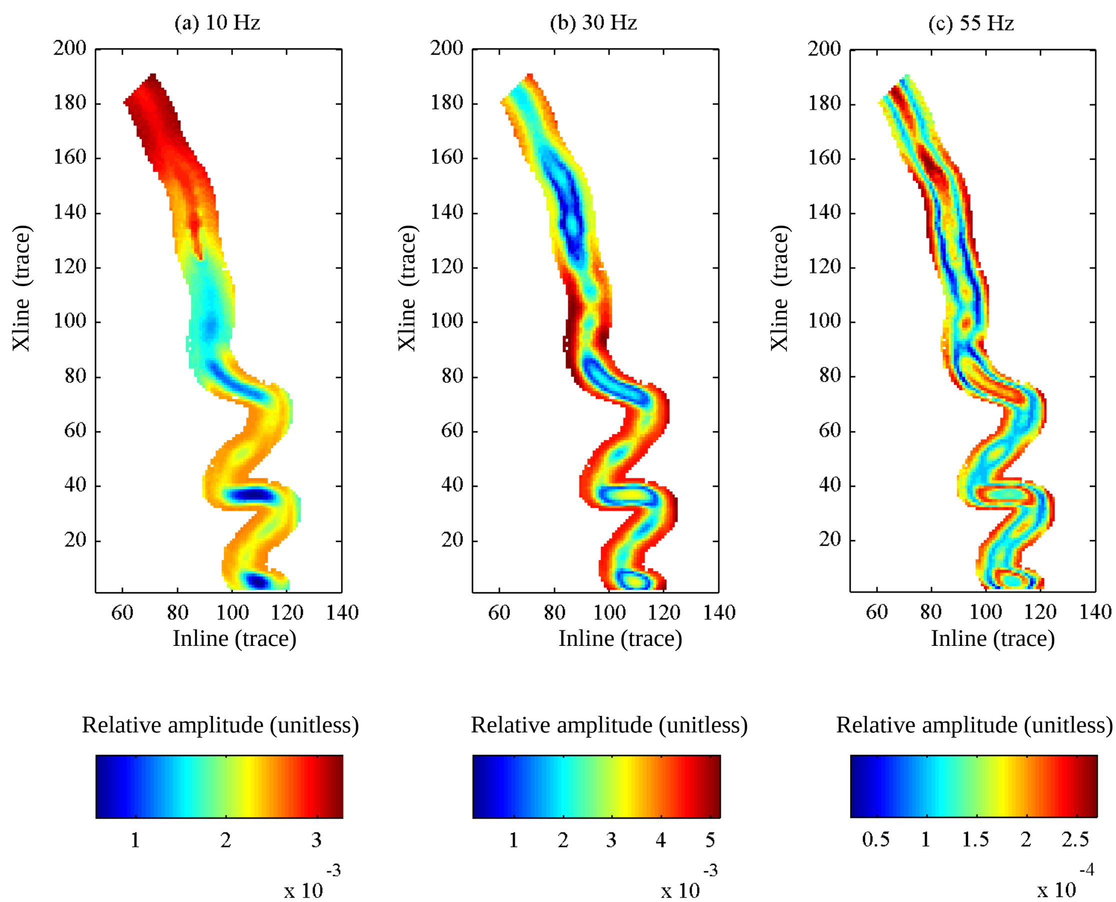

Figure 5.13 Single frequency (a) 10 Hz, (b) 30 Hz, and (c) 55 Hz map of only the channel from the picked seismic horizon.

Spectral decomposition is performed on the seismic data to generate multiple single frequency datasets. The algorithm used here is the Short-time Fourier Transform with a 120 ms boxcar window. Although this algorithm may not have the best time or frequency resolution compared to some newer methods, it is conceptually simple and also sufficient for this simple synthetic model data. Also, for the next few figures, only data that is directly in the channel is displayed to avoid confusion. Figure 5.13 shows the single frequency display of the studied channel at 10 Hz (a), 30 Hz (b), and 55 Hz (c). Notice in the 10 Hz display, spectral amplitude is generally higher in the north and south ends, and lower in middle of the channel. This is not indicative of channel thickness change. Although there are different patterns shown in the three panels, which are represent low, medium, and high frequency, however it is not clear how spectral amplitude for single frequency data can be related to thickness nor channel feature.

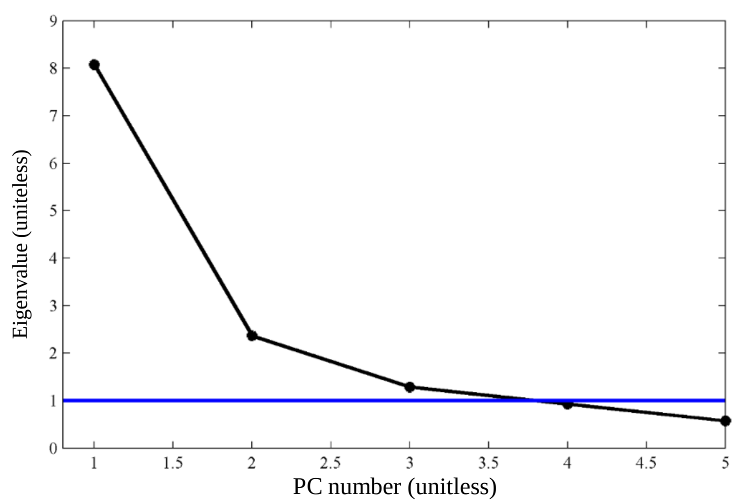

Figure 5.14 Typical eigenvalue-scree plot of a trace in the channel.

We conducted the spectral-PCA workflow as described in Figure 4.16. Based on the data, the first three PCs capture most of the information in single traces from 10 to 70 Hz

(Figure 5.14). The resultant spectral-PC-amplitude map of the studied channel using PC1 (a), PC2 (b), and PC3 (c) are shown in Figure 5.15. The general observation is that, the behavior of spectral-PC amplitudes are comparable to what is seen for the wedge model case. The channel mapped by PC1 is more continuous laterally, since PC1 is considered the non-tuning affected amplitude. PC2 highlights the thick part of the channel, as seen in Figure 5.12(a). Because the reflection pair of the channel is closer to the even pair model (Figure 5.8) as opposed to the odd pair model (Figure 5.6), it is conceptually understandable that high amplitude in tuning-affected PC2 corresponds to the section of the channel where thickness is around 40-45 ms, where it is close to the tuning thickness for a 20 Hz wavelet, similar to what's shown in the even reflection pair wedge model (Figure 5.8b). In addition, the PC3 amplitude map shows high values in the thinner part of the map, which is similar to what is seen in the odd reflection pair wedge model (Figure 5.6b).

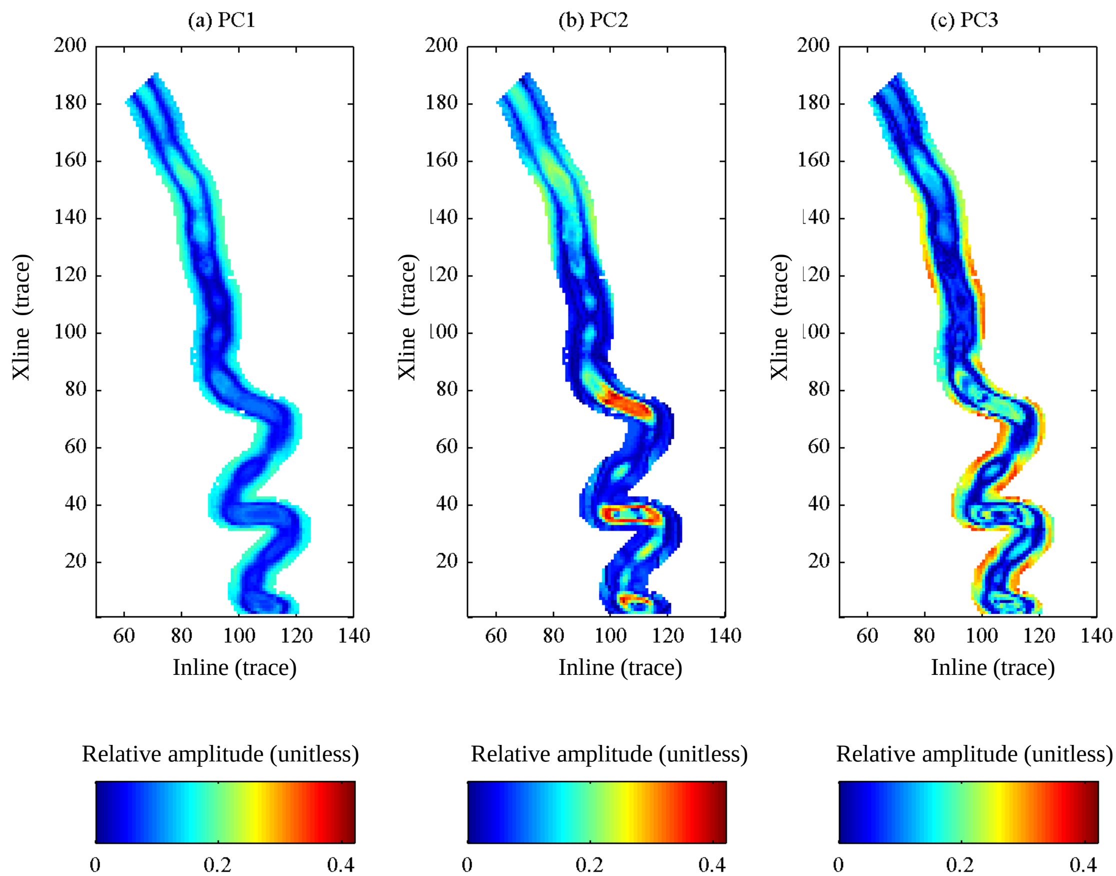

Figure 5.15 Spectral (a) PC1-, (b) PC2-, and (c) PC3-amplitude map of the studied channel.

Figure 5.16 shows cross-plots of the PC amplitudes for PC 1, 2, and 3 against the true channel thickness in the original impedance model. Mean value and standard deviation are calculated and plotted for each thickness and PC. Comparing the three panels, it is clear that PC1 has the lowest mean PC amplitudes and lowest variation, indicating that it is the one that is less affected by tuning. The PC2 and PC3 amplitude over thickness curve bears striking resemblance to the pure odd and even pair results, suggesting that spectral-PC analysis is able to extract individually the seismic responses of even and odd portions of the impulse pair.

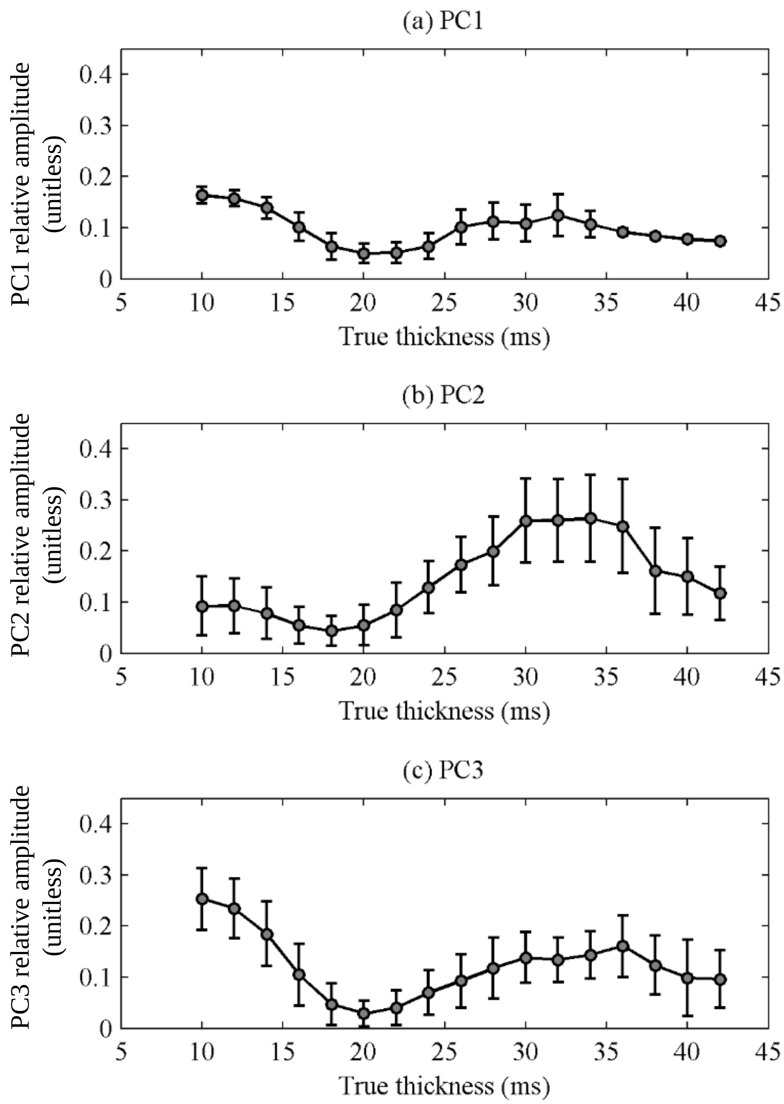

Figure 5.16 Channel thickness plotted against average-peak amplitudes of spectral (a) PC1, (b) PC2, and (c) PC3. Short bar indicates one standard deviation above or below average amplitude.

In summary, this synthetic channel model shows that spectral-PC amplitude seems to be working better in displaying layer thickness variation comparted to the original seismic data and single frequency maps. However, as shown in the wedge model, if we were to quantitatively relate thickness variation especially below tuning thickness using PC spectral amplitude, it is important that the layer reflection pair be exactly the same magnitude and opposite sign, i.e., an odd pair (Figure 5.6). Although from this example, it seems that the third PC is most sensitive to the odd component of the reflectivity. There are limitations however. To do quantitative thickness estimation, a few conditions might need to be met. For example, the center of the layer needs to be known. More importantly, response from the odd pair must be much larger than the noise. In the future, if we would apply techniques that could robustly separate the odd and even pair, the spectral-PC amplitude using only the odd pair should be able to map thickness quantitatively with higher confidence.

5.3 Real-data examples

5.3.1 Boonsville-field dataset in north Texas, USA

The spectral-PC amplitude method was used to map thickness variation in a karsted area in a 3-D post-stack time-migrated seismic data from the Boonsville field, Fort Worth Basin, United States (Hardage et al., 1996a). A time slice at 1.005 second two-way-time (TWT) is chosen for study (Figure 5.17a). Note that the dominant frequency around this time slice (using a 140 ms calculation window, Figure 5.17b) is relatively higher than common land seismic data. A cross-sectional view of seismic data (Figure 5.17c) shows multiple structural depressions resulting from deep karst sink holes in this area.

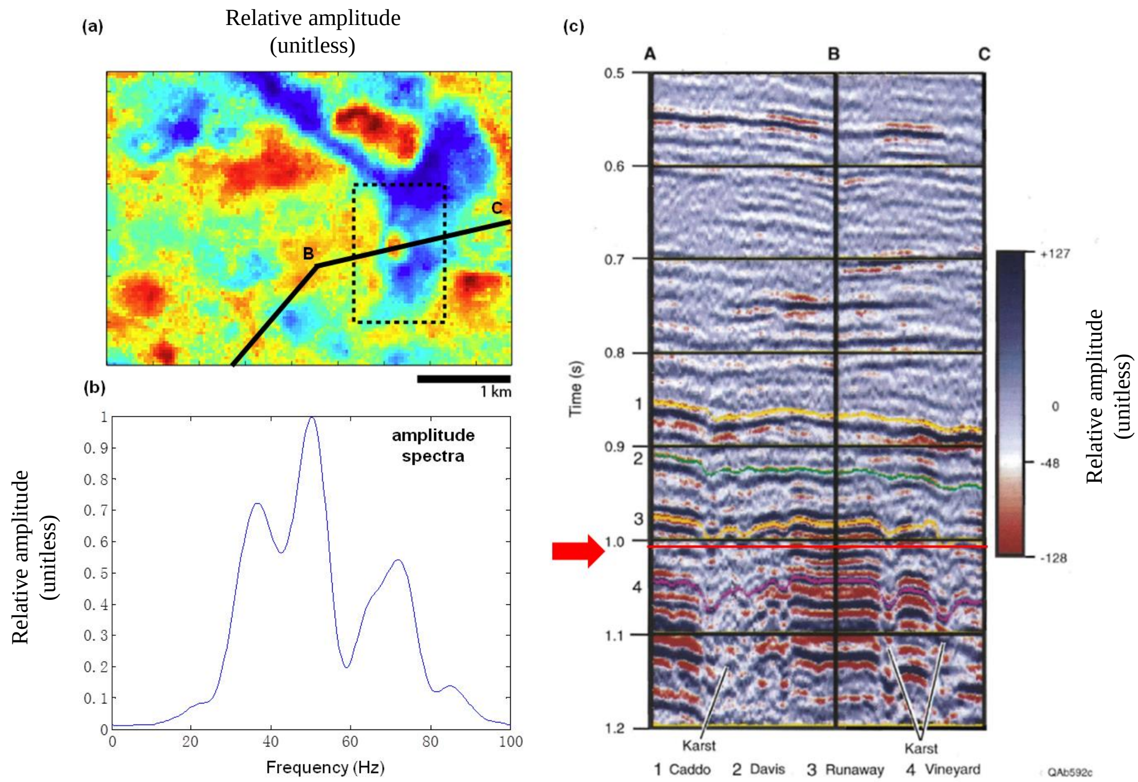

Figure 5.17 (a) Seismic-amplitude map at 1.005 second in the Boonsville-field dataset (red indicates hard reflection); (b) amplitude spectra around the time slice; (c) seismic profile that cross the time slice along the black line in (a) (Hardage et al., 1996).

The spectral-PC analysis was applied to the 3D data following the workflow in Figure 4.15. Based on the data, the first three PCs represent most of the information in single traces from 10 to 70 Hz. Although the real data is supposed to be more complex, as seen for the simple layer case (Figure 4.13 and 4.14), by rotation of the PC coefficients, it is much easier to find specific frequency contents represented by each PC. As shown in

Figure 4.15, as each spectral PC is associated with a certain frequency band, especially in a 3D setting, it would be more reasonable to "resort" and display spectral-PC amplitude of matching "characteristic" frequency bands, which should be the "non-tuning affected", "even pair affected", and "odd pair affected", as opposed to the conventional way to sort and display PCs strictly following the rank from high to low importance (1^{st}, 2^{nd}… etc.). Using the Boonsville field data, Figure 5.18 compares single frequency slices from spectral decomposition (a), spectral-PC amplitude without "resorting" or the conventional way (b), and PC spectral amplitude mapping with the "resorting" (c) on time slice 1.005 sec TWT. The 10, 40 and 75 Hz time slices are selected to represent interference patterns in low, medium and high frequency bands of seismic data. The conventional PC1 spectral attribute (b) recreates the pattern of the dominant (medium) frequency data, while the 2^{nd} and 3^{rd} PCs don't correlate to a specific frequency band or geological feature. After the Varimax rotation, and resorting, the PC1 amplitude is usually interpreted as not affected by tuning, PC2 and PC3 are interpreted as either affected by odd and even reflection pairs, and hence are indicative of thinner and thicker layers, respectively.

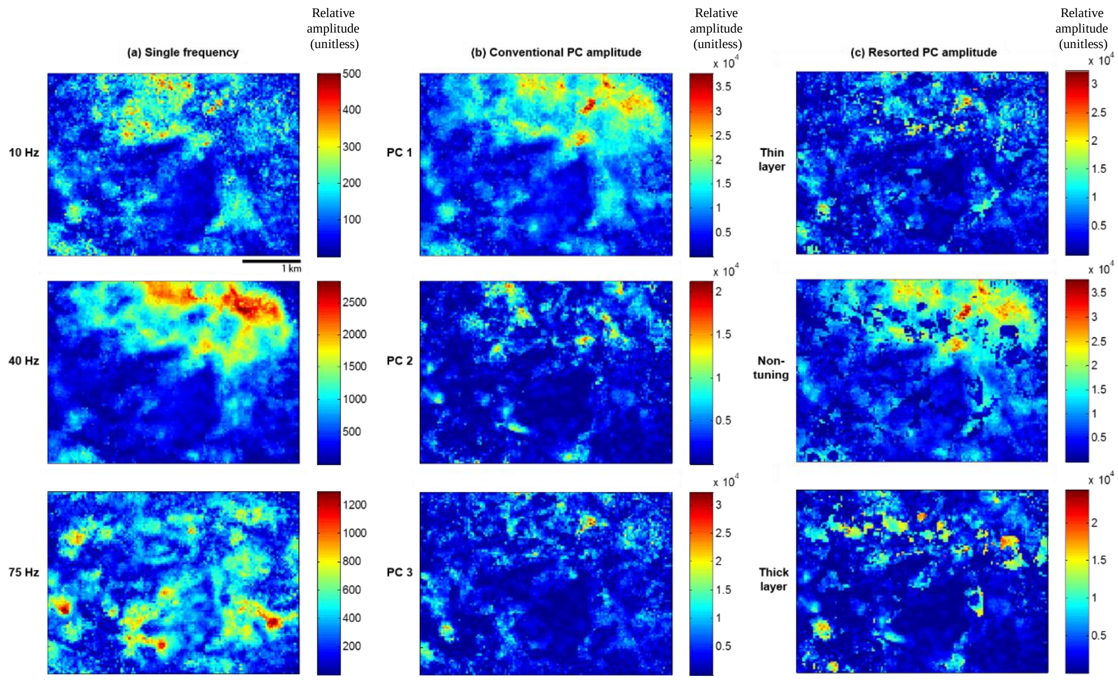

Figure 5.18 (a) Single-frequency image, (b) conventional spectral-PC amplitude, and (c) resorted spectral-PC-amplitude map in the Boonsville data at time 1.005 second.

Figure 5.19 illustrates color rendering of the three types of display: input 10, 40, and 75 Hz data (a), conventional PCs 1-2-3 (b), and the resorted "large, medium and small thickness" PCs (c). At a large scale, the spectral decomposition-based images show patterns like the original seismic (Figure 5.17a). The RGB composite image of single frequencies shows smooth color variations, with little indication of subtle features. In detail, the RGB composite image of conventional PCs (b) looks noisy thus inhibiting interpretation of frequency-dependent features. In comparison, the composite image of the Varimax rotated PCs (c) shows smooth large scale variation as well as subtle features. The feature highlighted in the squares (Figure 5.17a and 5.19) is interpreted as a sink hole due to karst depression of the Ellenburger group beneath the selected time slice (as interpreted on the seismic section; Figure 5.17c). The inner ring of this bulls-eye feature is dominated by the high frequency Varimax rotated PC attribute. This high frequency event indicates the maximum reduction of layer thickness, possibly due to stretching and/or thinning of rock layers caused by normal faulting induced by the karst depression.

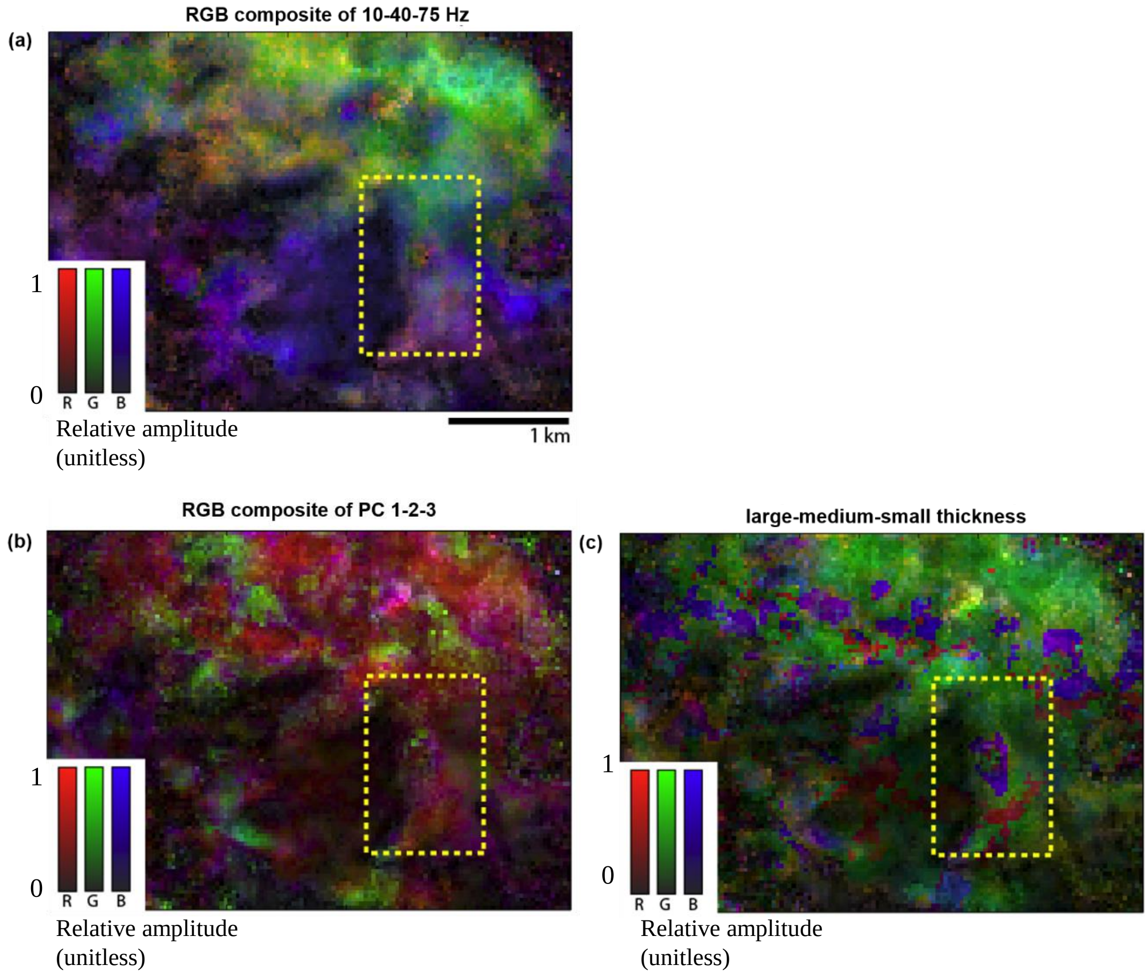

Figure 5.19 RGB rending at time slice 1.005 sec of the Boonsville-field dataset using (a) 10-40-75 Hz single frequency; (b) conventional PC1-2-3; and (c) resorted PCs of large-medium-small thickness.

5.3.2 Hoover-field dataset in the Gulf of Mexico

The Hoover field from the Alamos Canyon block of the Gulf of Mexico is located some 160 miles offshore south of Galveston, Texas, USA in 4800 feet of water (Figure 5.20). It utilized the world's deepest offshore drilling and production platform at that time. The main reservoir in this field is associated with a sand levee in a deep water turbidite system. The discovery and subsequent wells confirmed the amplitude-based extent of the reservoirs (Higgins, 1998).

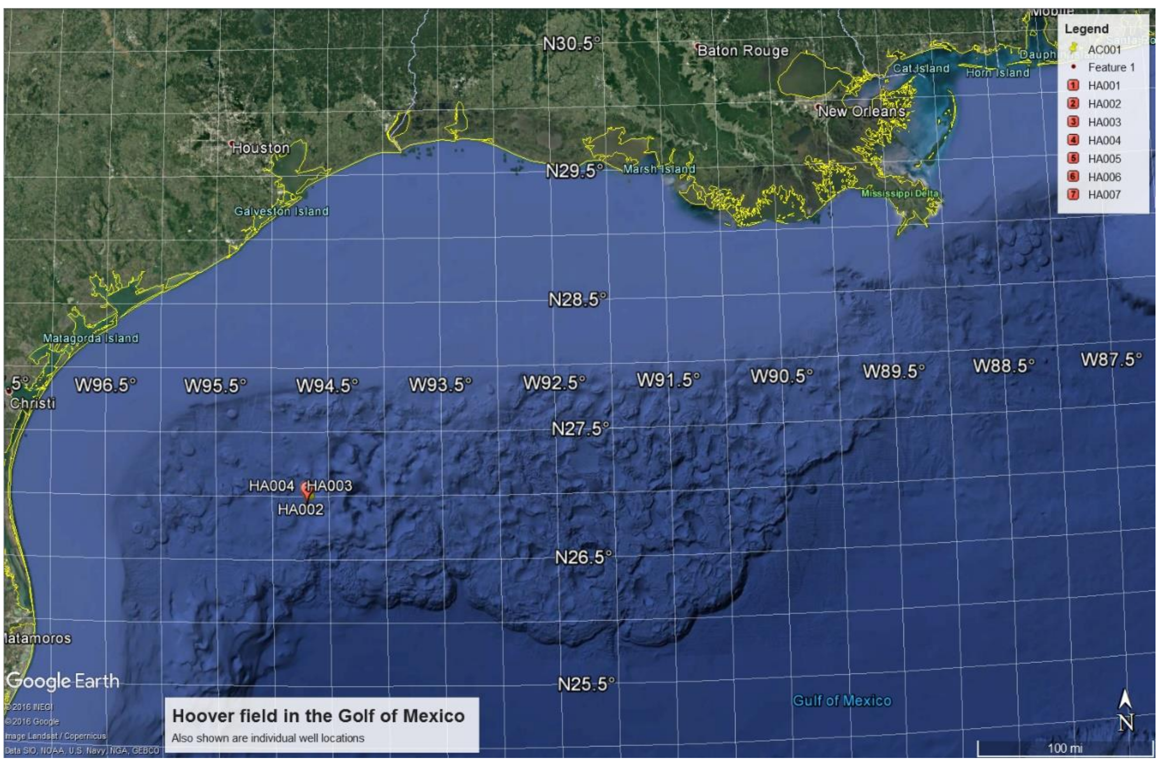

Figure 5.20 Geographic location of the Hoover field in the Gulf of Mexico.

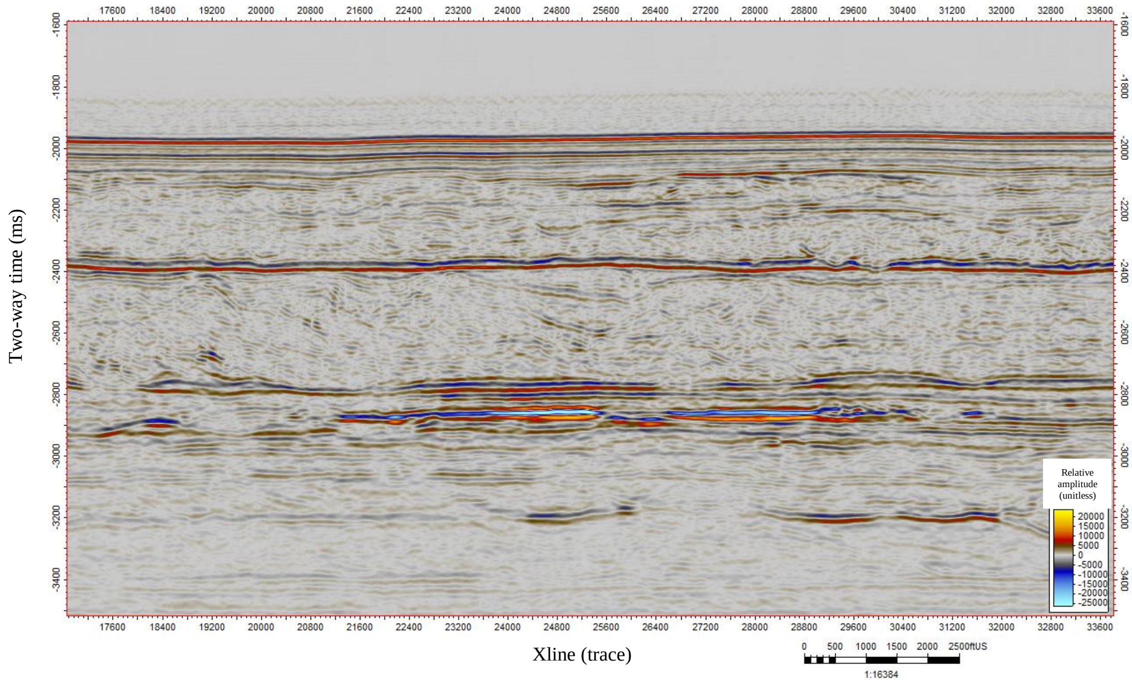

Figure 5.21 Amplitude of Inline 32795 (W-E direction) section from the Hoover-field-seismic data.

Figure 5.21 show a seismic amplitude section along Inline 32795 from the Hoover-field dataset. Reflectors in this region are generally flat, which is good for both imaging and interpretation. The water bottom reflection is located at depth of around 1980 ms two-way time. Two bright spots can be seen in this section at depth of around 2980 ms, which corresponds to levees (or splays) on both sides of the main channel (between Xline 25600 to 26400). The levee system associated with the channel is the main sand reservoir.

Figure 5.22 is the time structure map created by tracing the soft reflector associated with the main reservoir. In addition, Figure 5.23 show the seismic amplitude map extracted from the picked horizon. The black square in Figure 5.22 and the yellow dash square in Figure 5.23 show the area where spectral-PC analysis will be performed, which aims to map reservoir rock associated with the sand levee system.

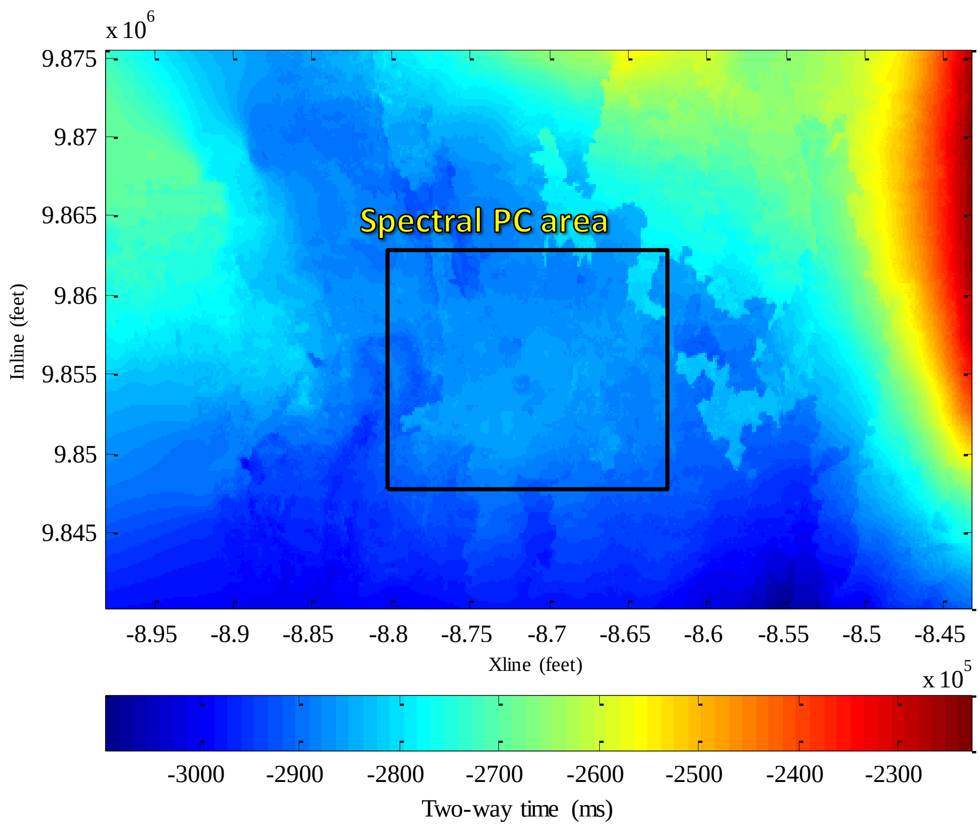

Figure 5.22 Time-structure map of interpreted horizon of the main reservoir in the Hoover-field-seismic data. Spectral-PC attributes are calculated in area surrounded by black line.

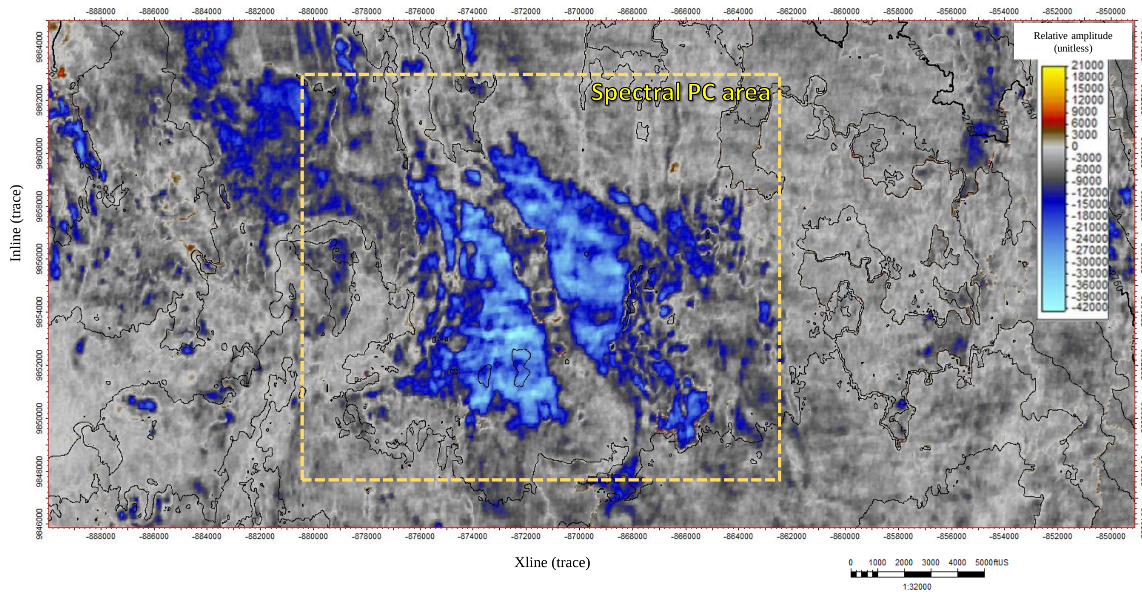

Figure 5.23 Amplitude map of interpreted horizon of the main reservoir in the Hoover-field-seismic data. Spectral-PC attributes are calculated in area surrounded by yellow dash line.

Spectral-PC result at well locations

Figure 5.24 shows the amplitude map of the picked seismic horizon (soft reflection) associated with the major oil reservoir, together with locations of the discovery well and development wells at which each well penetrates the main reservoir. Thickness of the sand are calculated from log data from the nine wells, which ranges from 36 to 102 feet, with a median thickness of 62 feet.

The first step for calculating spectral-PC-amplitude attribute is to find a usable wavelet amplitude spectrum for the seismic data. Water bottom reflections from the nine traces are extracted using a window to calculate a wavelet. Figure 5.25 shows the waveform of the water bottom reflection from the nine traces. Because the seismic data was sampled at a 4 ms-per-sample rate (blue curve), in order to smooth the waveform, a spline interpolation of the waveform is performed using 1 ms-per-sample rate (red curve) before calculating the wavelet. Figure 5.26 show the average amplitude spectrum and wavelet calculated from the windowed water bottom reflection events. The wavelet has a high spectral energy above noise between the frequencies 10 to 70 Hz. Hence, later spectral decomposition and PCA of the isofrequency data will apply the same range of frequencies.

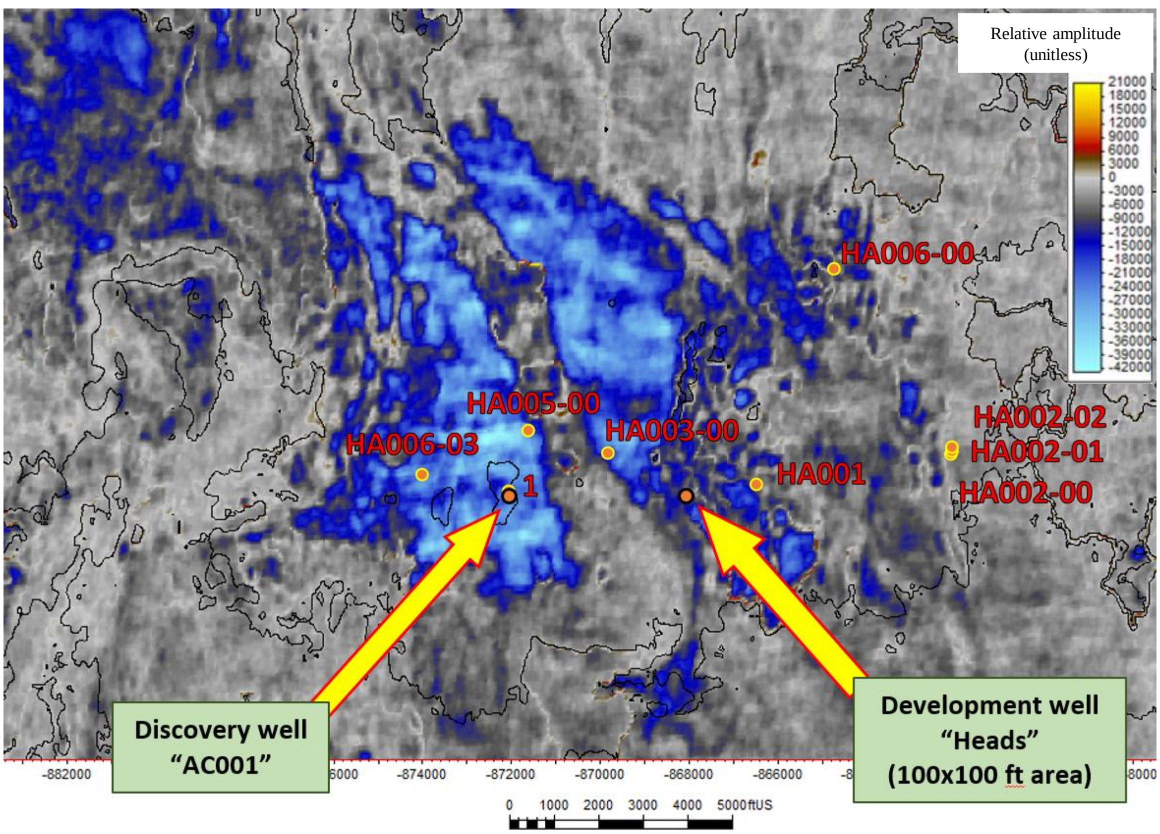

Figure 5.24 Seismic amplitude extracted from horizon of the main reservoir (soft reflection). Orange dots signifies location of wellheads and location at which each well penetrate the main reservoir.

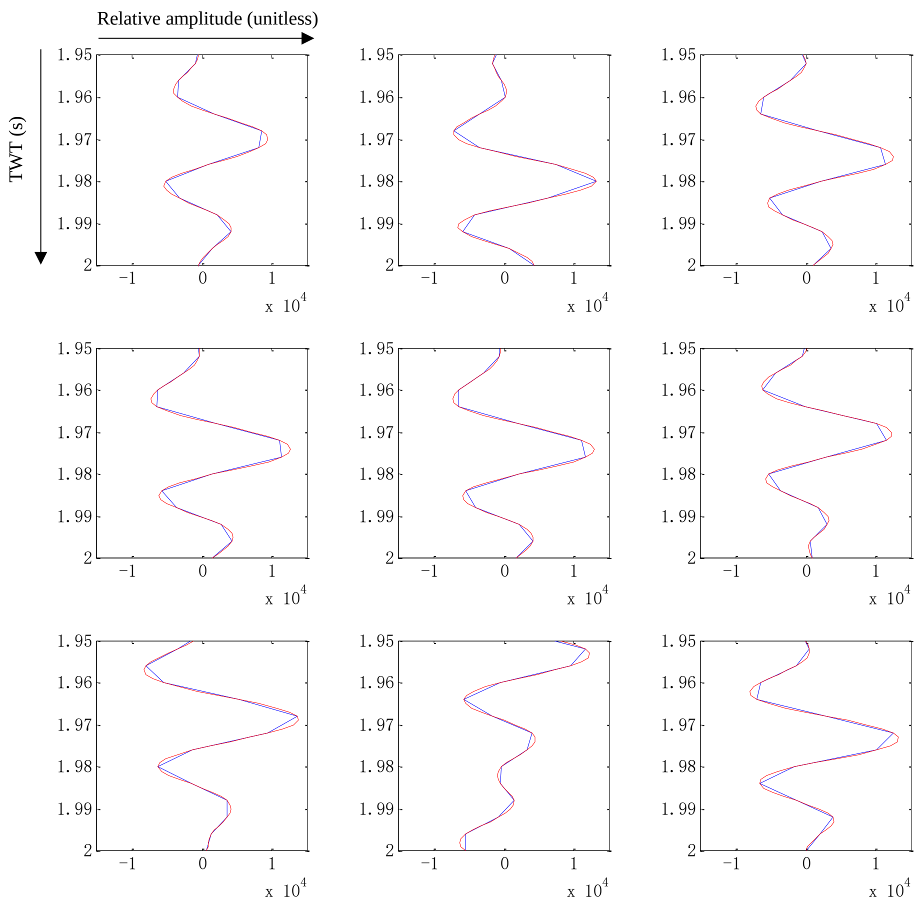

Figure 5.25 Waveform of water-bottom reflections from original (blue) and resampled (red) seismic traces where each well penetrates the reservoir in Figure 5.24.

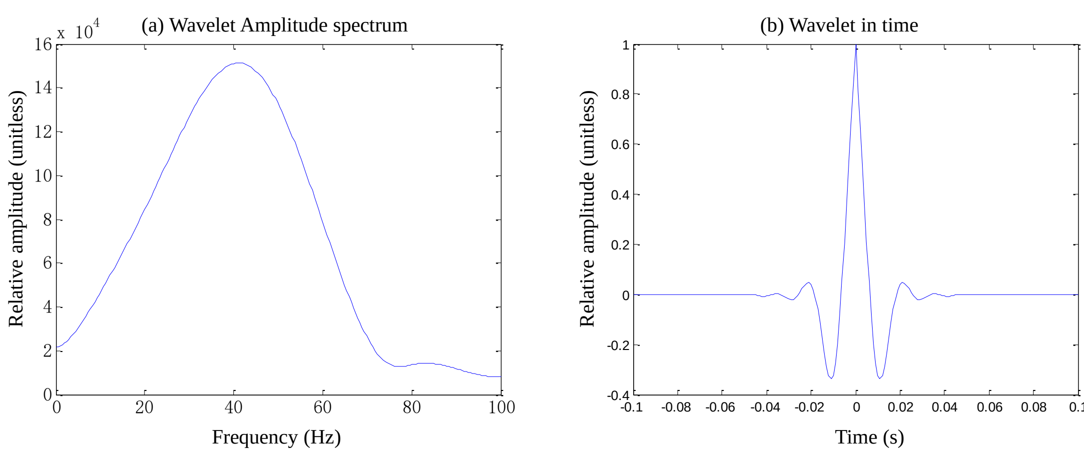

Figure 5.26 (a) Amplitude spectrum of the wavelet extracted from water-bottom reflections; (b) extracted wavelet in time domain.

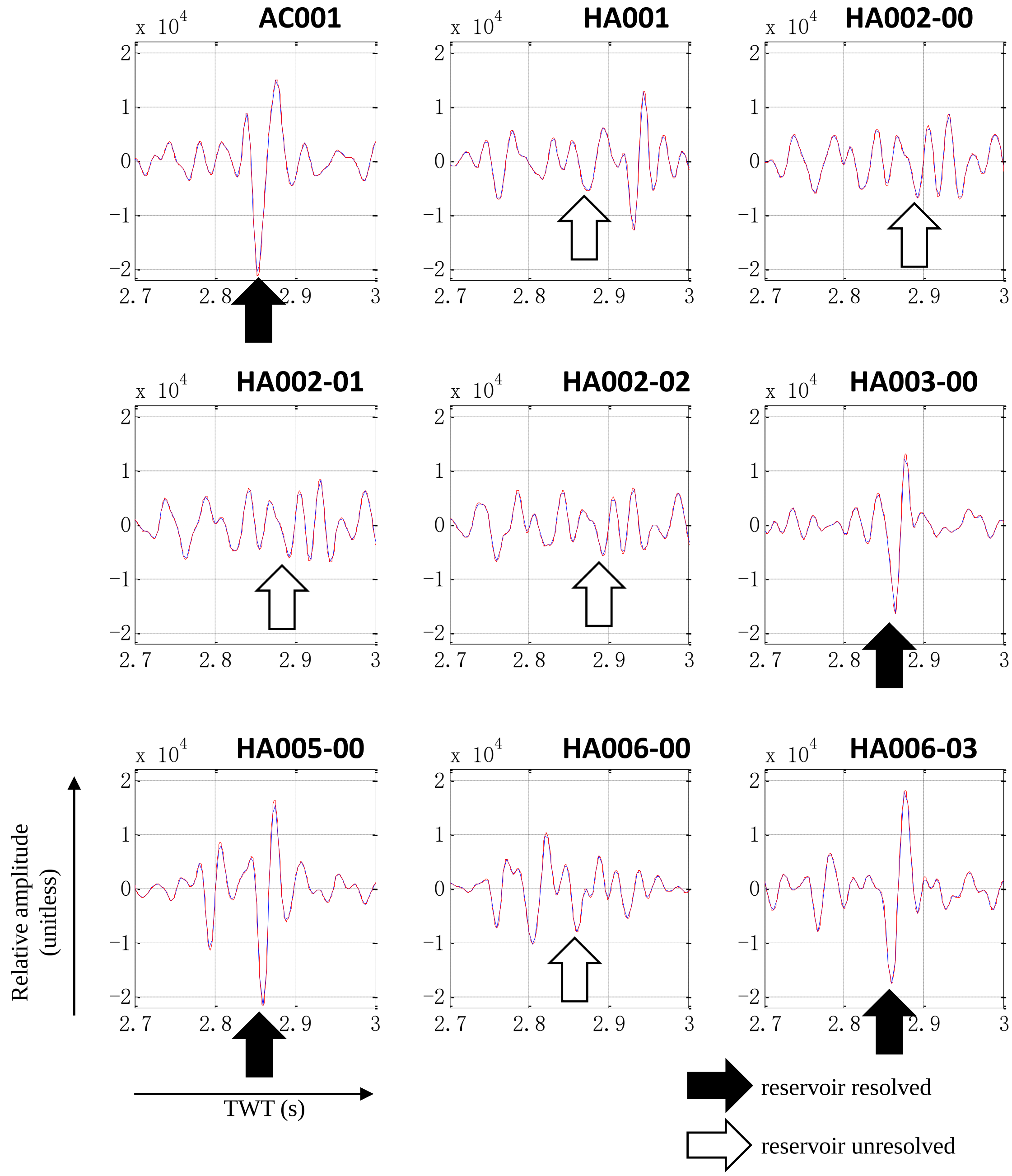

Figure 5.27 Seismic trace at locations where wells penetrate the reservoir.

Figure 5.27 show real seismic traces at locations where each well penetrates the reservoir, with arrows pointing to the interpreted reservoir location. Not all traces displays a clear 90-degree phase-shifted waveform, which is what's shown in the pure odd model (Figure 5.5b). This poor resolution of the reservoir is partly due to 1) having one stronger reflection above or below the interpreted reservoir reflection (trough); or 2) having multiple reflections of similar strength that are adjacent to the reservoir reflection. This suggest a spectral decomposition algorithm with higher time and frequency resolution (compared to short-time Fourier transform) might be able to improve the resolution of isofrequency-amplitude traces.

Spectral-PC-amplitude trace for all nine wells are calculated following the same workflow as in Figure 4.15, results are displayed in Figure 5.28. As in Figure 5.24, the only traces that show good 90-degree phase shifted waveforms (solid arrow) generate spectral-PC waveforms with the peak aligned with the center of the layer, as seen in all the synthetic examples, e.g., Figure 5.6(a, c).

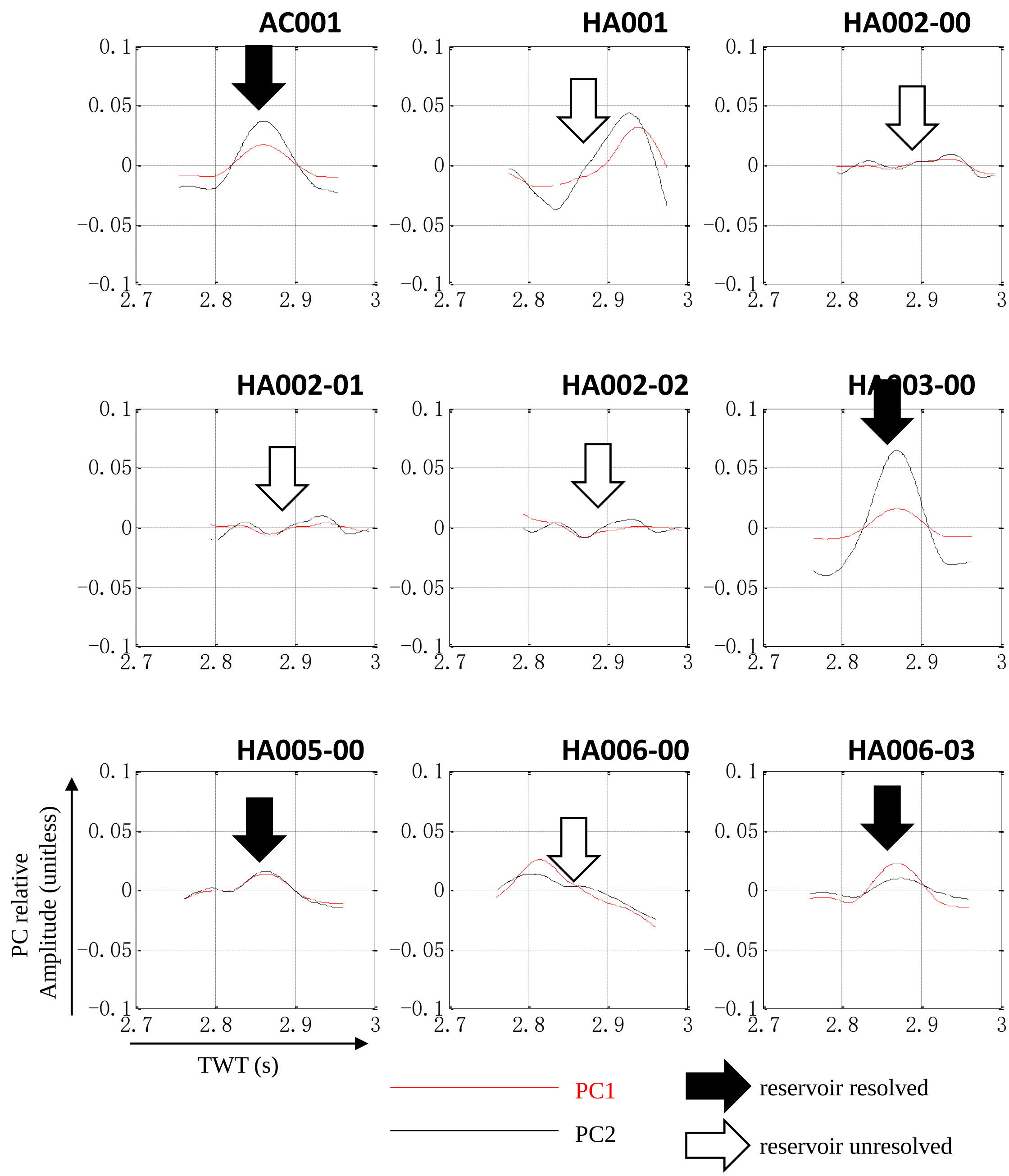

Figure 5.28 Spectral-PC-amplitude trace for PC1 and PC2 at well locations.

Comparing results from one-layer model, log-based model, and real-seismic trace

Reflection events in real geology are never simply pure odd or even pairs. In addition, usually there are more than only two reflectors in an analysis window. For example, the real logs shown in Figure 5.29 suggest that a clear oil-water contact exists at the bottom of the oil layer. As a result, the density log shows an increasing ramp as oppose to sharp step. Figure 5.30 compares spectral-PC peak amplitude, at different thicknesses, of synthetic data from a model containing one simple low-impedance layer to the synthetic data created based on blocked true log reflectivity. Although spectral-PC amplitude from the log-based model is generally larger than that in the simple model, a clear linear trend can be seen. In addition, Figure 5.31 compares spectral-PC amplitude from the simple model data to the true seismic traces from a well where the reservoir can be resolved (thick enough). Although real geology can be more complex than the simple one-layer wedge model (Figure 5.29), the linear trend suggest that, due to the relatively flat geology and good lateral continuity in this region, the spectral-PC-amplitude attribute can be indicative of lateral variation of equivalent thickness in the analysis window.

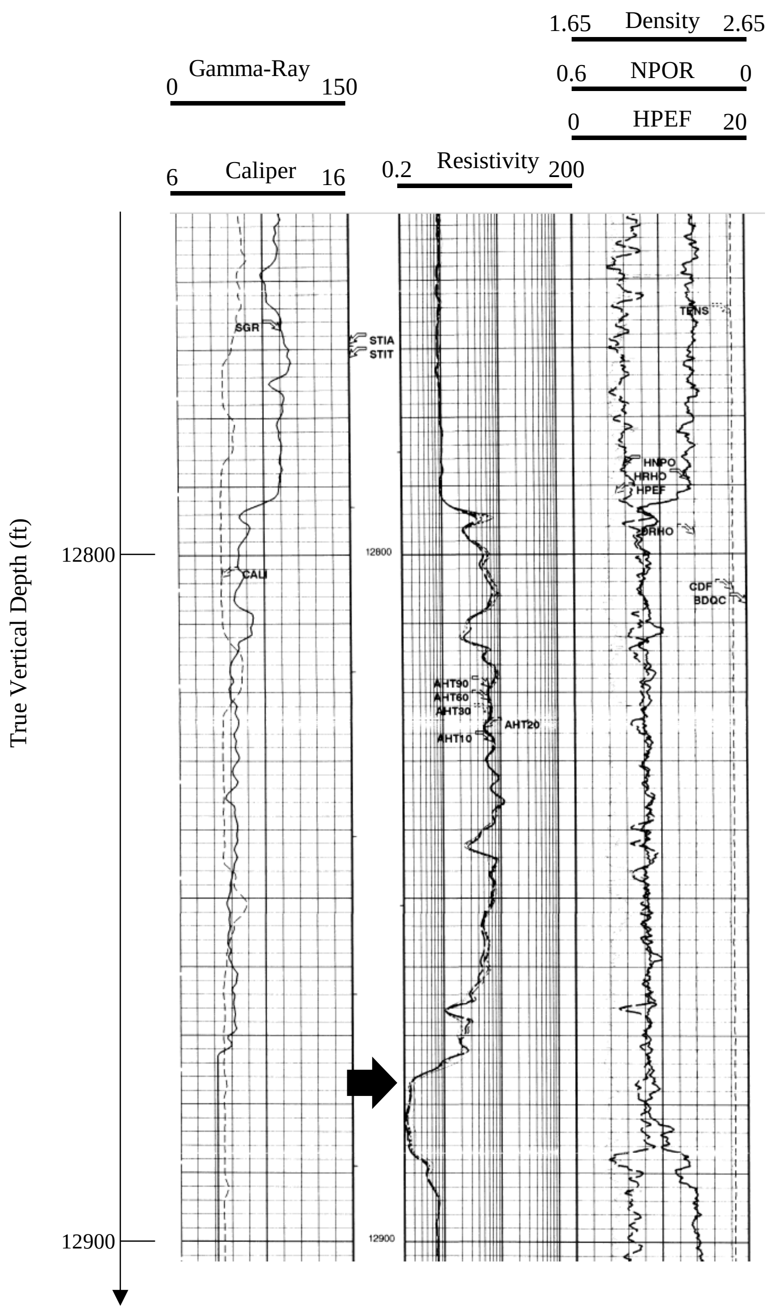

Figure 5.29 Gamma-ray, caliper, resistivity, density, porosity, and HPEF logs from discovery well AC001. Black arrow indicates oil-water contact.

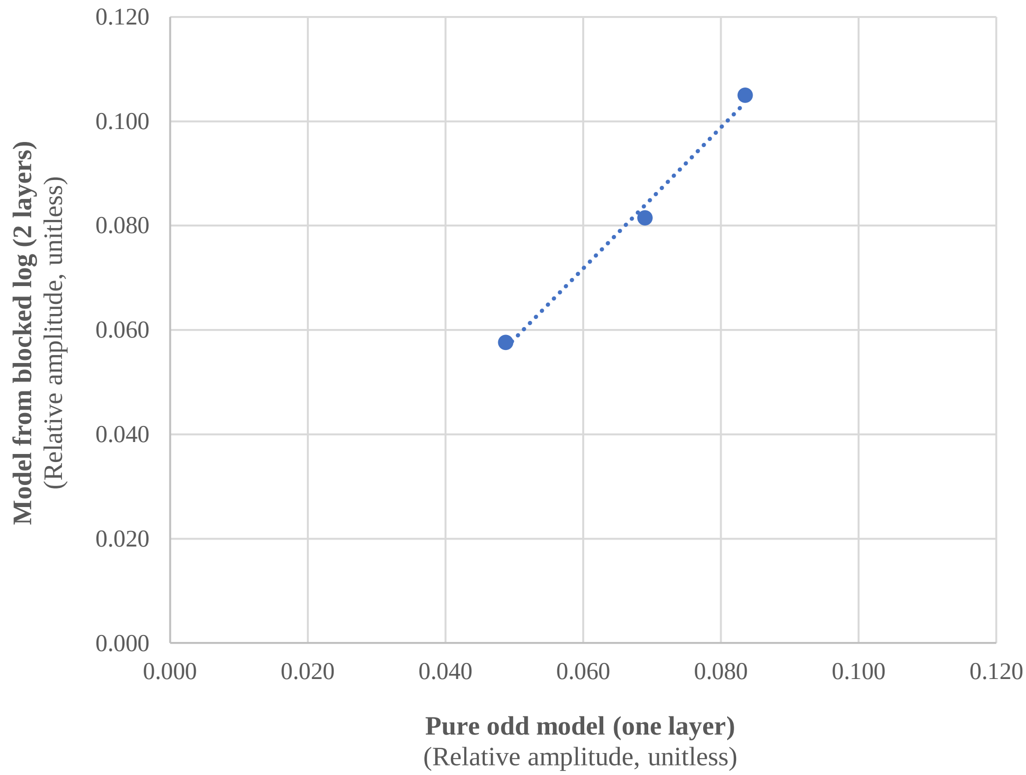

Figure 5.30 Comparison between spectral-PC amplitude results of synthetic data from pure one-layer-odd model and log-based model.

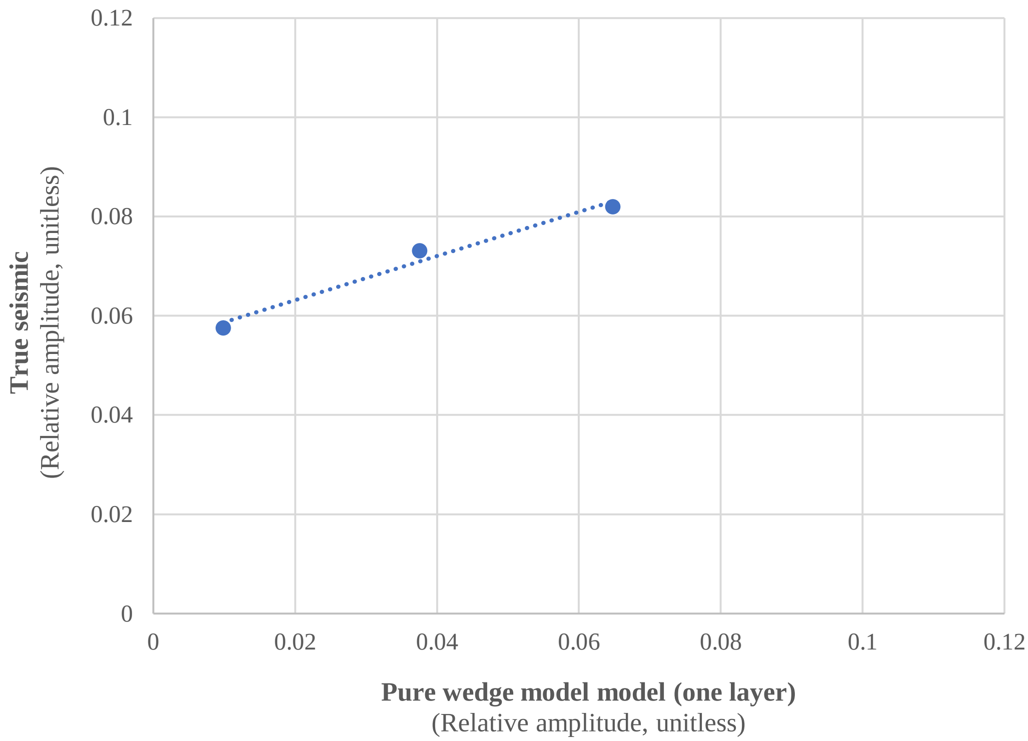

Figure 5.31 Comparison between spectral-PC amplitude results of synthetic data from pure one-layer-odd model and real-seismic data at well locations.

Mapping spectral-PC amplitude

Figure 5.32(a) and Figure 5.33 (a) display spectral PC1 and PC2 amplitude attributes computed within the analyzed area (Figure 5.22 and 5.23). Extent of the main sand reservoir is interpreted and shown in Figure 5.32(b) and Figure 5.33(b). The main sand reservoir has clearly lower PC amplitude compared to the surrounding area. This can be interpreted as relatively greater equivalent layer thickness of the reservoir. We can also see the same trend from the synthetic wedge model for an isolated low impedance layer (Figure 5.31).

Comparing the interpreted reservoir extent from spectral-PC attributes and the original seismic (Figure 5.34), we see a good match on the upper boundary of the bright spot. At the lower part of the analyzed window, the reservoir boundary interpreted from spectral PC (yellow dash) seems to extend further away from the bright spot while maintaining the overall shape. This on one hand, suggests that the spectral-PC attribute is, as shown in the synthetic example (Figure 5.4), independent of layer reflectivity or seismic amplitude. On the other hand, the southern edge of bright spot could suggest the location of the oil-water contact, which is clearly defined in numerous resistivity logs in this region (e.g., Figure 5.29).

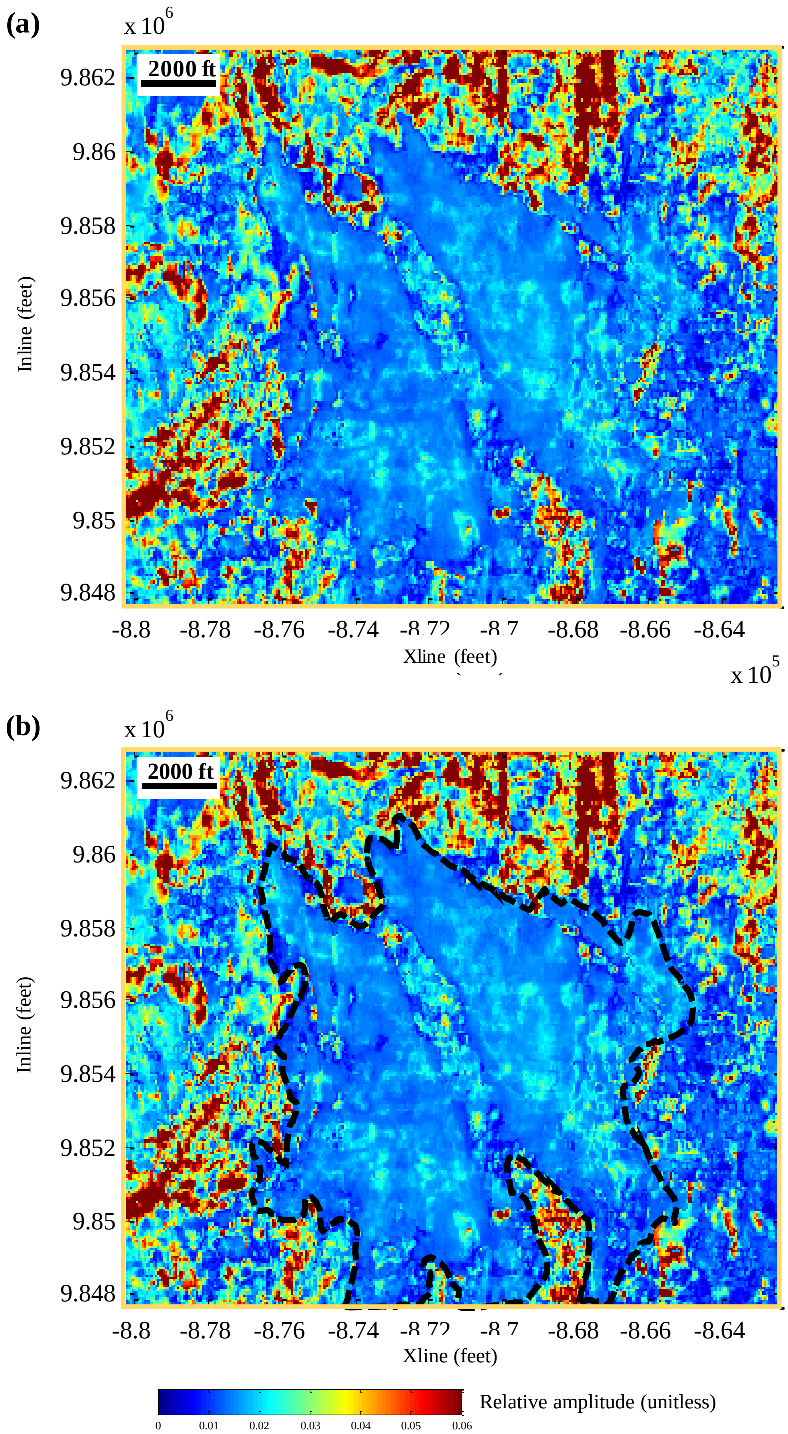

Figure 5.32 Spectral-PC1-amplitude-attribute map (a) and interpreted extent of the reservoir (b, dash line) around the sand levee.

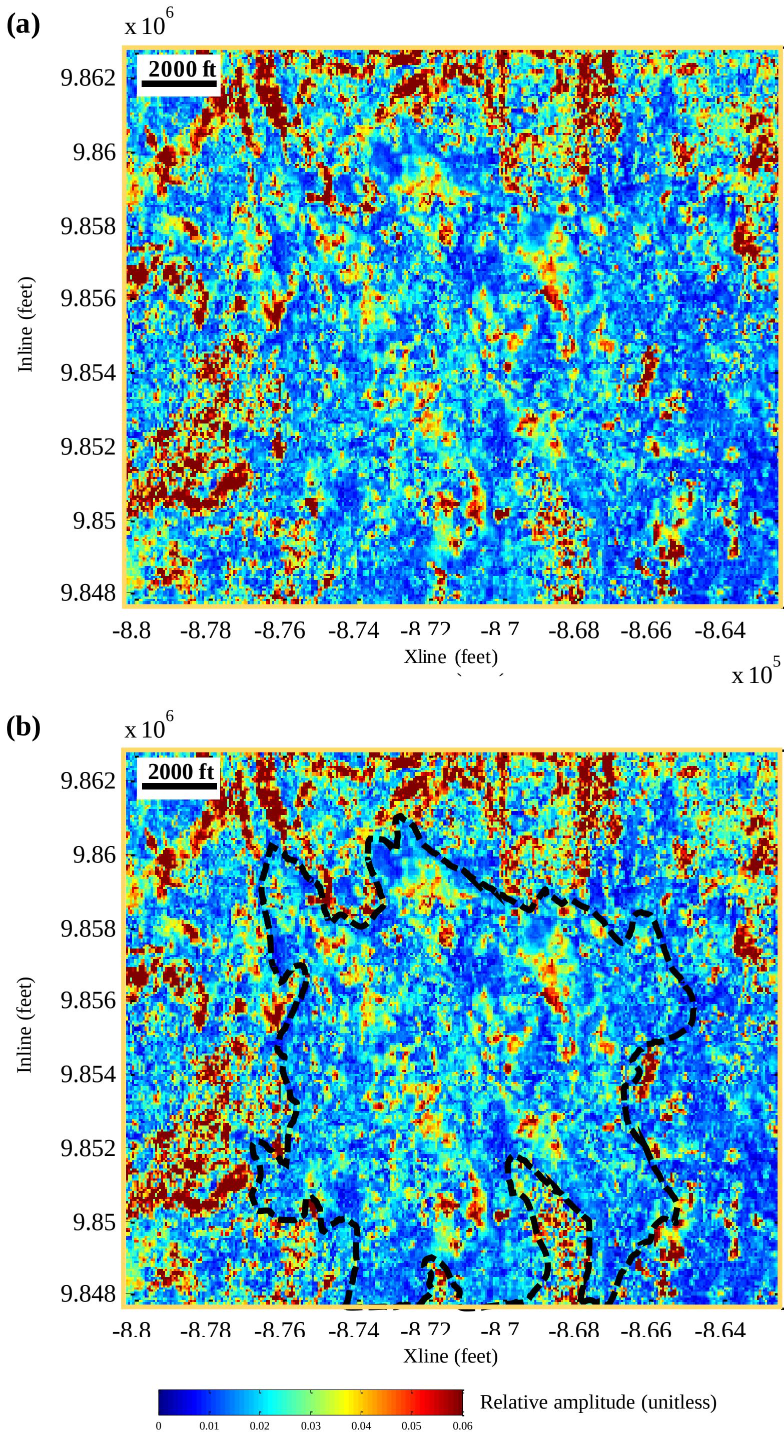

Figure 5.33 Spectral-PC2-amplitude-attribute map (a) and interpreted extended of the reservoir (b, dash line) around the sand levee.

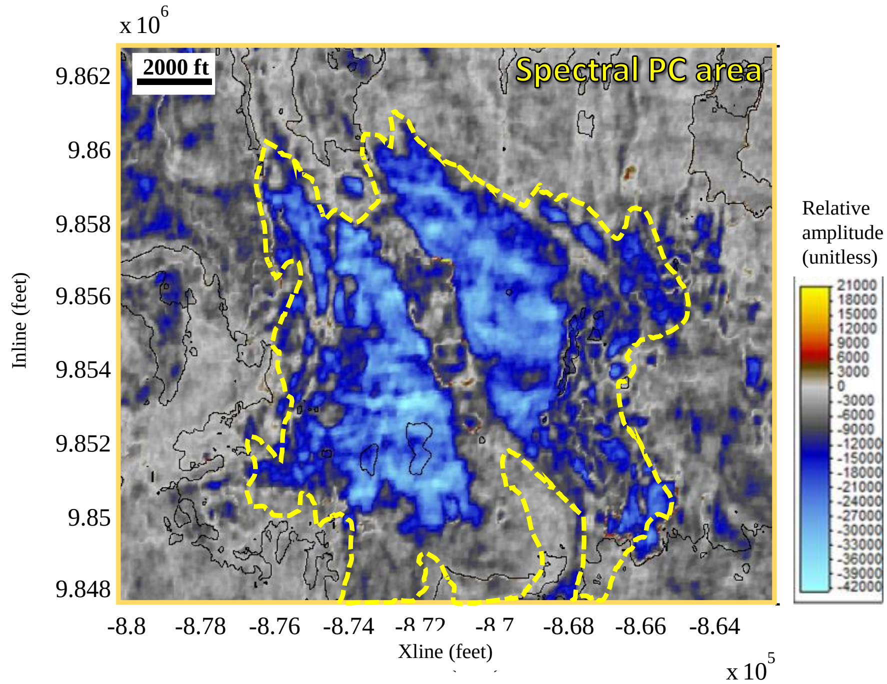

Figure 5.34 Seismic-amplitude map and extended of the reservoir interpreted from spectral-PC attribute (yellow dash curve) around the sand levee.

Chapter 6

Conclusion

The complex nature of seismic amplitude involves thin-layer tuning, fluid involved effects, and lateral wavelet variation besides the conventional understanding of simply reflection strength. First of all, the reflectivity series and seismic waveform of a generalized simple layer can be separated into unique even and odd components. Particularly, the odd and even component of the seismic waveform have different tuning curves. The odd component exhibits maximum constructive interference at the tuning time thickness; while the even component exhibits maximum destructive interference at the tuning time thickness and maximum constructive interference at zero thickness. This discrepancy of odd and even component in amplitude-layer thickness relationship shows that they have different sensitivity to layer thickness. By dividing the data amplitude spectrum by the amplitude spectrum of the wavelet within a usable band, the peak frequency amplitudes are independent of thickness. Comparing peak frequency amplitudes for even and odd components to that of the total waveform, provides clues as to the nature of the layering, as to either a "hard or soft streak" or a "staircase" shaped impedance model.

Principal component analysis (PCA) of isofrequency-amplitude trace data delineates thin-layer-thickness variation by taking advantage of correlation relationship between isofrequency traces. Isofrequency traces tends to be correlated between those at frequency notches, and amongst those not at spectral nulls. By extracting amplitude associated with notch frequencies, the spectral-PC analysis quickly examines the vast isofrequency-amplitude dataset and produces spectral-PC amplitude that is indicative to thickness. Three spectral-PC amplitudes individually delineate amplitudes from: 1) an isolated reflection not affected by tuning; 2) tuning of an even reflection pair; and 3) tuning of an odd reflection pair, in synthetic 2-D wedges and a 3-D synthetic turbidite model. Results from the PC spectral amplitude demonstrate more clearly a karst depression on the Boonsville dataset. In an offshore Gulf of Mexico data example, spectral-PC attributes show similar trends as the synthetic model, when comparing spectral-PC amplitude to true log-based reservoir thickness.

Appendix A

Time-domain-seismic attributes on various wedge models

We tested a series of time domain seismic attributes on four wedge models with (1) odd reflection pair ($r_1 = -1$, $r_2 = 1$); (2) even reflection pair ($r_1 = 1$, $r_2 = 1$); (c) mixed reflection pair ($r_1 = -1$, $r_2 = 0.5$); and (d) mix reflection pair ($r_1 = 1$, $r_2 = 0.5$).

The attributes tested are: Figure A.1: peak amplitude, envelope, second derivative. Figure A.2: peak-peak / peak-trough time. Figure A.3: peak amplitude times peak-peak / peak-trough time. Figure A.4: Peak instantaneous frequency. Figure A.5: Response frequency (peak frequency at peak of envelope). Figure A.6: Sweetness (dividing reflection strength by the square root of instantaneous frequency). Figure A.7: Response sweetness.

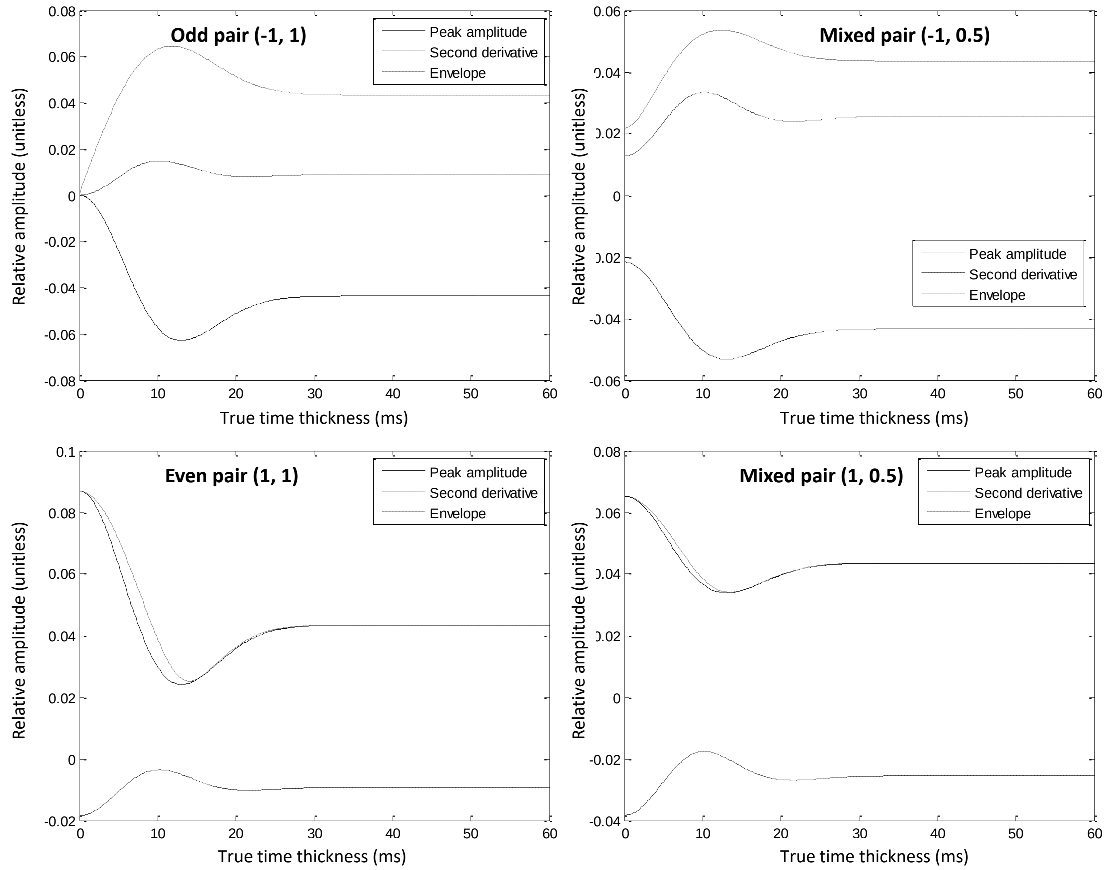

Figure A.1 Peak amplitude, envelope, second derivative of waveform of the wedge model.

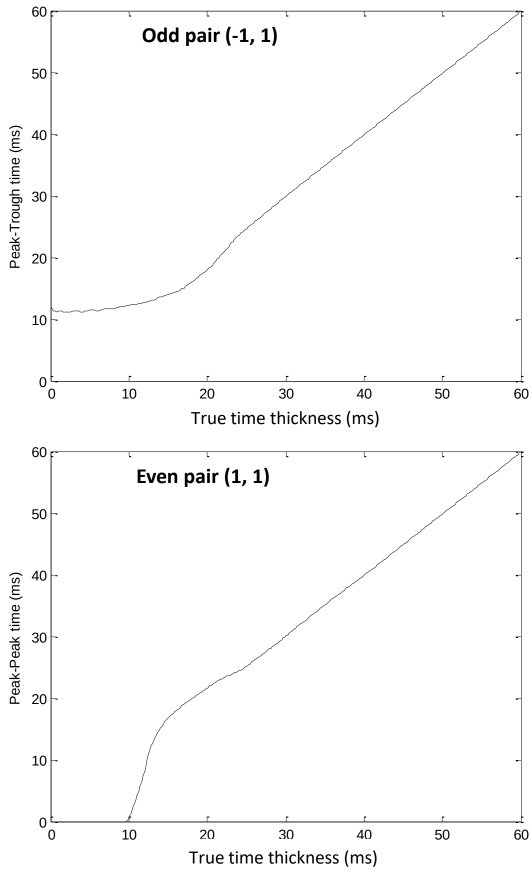

Figure A.2 Peak-peak / peak-trough time of the wedge model.

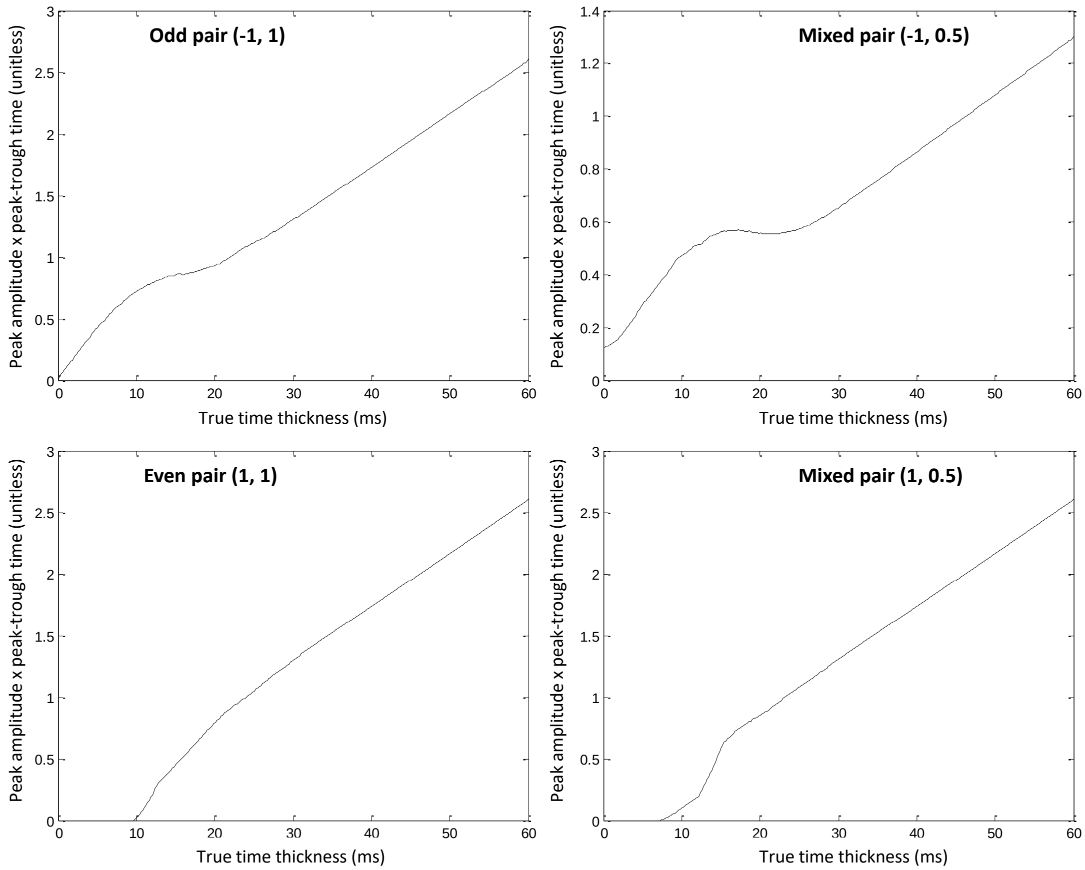

Figure A.3 Peak amplitude multiply peak-peak / peak-trough time of the wedge model.

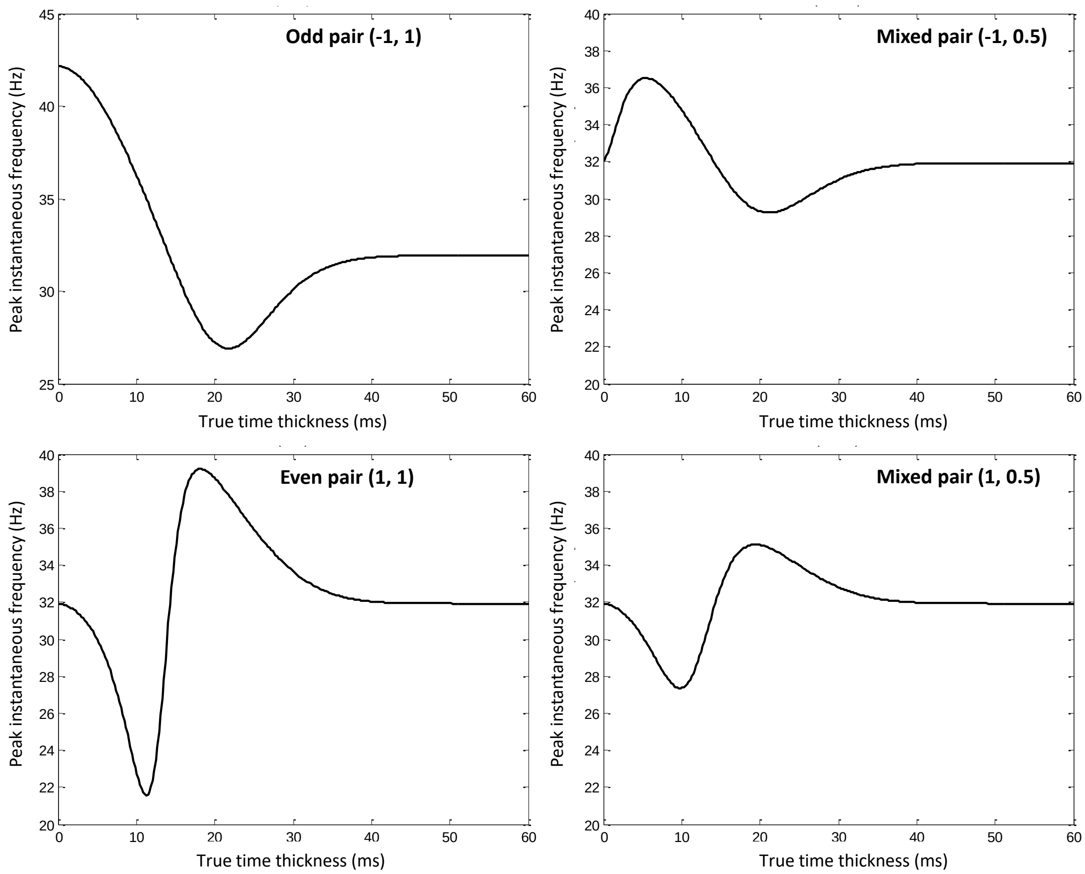

Figure A.4 Peak-instantaneous frequency of the wedge model.

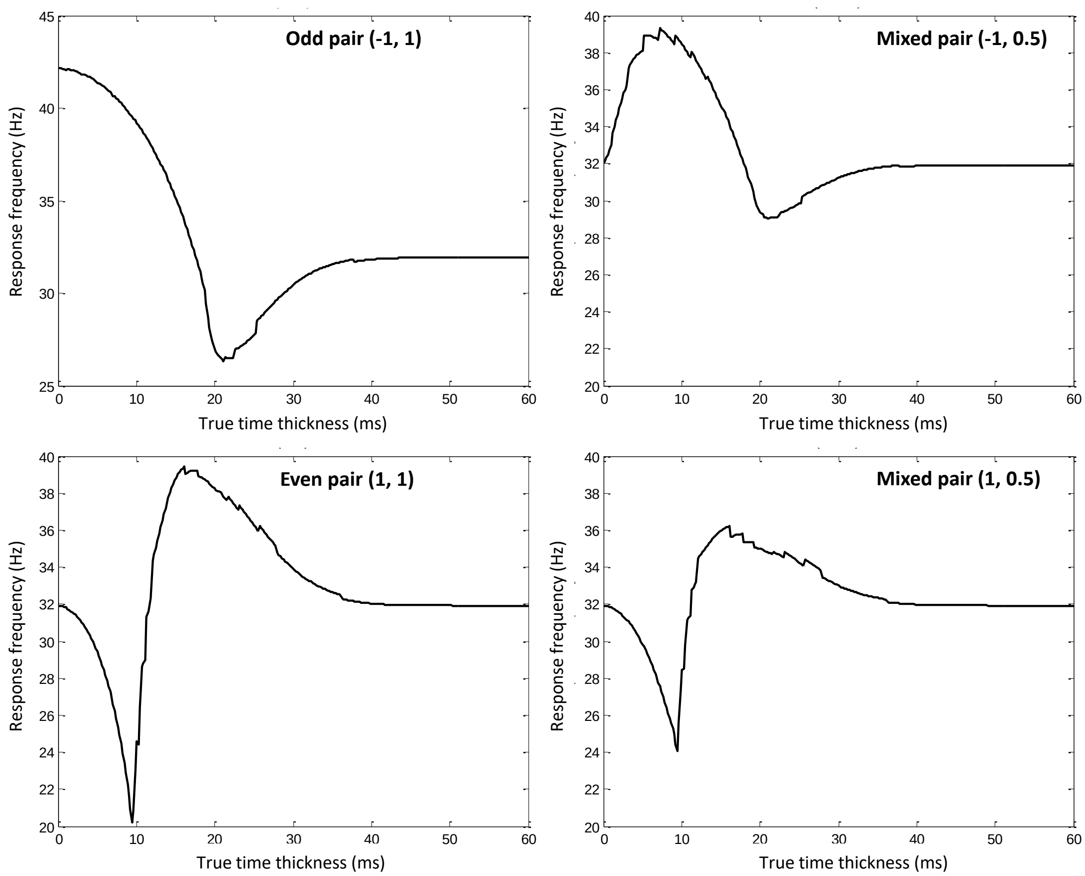

Figure A.5 Response frequency of the wedge model.

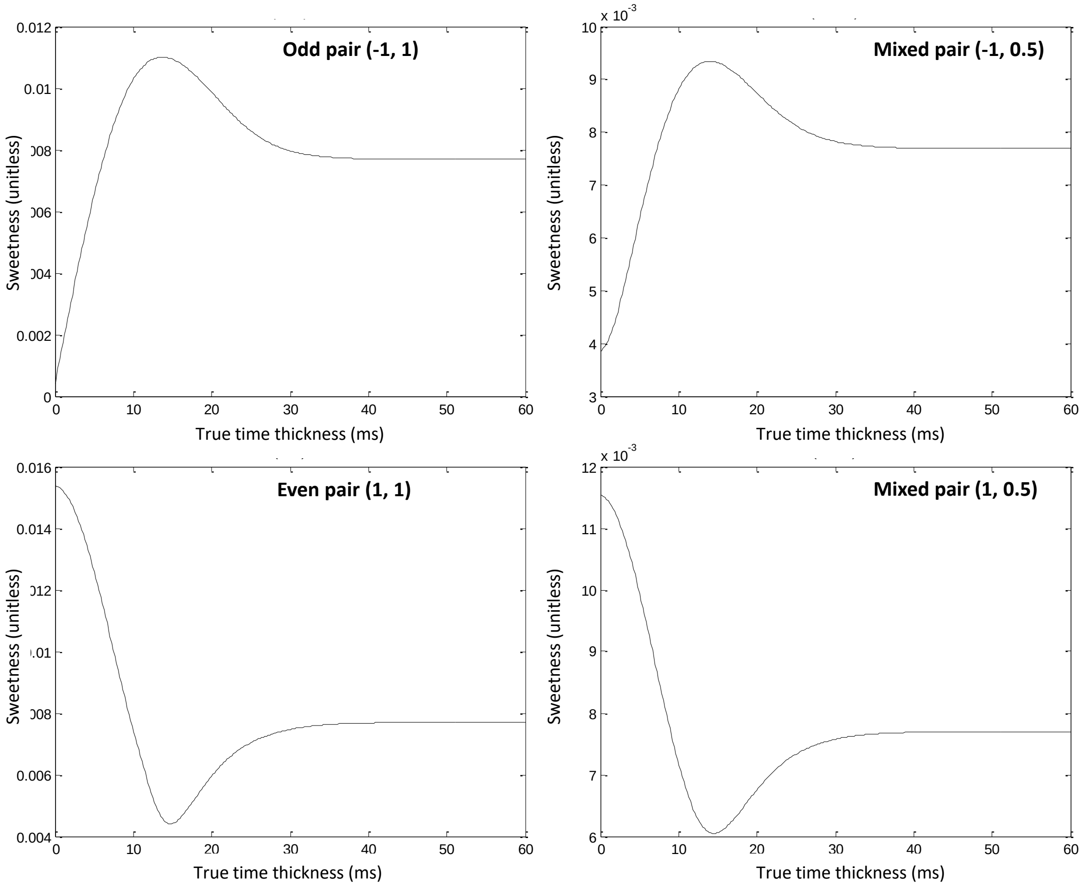

Figure A.6 Sweetness of the wedge model.

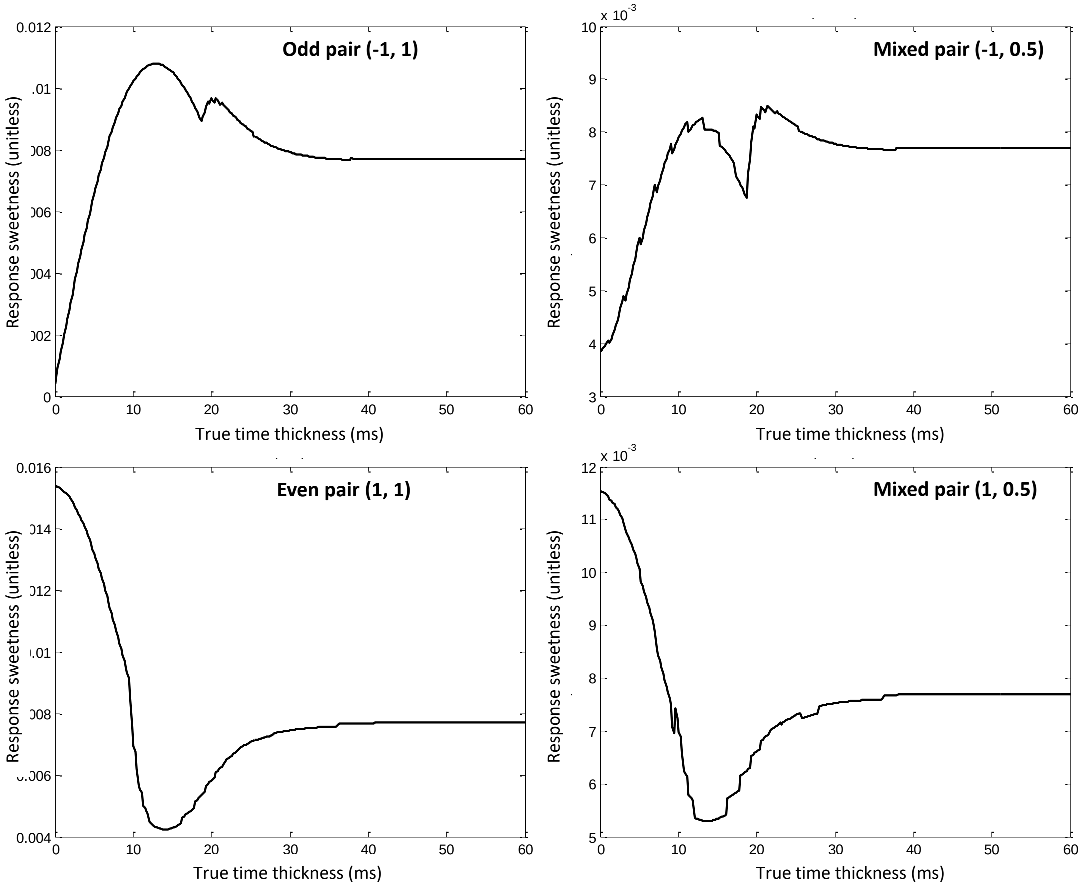

Figure A.7 Response sweetness of the wedge model.

Appendix B

Workflow for Separating Even- and Odd- Components of an Arbitrary-Reflection Pair

For any arbitrary seismic reflection pair of seismogram, it is possible to separate the even and odd part of the data using simply Fourier transform once the center is decided. Figure B1 describes the general workflow and MATLAB code example for this workflow. The general idea is to perform Fourier transform to the data, take the real and imaginary part separately, and use inverse Fourier transform to convert the real and imaginary part back to time domain individually, then the even and odd part of the data is obtained, respectively.

An example of a 10 ms mixed reflection pair is used to show the workflow as presented in Figure B2, B3, and B4, for its time representation, amplitude spectrum, and phase diagram, respectively. A seismogram is created by convolving the same reflection pair to a 30 Hz Ricker wavelet. The same workflow is also able to separate the even and odd part just like the reflection pair, as shown in Figure B5, B6, and B7, for its time representation, amplitude spectrum, and phase diagram, respectively.

Also a spectral division can be used to remove the effect of wavelet spectrum and recover amplitude spectrum of reflection pair once the amplitude spectrum of wavelet is known. An example using a 40 ms thick mixed reflection layer and 30 Hz wavelet. The spectral division can be performed on either the amplitude spectrum of original seismic waveform (Figure B8), even part of the waveform (Figure B9), or odd part of the waveform (Figure B10).

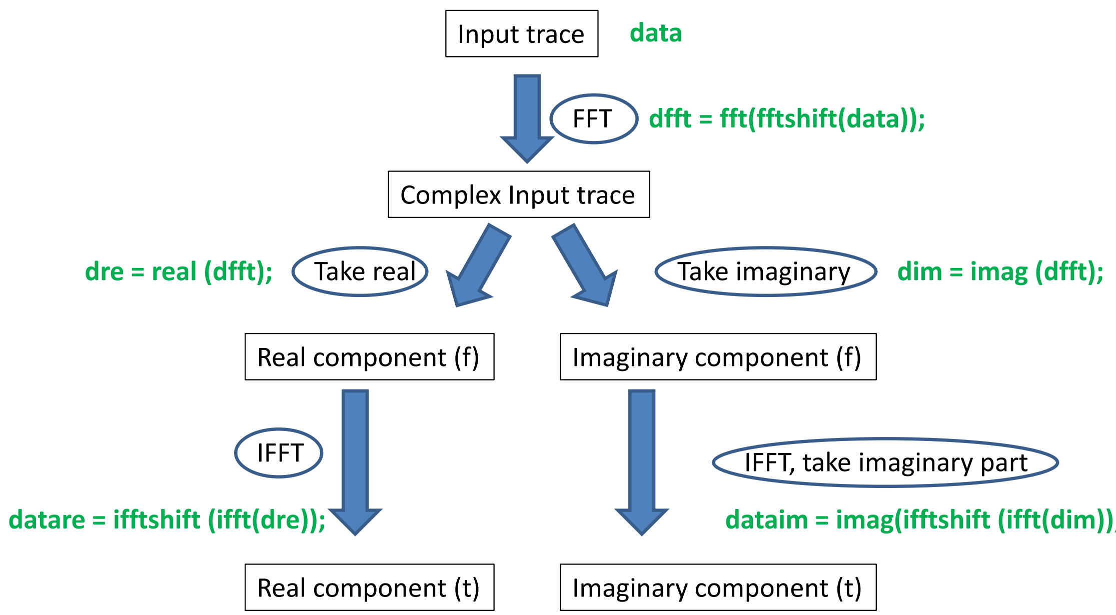

Note: **fftshift** and **fftshift** are MATLAB function that shift data so that MATLAB process the data with time zero at actual center.

Figure B.1 Workflow of separating the real and imaginary component of any Fourier series using Fourier transform.

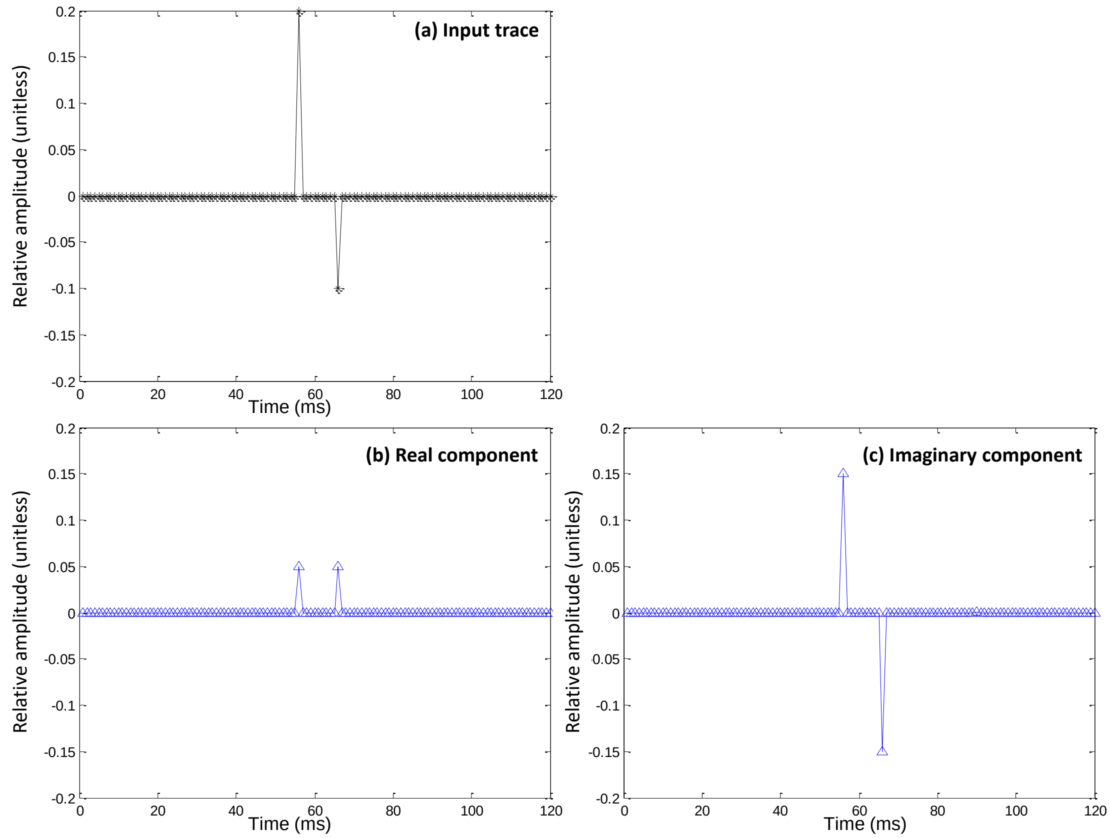

Figure B.2 A mixed reflection pair (a), the even part (b), and odd part (c).

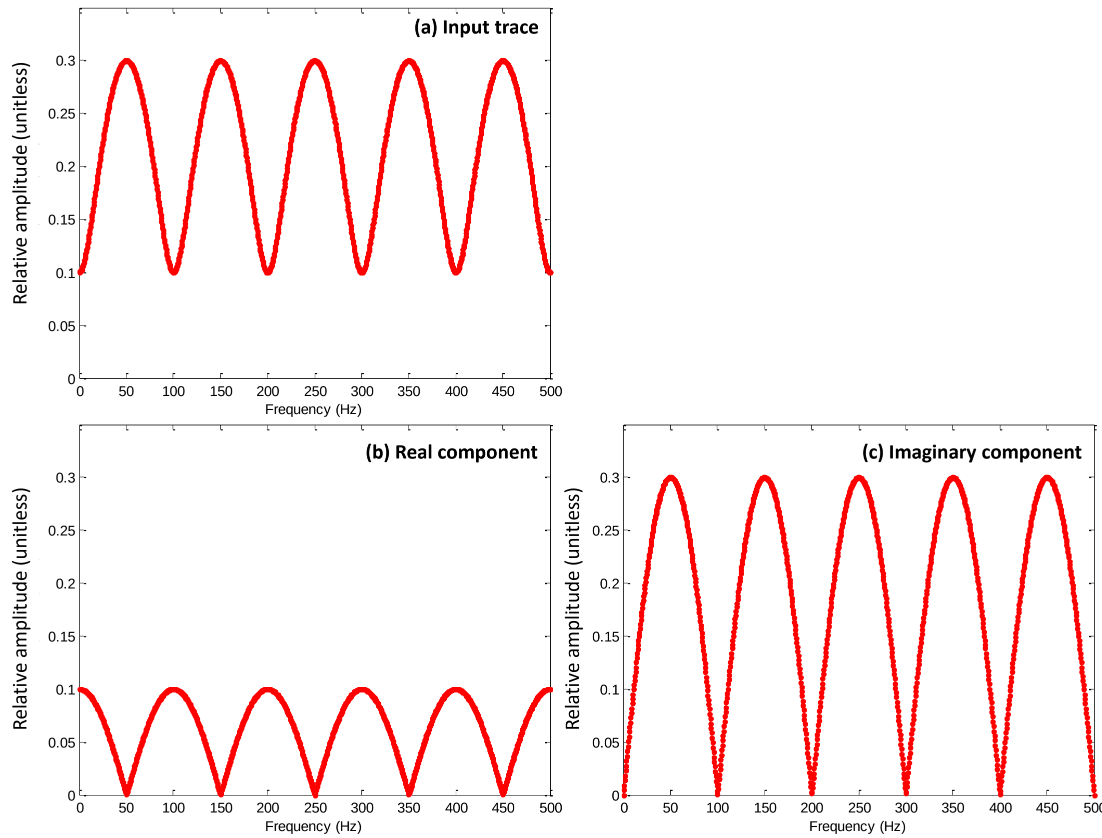

Figure B.3 Amplitude spectrum of a mixed-reflection pair (a), the even part (b), and odd part (c).

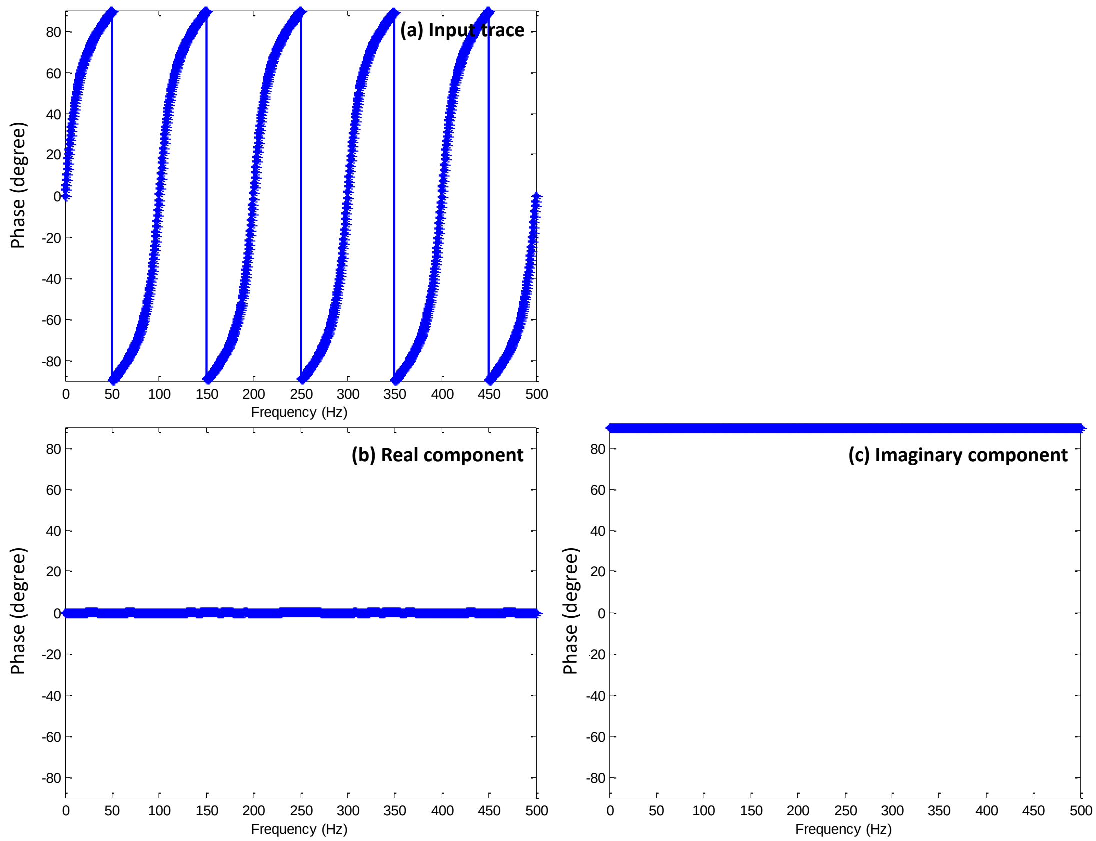

Figure B.4 Phase spectrum of a mixed-reflection pair (a), the even part (b), and odd part (c).

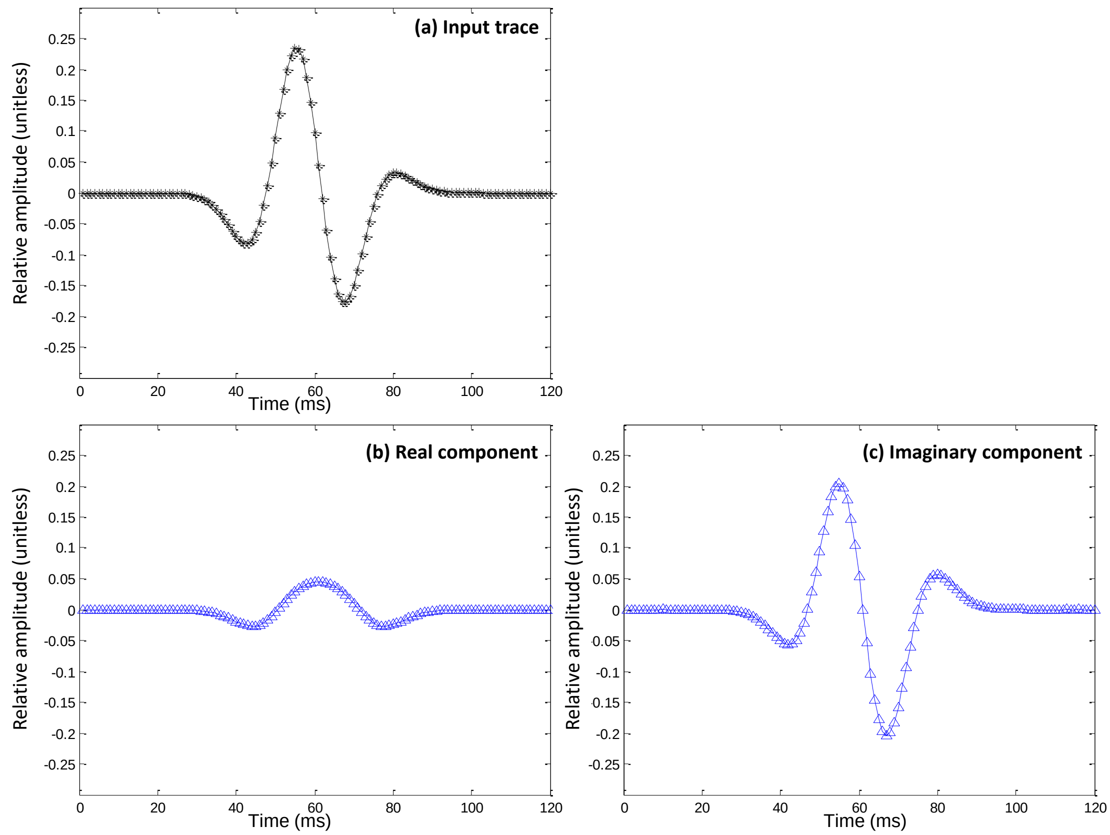

Figure B.5 Seismogram of a mixed-reflection pair from 10 ms layer convolved with 30 Hz Ricker wavelet (a), the even part (b), and odd part (c).

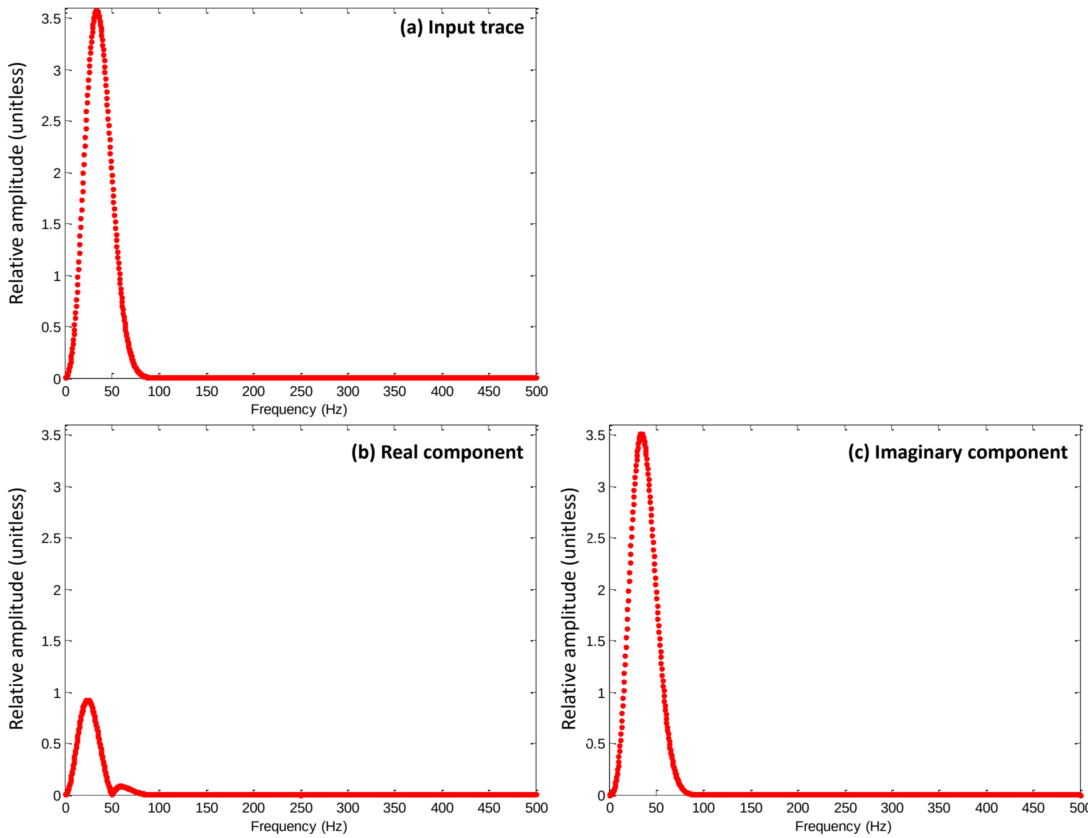

Figure B.6 Amplitude spectrum of a mixed-reflection pair from 10 ms layer convolved with 30 Hz Ricker wavelet (a), the even part (b), and odd part (c).

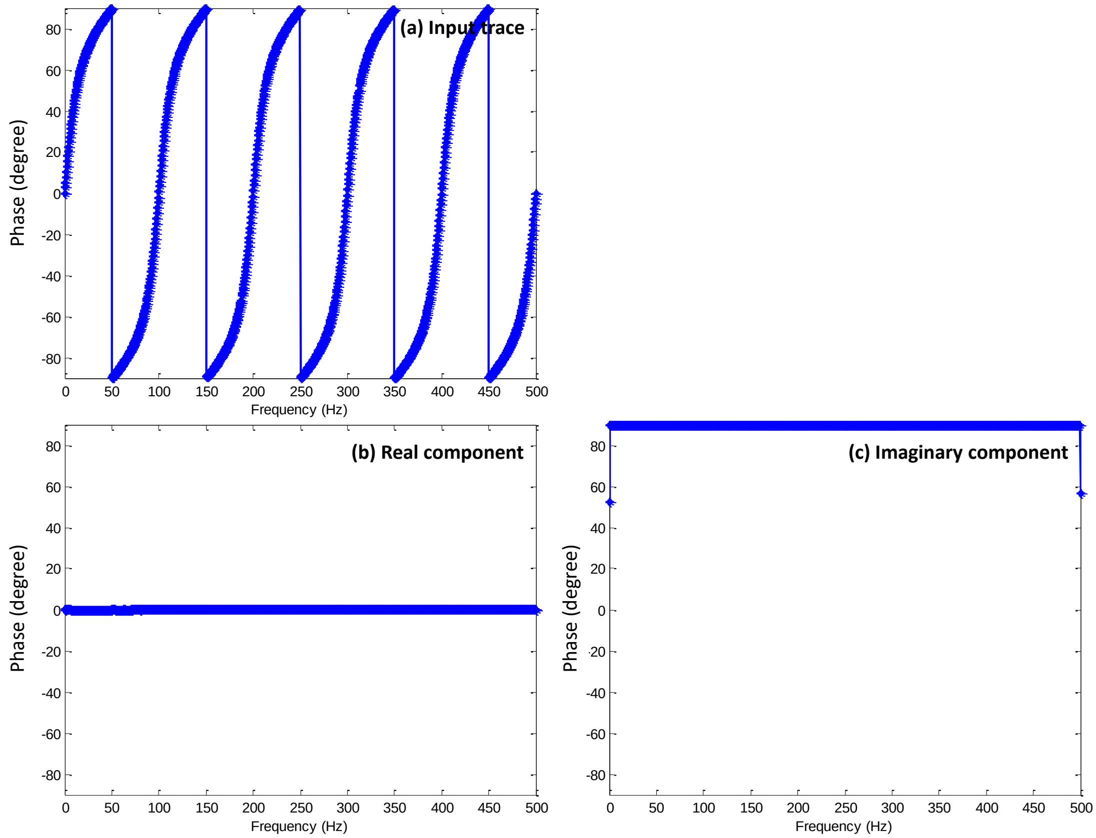

Figure B.7 Phase diagram a mixed-reflection pair from 10 ms layer convolved with 30 Hz Ricker wavelet (a), the even part (b), and odd part (c).

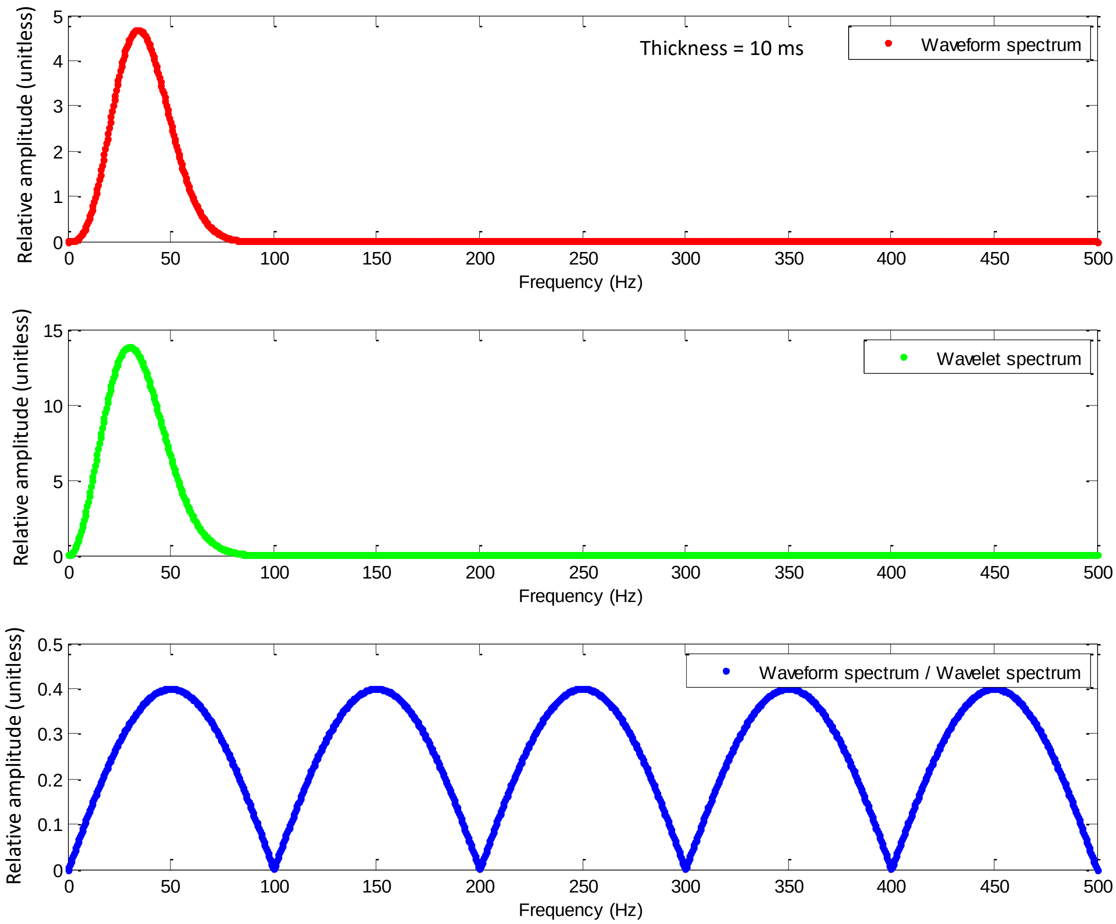

Figure B.8 Amplitude spectrum of signal from a 40-ms-thick layer (upper); 30 Hz Ricker wavelet (middle); quotient of signal and wavelet amplitude spectrum (lower).

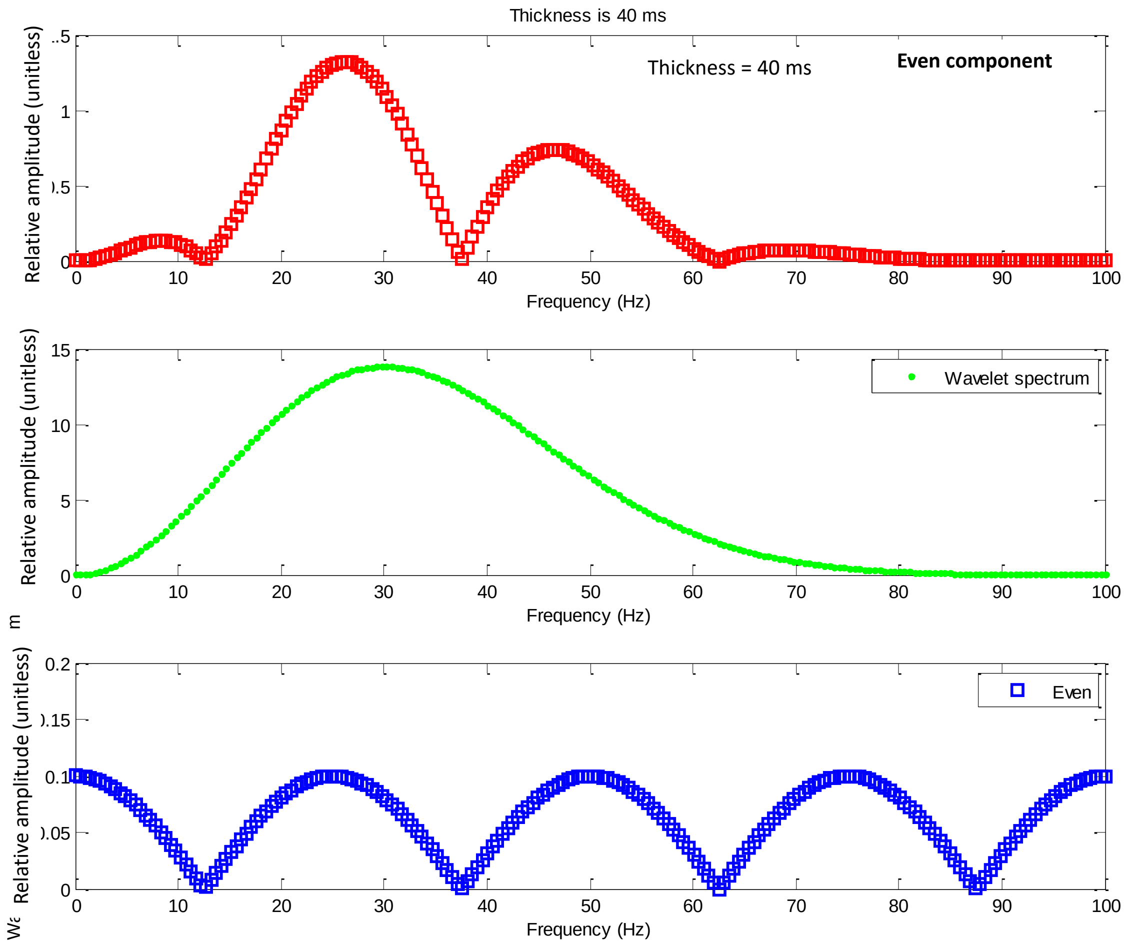

Figure B.9 Amplitude spectrum of even part of signal from a 40-ms-thick layer (upper); 30 Hz Ricker wavelet (middle); quotient of signal even part and wavelet amplitude spectrum (lower).

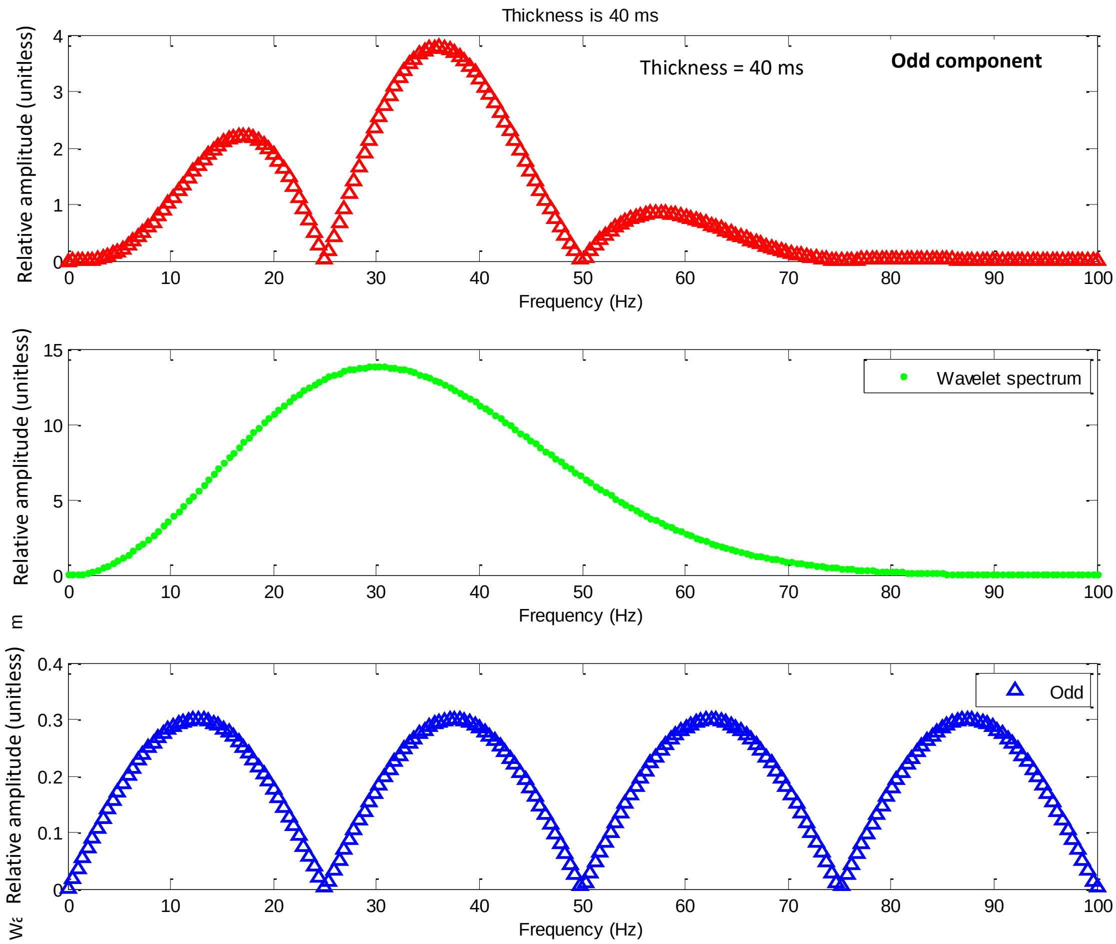

Figure B.10 Amplitude spectrum of odd part of signal from a 40-ms-thick layer (upper); 30 Hz Ricker wavelet (middle); quotient of signal odd part and wavelet amplitude spectrum (lower).

Appendix C

An algorithm for Varimax rotation of PC coefficient matrix

One of the conceptually simple algorithm to solve the argument of maximum PC coefficient matrix (R') is by performing bivariate rotations iteratively. Each iteration begins with selection of two columns in the m-by-p R' matrix, R_i and R_j, which defines a 2-dimension plane within the p-dimension hyperspace. Next, the angle for rotation in the selected 2-d plane can be calculated by the following equation (Kaiser, 1958).

$$\Phi = \frac{1}{4} tan^{-1} \frac{2\left[n \sum(R'^2_i - R'^2_j)(2R'_i R'_j) - \sum(R'^2_i - R'^2_j) \sum(2R'_i R'_j)\right]}{p\left\{\sum\left[\left(R'^2_i - R'^2_j\right)^2 - (2R'_i R'_j)^2\right]\right\} - \left\{\left[\sum\left(R'^2_i - R'^2_j\right)\right]^2 - \left[\sum\left(2R'_i R'_j\right)\right]^2\right\}}$$

The rotation of the selected two columns is performed by multiplying it to a rotation matrix $\begin{bmatrix} cos\,\Phi & -sin\,\Phi \\ sin\,\Phi & cos\,\Phi \end{bmatrix}$. As a result, data points in this 2-d plane now have the highest variation along the new axes, i.e., are closest to the two axes. After that, rotation is performed on different pairs of columns. The total number of rotations for each iteration depends on p, the number of columns in R' that is used. The value of i range from 1 to p, j range from $(i+1)$ to p. By counting combination, the number of rotations for each iteration is C_2^p. The iteration continues until a small enough rotation angle is reached, indicating the Varimax criterion is met in all p dimensions (columns) in R'.

Another algorithm that is computationally more efficient using singular value decomposition can be find in Lawley and Maxwell (1971).

REFERENCES

Bracewell, R., 1986, The Fourier Transform and its Applications, McGraw-Hill Publ. Co., New York City.

Castagna, J. P., S. Sun, and R. W. Siegfried, 2003, Instantaneous spectral analysis: Detection of low-frequency shadows associated with hydrocarbons. The Leading Edge, 22, 120-127.

Chakraborty, A., D. Okaya, 1995, Frequency-time decomposition of seismic data using wavelet-based methods: Geophysics, 60, 1906-1916.

Chen, G., G. Matteucci, B. Fahmy, and C. Finn, 2008, Spectral-decomposition response to reservoir fluids from a deepwater West Africa reservoir. Geophysics, 73, C23-C30.

Chung, H., and D. C. Lawton, 1995, Frequency characteristics of seismic reflections from thin beds. Canadian Journal of Exploration Geophysicists, 31, 32-37.

Gabor D., 1946, Theory of communication. Part 1: The analysis of information. Journal of the Institution of Electrical Engineers-Part III: Radio and Communication Engineering. 1946, 93:429-441.

Fomel, S., E. Landa, and M. T. Taner, 2007, Poststack velocity analysis by separation and imaging of seismic diffractions. Geophysics, 72, U89-U94.

Guo, H., K. J. Marfurt, and J. L. Liu, 2009, Principal component spectral analysis. Geophysics, 74, P35-P43.

Hardage, B. A., D. L. Carr, D. E. Lancaster, J. L. Simmons, R. Y. Elphick, V. M. Pendleton, and R. A. Johns, 1996, 3-D seismic evidence of the effects of carbonate karst collapse on overlying clastic stratigraphy and reservoir compartmentalization. Geophysics, 61, 1336-1350.

Higgins, J. W., D. Chergotis, and J. C. Nania, 1998, Hoover: A Significant Oil Discovery in the Western Gulf of Mexico Deepwater. Houston Geological Society Bulletin, 40, 17 and 19.

Jolliffe, I., 2002, Principal component analysis, Springer.

Kaiser, H. F., 1958, The varimax criterion for analytic rotation in factor-analysis. Psychometrika, 23, 187-200.

Kallweit, R. S., and L. C. Wood, 1982, The limits of resolution of zero-phase wavelets. Geophysics, 47, 1035.

Khare, V., and A. Martinez, 2008, Estimation of sub-tuned reservoir thickness from amplitudes at different seismic bandwidths — a time-domain approach. SEG Technical Program Expanded Abstracts, 2968-2972.

Korneev, V. A., G. M. Goloshubin, T. M. Daley, and D. B. Silin, 2004, Seismic low-frequency effects in monitoring fluid-saturated reservoirs. Geophysics, 69, 522-532.

Lawley, D. N., and A. E. Maxwell, 1971, Factor analysis as a statistical method. JSTOR.

Levy, S., and D. W. Oldenburg, 1987, Automatic Phase Correction of Common-Midpoint Stacked Data. Geophysics, 52, 51-59.

Li, Y. D., X. D. Zheng, and Y. Zhang, 2011, High-frequency anomalies in carbonate reservoir characterization using spectral decomposition. Geophysics, 76, V47-V57.

Liner, C. L., and B. G. Bodmann, 2010, The Wolf ramp: Reflection characteristics of a transition layer. Geophysics, 75.

Liu, J. L., and K. J. Marfurt, 2007, Instantaneous spectral attributes to detect channels. Geophysics, 72, P23-P31.

Marfurt, K. J., and R. L. Kirlin, 2001, Narrow-band spectral analysis and thin-bed tuning. Geophysics, 66, 1274-1283.

Partyka, G., J. Gridley, and J. Lopez, 1999, Interpretational applications of spectral decomposition in reservoir characterization. The Leading Edge, 18, 353-360.

Puryear, C. I., and J. P. Castagna, 2008, Layer-thickness determination and stratigraphic interpretation using spectral inversion: Theory and application. Geophysics, 73, R37-R48.

Sinha, S., P. S. Routh, P. D. Anno, and J. P. Castagna, 2005, Spectral decomposition of seismic data with continuous-wavelet transform. Geophysics, 70, P19-P25.

Taner, M. T., F. Koehler, and R. E. Sheriff, 1979, Complex Seismic Trace Analysis. Geophysics, 44, 1041-1063.

Wallet, B., and K. Marfurt, 2008, A grand tour of multispectral components: A tutorial. The Leading Edge, 27, 334-341.

Widess, M. B., 1973, How thin is a thin bed? : Geophysics, 38, 1176-1180.

Wiggins, R. A., 1978, Minimum entropy deconvolution. Geoexploration, 16, 21-35.

Yang, M. 2003, Monochromatic AVO: An indicator that sees through wave interference, SEG Technical Program Expanded Abstracts. 208-210.